Report No.488

epa Research

Habitat Mapping, Assessment and Monitoring with High-resolution Unoccupied Aerial Vehicle Imagery (iHabiMap)

Authors: John Connolly, Charmaine Cruz, James R. Martin, Jerome O Connell, Kevin McGuinness and Philip M. Perrin

www.epa.ie

Rialtas na hÉireann
Government of Ireland

Environmental Protection Agency

The EPA is responsible for protecting and improving the environment as a valuable asset for the people of Ireland. We are committed to protecting people and the environment from the harmful effects of radiation and pollution.

The work of the EPA can be divided into three main areas:

Regulation: Implementing regulation and environmental compliance systems to deliver good environmental outcomes and target those who don't comply.

Knowledge: Providing high quality, targeted and timely environmental data, information and assessment to inform decision making.

Advocacy: Working with others to advocate for a clean, productive and well protected environment and for sustainable environmental practices.

Our Responsibilities Include:

Licensing

- Large-scale industrial, waste and petrol storage activities;
- Urban waste water discharges;
- The contained use and controlled release of Genetically Modified Organisms;
- Sources of ionising radiation;
- Greenhouse gas emissions from industry and aviation through the EU Emissions Trading Scheme.

National Environmental Enforcement

- Audit and inspection of EPA licensed facilities;
- Drive the implementation of best practice in regulated activities and facilities;
- Oversee local authority responsibilities for environmental protection;
- Regulate the quality of public drinking water and enforce urban waste water discharge authorisations;
- Assess and report on public and private drinking water quality;
- Coordinate a network of public service organisations to support action against environmental crime;
- Prosecute those who flout environmental law and damage the environment.

Waste Management and Chemicals in the Environment

- Implement and enforce waste regulations including national enforcement issues;
- Prepare and publish national waste statistics and the National Hazardous Waste Management Plan;
- Develop and implement the National Waste Prevention Programme;
- Implement and report on legislation on the control of chemicals in the environment.

Water Management

- Engage with national and regional governance and operational structures to implement the Water Framework Directive;
- Monitor, assess and report on the quality of rivers, lakes, transitional and coastal waters, bathing waters and groundwaters, and measurement of water levels and river flows.

Climate Science & Climate Change

- Publish Ireland's greenhouse gas emission inventories and projections;
- Provide the Secretariat to the Climate Change Advisory Council and support to the National Dialogue on Climate Action;
- Support National, EU and UN Climate Science and Policy development activities.

Environmental Monitoring & Assessment

- Design and implement national environmental monitoring systems: technology, data management, analysis and forecasting;
- Produce the State of Ireland's Environment and Indicator Reports;
- Monitor air quality and implement the EU Clean Air for Europe Directive, the Convention on Long Range Transboundary Air Pollution, and the National Emissions Ceiling Directive;
- Oversee the implementation of the Environmental Noise Directive;
- Assess the impact of proposed plans and programmes on the Irish environment.

Environmental Research and Development

- Coordinate and fund national environmental research activity to identify pressures, inform policy and provide solutions;
- Collaborate with national and EU environmental research activity.

Radiological Protection

- Monitoring radiation levels and assess public exposure to ionising radiation and electromagnetic fields;
- Assist in developing national plans for emergencies arising from nuclear accidents;
- Monitor developments abroad relating to nuclear installations and radiological safety;
- Provide, or oversee the provision of, specialist radiation protection services.

Guidance, Awareness Raising, and Accessible Information

- Provide independent evidence-based reporting, advice and guidance to Government, industry and the public on environmental and radiological protection topics;
- Promote the link between health and wellbeing, the economy and a clean environment;
- Promote environmental awareness including supporting behaviours for resource efficiency and climate transition;
- Promote radon testing in homes and workplaces and encourage remediation where necessary.

Partnership and Networking

- Work with international and national agencies, regional and local authorities, non-governmental organisations, representative bodies and government departments to deliver environmental and radiological protection, research coordination and science-based decision making.

Management and Structure of the EPA

The EPA is managed by a full time Board, consisting of a Director General and five Directors. The work is carried out across five Offices:

1. Office of Environmental Sustainability
2. Office of Environmental Enforcement
3. Office of Evidence and Assessment
4. Office of Radiation Protection and Environmental Monitoring
5. Office of Communications and Corporate Services

The EPA is assisted by advisory committees who meet regularly to discuss issues of concern and provide advice to the Board.

Habitat Mapping, Assessment and Monitoring with High-resolution Unoccupied Aerial Vehicle Imagery (iHabiMap)

Authors: John Connolly, Charmaine Cruz, James R. Martin, Jerome O Connell, Kevin McGuinness and Philip M. Perrin

Leading organisation: Trinity College Dublin, Dublin City University, BEC Consultants Ltd and Proveye Ltd

What did this research aim to address?

The research demonstrated how Unmanned Aerial Vehicle (UAV) and computer machine learning technology offer an alternative complementary approach to map, assess and monitor habitats. Habitat assessment carried out by qualified ecologists during field visits, is demanding and time-consuming, particularly in remote and inaccessible areas.

The developed approach used a combination of botanical and UAV surveys, image analysis and machine learning to develop methods to accurately map Annex1 habitats in grassland (one site in Glenasmole, Co. Dublin), upland (two sites in Slieve Mish, Co. Kerry and Kippure gates, Co. Wicklow) and coastal (two sand dunes sites in Maharees, Co. Kerry and Bull Island and one saltmarsh site in Bull Island). This novel integration of ecological, AI and Geospatial knowledge produced highly accurate maps of vegetation.

This newly developed methodology would be highly beneficial to the National Parks and Wildlife Service (NPWS), who are legally obliged, under Article 17 of the Habitats Directive (HD), to conduct an assessment of Annex I habitats throughout Ireland, every six years and also complete assessments for reporting under the Water Framework Directive.

What did this research find?

The integration of expert knowledge from experienced ecologists with high resolution UAV, Geospatial and AI expertise in the iHabiMap project produced very accurate habitat maps (accuracies >90%). iHabiMap demonstrates the feasibility to use this method to map habitats over large areas in a routine fashion.

Some insights: Relatively homogeneous habitats that occur in undulating or gently sloping terrain can be characterised by UAV remote sensing with high accuracy. Habitats with distinct spectral signatures and typically defined by elevation (coastal dunes) can be very accurately mapped with UAV multispectral and topographic information.

Heterogeneous habitats, occurring in mosaics e.g. upland habitats, can be more challenging to characterise due to complex spectral characteristics. High-altitude or rugged terrain leads to data quality issues, including shadowing effects and variations in UAV sensors' perspectives due to steep slopes and changing elevations.

Optical UAV remote sensing may not be suitable for classifying understory habitats. Dense canopies often obstruct the sensor's view of the ground, making understory vegetation difficult to detect. Future studies could explore other sensors, such as LiDAR, which can penetrate the canopy more effectively.

How can the research findings be used?

The main target audience is the NPWS and private companies operating in the ecological monitoring and assessment space. To facilitate the implementation and roll out of the research, in the land cover types assessed in iHabiMap, additional technical capability would likely be needed by NPWS to make operational use of the methodology. Further research should also be carried out to determine; 1. how transferable and interoperable the model is in different environments and 2. how to roll this out to areas of interest across the country.

The methods developed in this research can be applied to monitor degradation and rehabilitation of Dune systems, Salt Marshes, Uplands and Grasslands nationally. The methods are excellent for the implementation of monitoring, reporting and verification for policies such as the Nature Restoration Law.

EPA RESEARCH PROGRAMME 2021–2030

Habitat Mapping, Assessment and Monitoring with High-resolution Unoccupied Aerial Vehicle Imagery (iHabiMap)

(2018-NC-LS-4)

EPA Research Report

Prepared for the Environmental Protection Agency

by

Trinity College Dublin, Dublin City University, BEC Consultants Ltd and Proveye Ltd

Authors:

John Connolly, Charmaine Cruz, James R. Martin, Jerome O Connell, Kevin McGuinness and Philip M. Perrin

ENVIRONMENTAL PROTECTION AGENCY
An Ghníomhaireacht um Chaomhnú Comhshaoil
PO Box 3000, Johnstown Castle, Co. Wexford, Ireland

Telephone: +353 53 916 0600 Fax: +353 53 916 0699
Email: info@epa.ie Website: www.epa.ie

ACKNOWLEDGEMENTS

This report is published as part of the EPA Research Programme 2021–2030. The EPA Research Programme is a Government of Ireland initiative funded by the Department of Climate, Energy and the Environment. It is administered by the Environmental Protection Agency, which has the statutory function of co-ordinating and promoting environmental research.

The authors would like to acknowledge the members of the project steering committee, namely Gavin Smith (EPA), Gemma Weir (National Parks and Wildlife Service), Kevin Lydon (EPA), Monica Rivas Casado (Cranfield University), Paul Scholefield (Lancaster University) and Lisa Johnson and Siobhan Murphy (project managers on behalf of EPA Research).

The authors would also like to thank the Dublin City University Insight Centre and Trinity College Dublin research office for administrative support. Many landowners generously granted permission to access their lands, including Tom McCarthy and Michael Anderson who gave access to their grasslands in Glenasmole. We would also like to thank County Wicklow and County Kerry rangers (National Parks and Wildlife Service), Dr Eugene Farrell (University of Galway) and the Maharees Conservation Association.

Finally, this report is dedicated to the memory of our co-author and colleague Dr Kevin McGuinness (Dublin City University), who unfortunately passed away suddenly in summer 2023.

Cover image: Drone image taken in the Maharees, Co. Kerry, with the Brandon Mountains in the distance.

DISCLAIMER

This report is based on research carried out/data from March 2019 to August 2023. More recent data may have become available since the research was completed.

The EPA Research Programme addresses the need for research in Ireland to inform policymakers and other stakeholders on a range of questions in relation to environmental protection. These reports are intended as contributions to the necessary debate on the protection of the environment.

EPA RESEARCH PROGRAMME 2021–2030
Published by the Environmental Protection Agency, Ireland

ISBN: 978-1-80009-293-8 June 2025

Price: Free Online version

Project Partners

John Connolly
Discipline of Geography, School of Natural Sciences
Trinity College Dublin
Dublin 2
Ireland
Email: john.connolly@tcd.ie

Charmaine Cruz
Discipline of Geography, School of Natural Sciences
Trinity College Dublin
Dublin 2
Ireland
Email: ccruz@tcd.ie

James R. Martin
BEC Consultants Ltd
65 Holywell
Dundrum
Dublin
D14 P5W0
Ireland
Email: jmartin@botanicalenvironmental.com

Philip M. Perrin
BEC Consultants Ltd
65 Holywell
Dundrum
Dublin
D14 P5W0
Ireland
Email: pperrin@botanicalenvironmental.com

Kevin McGuinness
School of Electronic Engineering and Insight SFI Research Centre for Data Analytics
Dublin City University
Dublin 9
Ireland

Jerome O Connell
Proveye Ltd
NovaUCD
University College Dublin
Dublin 4
Ireland
Email: joconnell@proveye.io

Contents

List of Figures

List of Tables

Executive Summary

The increasing decline in habitats has spurred the development of conservation-related legislation that includes monitoring, reporting and verifying. Field surveys are often part of monitoring, reporting and verifying, but they can be time-consuming and resource-intensive, particularly over large remote areas. Advancements in remote sensing and machine learning can be integrated with field surveys to improve their efficiency and effectiveness. However, this integration has not been well examined in an Irish context. The iHabiMap project explored the integration of remote sensing data with machine learning techniques, developing robust and repeatable methodologies to map Irish examples of habitats listed under Annex I of the EU Habitats Directive. iHabiMap focused on coastal, grassland and upland habitats but the method is transferable to other habitat types.

The effectiveness of processing remote sensing data acquired by unoccupied aerial vehicles (UAVs) using machine learning tools to accurately map highly dynamic and fine-scale mosaics of habitats in a coastal dune environment was assessed. UAV images have very high spatial resolution (centimetre level). They facilitate flexible temporal acquisition, aligning with key phenological stages of vegetation communities. Here, the imagery and field data were acquired during the 2020 and 2021 growing seasons between May and October. Orthomosaics and topographic data were generated using the structure-from-motion technique. The datasets were processed and analysed using the random forest machine learning technique to classify the dune habitats. Combining multiple UAV datasets acquired throughout the growing season achieved higher classification accuracy than single image acquisitions (92.37% vs 84.09%, respectively). Inclusion of topographic data consistently improved accuracy. The best time to acquire data for dune habitat mapping was during the flowering period. iHabiMap produced highly accurate maps detailing habitat distribution and vulnerable areas, which can be used for land use management.

The method was adapted for monitoring, reporting and verifying the location and expansion of invasive species. UAV-acquired imagery and deep learning techniques created detailed maps of an invasive species (*Spartina anglica*) in a saltmarsh. The development of robust deep learning models is challenging owing to the requirement for large and diverse labelled training data. The creation of labelled data is time- and resource-intensive. This limitation restricts the transferability of deep learning models. The study implemented a deep learning semantic segmentation on UAV imagery, testing different model parameters to determine an effective network structure. Data augmentation and pseudo-labelling were used to increase the amount and diversity of labelled data. The best model network achieved a mean Intersection over Union score of 0.832. The model trained on the augmented and pseudo-labelled data achieved a mean Intersection over Union score of 0.712 on independent data. This result suggests the potential for using data augmentation and pseudo-labelling techniques to create more robust models. Automating invasive species mapping through deep learning is a significant step towards more efficient assessment of habitat conditions.

UAVs are currently impractical for mapping extensive habitats such as uplands, as they have limited battery life, require visual lines of sight and have specified maximum flight altitudes (120 m in Ireland). High-resolution (2 m) satellite imagery can overcome these issues. Chapter 4 investigates the impact of varying spatial resolution on classification accuracy. Moreover, a fuzzy classification technique based on random forest was implemented, as upland habitats are typically heterogeneous, complex mosaics. The classifications from the 2-m-resolution images were generally more accurate than the 10-m-resolution images (80.34% vs 73.55%, respectively). Fuzzy classified maps deliver more insights into habitat composition. Generated habitat probabilities estimate the spatial confidence of classification over an area. In this way, more targeted assessments of high uncertainty areas can be recommended.

Overall, the combined use of high-resolution remote sensing data and machine learning techniques offers significant potential for accurate systematic habitat mapping in Ireland and beyond. The detailed maps produced here provide critical information to inform the monitoring, reporting and verifying of habitats.

1 Introduction

1.1 Background

The 8th Environment Action Programme of the EU states that its priority objectives are to protect, preserve and restore biodiversity and to enhance the EU's natural capital (EU, 2022). Natural capital includes ecosystems that provide vital services such as climate regulation and biodiversity (Millennium Ecosystem Assessment, 2003). The EU's Biodiversity Strategy for 2030 aims to maintain and enhance ecosystem services in Europe (EC, 2020). Nature legislation has been implemented through legally binding directives (e.g. the Habitats Directive (HD; Council Directive 92/43/EEC)) as well as the EU Biodiversity Strategy (Maes *et al*., 2020). Despite this, many ecosystems are degraded and have lost capacity to deliver their services (EC, 2011). The 2020 *State of the Environment Report* found that Ireland's environment is predominantly poor or very poor and that 85% of EU protected habitats have an unfavourable status (EPA, 2020). Under Article 17 of the HD, the National Parks and Wildlife Service (NPWS) conducts an assessment of Annex I habitats throughout Ireland every 6 years; the latest assessment was published in 2019 (NPWS, 2019). However, these assessments can be based only on available data. Habitat mapping, assessment and monitoring surveys provide data to support these HD assessments as well as helping to meet the reporting requirements of the Water Framework Directive (Directive 2000/60/EC). Much of the survey work conducted for Annex I habitat mapping and monitoring is carried out by qualified ecologists during field visits (e.g. Martin *et al*., 2018; Perrin *et al*., 2014a). Botanical field surveys can occur in remote and relatively inaccessible environments and can be demanding and time-consuming. It is therefore challenging to regularly survey an adequate sample of Ireland's Annex I habitats. Rapid advances in unoccupied aerial vehicle (UAV) and computer machine learning technologies offer a complementary and supportive approach to mapping, assessing and monitoring habitats throughout Ireland. These innovative technologies may enable the cost-effective implementation of the mapping, assessment and monitoring work undertaken by ecologists using standard classification schema (Fossitt, Irish Vegetation Classification).

1.2 Project Objectives

- To develop the methodologies and analytical approaches to determine if UAVs, satellite imagery and machine learning can effectively map, assess and monitor a range of Annex I habitats.
- To produce ecologically classified maps using the random forest (RF) machine learning algorithm to facilitate reproducible mapping, assessments and monitoring of key Annex I habitats, over time, with high-resolution UAV data.
- To utilise satellite data to enable the mapping, assessment and monitoring of habitats on a broader regional scale.

2 Assessing the Effectiveness of Unoccupied Aerial Vehicle Data for Accurate Mapping in Coastal Dune Habitats

2.1 Introduction

The European coastline is frequently bordered by coastal dunes (Doody, 2013). They form a spatially narrow yet complex mosaic of dynamic habitats parallel to the shoreline (Psuty, 2007). Coastal dunes are formed as sand-sized sediment is transported inland by onshore winds and trapped by vegetation. They are characterised by high flora diversity (Doody, 2013). They also provide important ecosystem services, including coastal defences, habitats for wildlife and carbon sequestration (Parker *et al*., 2016), and can be a source of sand to replenish beaches that have experienced erosion (Barbier *et al*., 2011).

In the EU, dune habitats are included in Annex I of Council Directive 92/43/EEC on the conservation of natural habitats and wild fauna and flora (the HD). The HD is an EU legal framework that aims to protect a wide range of rare, endangered and vulnerable habitats (those listed in Annex I) by requiring each Member State to monitor these habitats within its territory and report its findings to the European Commission on a 6-yearly basis (EU, 1992).

Within Ireland there are eight Annex I coastal dune habitats, and two other Annex I habitats are also often found in association with dune systems (see Table 2.1). These habitats are vulnerable to natural hazards, including climate change, and to human pressures, which can lead to habitat degradation and biodiversity loss (Delaney *et al*., 2013). In 2019, these 10 Annex I coastal habitats were assessed as having an unfavourable-inadequate or unfavourable-bad status (NPWS, 2019). This assessment result has remained largely unchanged in the past three HD reporting cycles in 2008, 2013 and 2019 (NPWS, 2008, 2013a, 2019). Therefore, assessment and monitoring of these vulnerable habitats is critical to identify key conservation issues, measure threat status, and develop and evaluate management and restoration programmes (EC, 2022).

Habitat mapping is a fundamental task for generating the data required for monitoring habitats under the HD. Most habitat mapping is conducted by ecologists in the field. While these surveys can provide detailed habitat information, manual methods alone can limit the size and temporal scope of the survey, primarily because of cost (Mack *et al*., 1997). Remote sensing offers an advantage over the traditional field-based mapping techniques, as it may capture data more frequently and across larger areas (Jensen, 2014). However, monitoring coastal dune habitats with freely available medium spatial resolution (> 10 m) satellite imagery is difficult, e.g. when mapping very narrow areas of patchy mobile dunes and identifying small-sized disturbed areas within the habitats caused by human tracks and coastal erosion (Ettritch *et al*., 2018; Marzialetti *et al*., 2019). For this reason, the classification output from this imagery can result in inaccurate spatial and botanical information about dune status, as higher resolution data are needed to capture this detailed information.

Recent advancements in remote sensing platforms and sensors, such as the development of UAVs, have enabled high-resolution mapping of habitats and vegetation (Gonçalves *et al*., 2016; Kattenborn *et al*., 2019a; Michez *et al*., 2016; Müllerová *et al*., 2021; van Iersel *et al*., 2018). UAVs can acquire centimetre-level spatial resolution imagery. They are also characterised by high levels of efficiency and flexibility in image acquisition of small (< 20 ha) areas because they generally have low operational costs, and the high temporal resolution of the images is suitable for complex environments (Eisenbeiss, 2009; Manfreda *et al*., 2019; Pajares, 2015; Yan *et al*., 2009).

In recent years, several UAV-based studies have implemented machine learning algorithms for image classification and habitat mapping because of the

excellent classification results and fast processing time (Han *et al*., 2019; Lu and He, 2017; van Iersel *et al*., 2018). RF is one of the most widely used of these algorithms (Belgiu and Drăgut, 2016; Pal, 2005). RF (Breiman, 2001) is a non-parametric, supervised machine learning algorithm that uses a collection of decision trees to solve a classification task. Each tree in an RF model generates a prediction, and the final prediction is determined by majority voting (Fawagreh *et al*., 2014). This allows large volumes of highly correlated variables to be ingested and processed without data redundancy affecting the model performance. The efficiency of RF in processing large datasets makes it appropriate for multitemporal analyses of UAV images. RF was selected as the preferred classification method owing to the reported high level of accuracy in vegetation mapping using various remote sensing data (Amani *et al*., 2017; Barrett *et al*., 2016; Raab *et al*., 2018; Villoslada *et al*., 2020).

In habitat mapping, image acquisition timing is an important factor, since plant communities within a habitat may be more distinct from the surrounding vegetation at a particular time of the growing season (Marcinkowska-Ochtyra *et al*., 2019). The use of multitemporal images in habitat mapping can increase the classification accuracy compared with maps produced from images collected at a single time period (Marcinkowska-Ochtyra *et al*., 2019; Schmidt *et al*., 2014; van Iersel *et al*., 2018). Several studies have used multitemporal UAV images in mapping of habitats and vegetation (Belcore *et al*., 2021; Michez *et al*., 2016; van Iersel *et al*., 2018); however, very few studies have been carried out on coastal dune habitats (Taddia *et al*., 2019). Given the complexity of coastal dune habitats, there is an opportunity to utilise high temporal resolution UAV data to determine the optimal time period to facilitate better discrimination between these habitats.

In this study, we aimed to assess the effectiveness of UAV remote sensing for mapping complex coastal dune habitat types. More specifically, we aimed to (1) determine how classification accuracy varies when using multitemporal images acquired throughout the growing season, (2) identify how the inclusion of UAV-derived topography affects the classification accuracy and (3) identify the optimum time to differentiate coastal dune habitats. These aims were achieved by integrating high-resolution UAV imagery with data from field surveys, and different habitat types were classified using the RF algorithm.

2.2 Materials and Methods

2.2.1 Study site description

The study area was a 37-ha coastal dune site located on the Magharees Peninsula (52°17′22″N, 10°1′31.00″W), County Kerry, Ireland. The Magharees Peninsula is a sand spit, about 5 km long, with an extensive area of fixed dunes containing several dune slacks (Delaney *et al*., 2013; NPWS, 2013b). This dune site is designated as part of the large Tralee Bay and Magharees Peninsula, West to Cloghane Special Area of Conservation (SAC) (code 002070; the area is approximately 11,627 ha) site of the Natura 2000 network (Figure 2.1) (NPWS, 2018). Six HD Annex I dune habitats are present within the study area: 1210, 2110, 2120, 2130, 2170 and 2190 (Table 2.1). One of these, 2130 (grey dunes), is a priority habitat that requires particular protection as it is in danger of disappearance within the EU territory (NPWS, 2019). Other common habitats present within the study area, which are not listed in Annex I of the HD, were categorised based on the Fossitt classification scheme (see Table 2.1). The Fossitt scheme is a standard guide for identifying and describing habitats in Ireland (Fossitt, 2000). It is important to determine the locations and sizes of these habitats, as some of them represent disturbance to the dune system (e.g. exposed sand, recolonising bare ground and the presence of non-native species).

2.2.2 General workflow

A replicable workflow using multitemporal high-resolution UAV imagery and field data acquired during the vegetation-growing season was used to characterise different habitat types. Several raster layers were generated from the UAV-derived photogrammetric products, including an image mosaic and a digital surface model (DSM). These layers, together with the field data as reference samples, were used to train the RF-based classification of each target habitat type. The trained model was then applied to the image mosaic to produce a spatially continuous map of habitats within the study area. These processes are

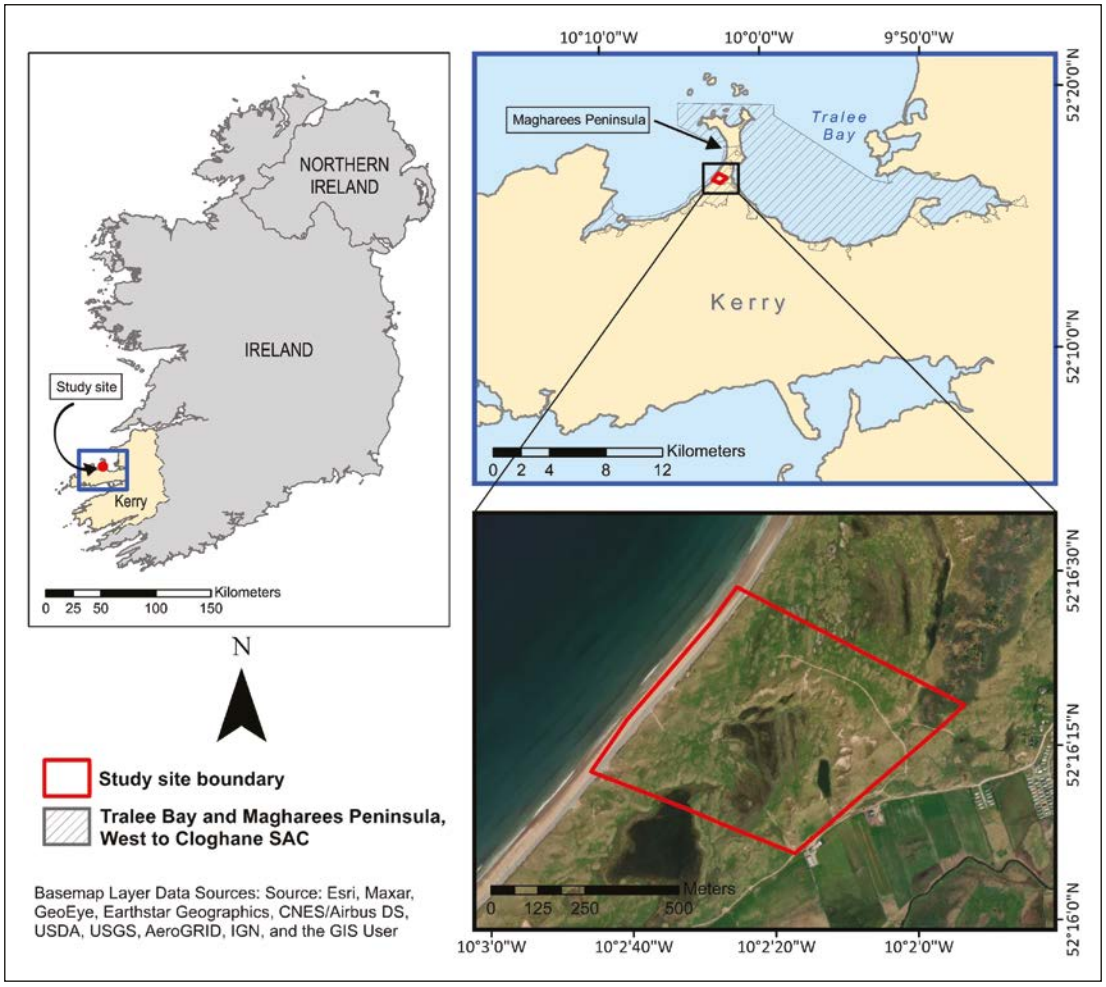

Figure 2.1. Inset map showing the location of the study site in County Kerry, Ireland (left); the boundary of the Tralee Bay and Magharees Peninsula, West to Cloghane SAC (upper right); and the boundary of the study site (lower right). Reproduced from Cruz *et al*. (2023a); licensed under CC BY 4.0 (https://creativecommons.org/licenses/by/4.0/).

illustrated in a flow diagram (Figure 2.2). Each step in the diagram is discussed in detail in the following subsections.

Step 1: field surveys

Image acquisition. Field campaigns were conducted during the growing season in 2020: May (early), July (mid) and October (late), under suitable flying conditions (i.e. clear sky with low wind speed). High-resolution imagery (6 cm) was acquired using a DJI Phantom 4 Multispectral UAV sensor (https://www.dji.com/p4-multispectral/specs) with five spectral bands: blue, green, red, red edge and near-infrared. Five ground control points (GCPs) were evenly distributed throughout the study area to spatially reference the UAV-acquired images, following recommendations by Assmann *et al*. (2019) and Mesas-Carrascosa *et al*. (2015). The coordinates at the centre of each GCP were measured and recorded using an Emlid Reach RS+ Global Navigation Satellite System (GNSS) device (https://emlid.com/reachrs/) through the real-time kinematic technique, with the observation time set to 2 minutes. This technique works by using a nearby base station or reference network with known positions to provide real-time corrections to GNSS measurements, allowing them to achieve centimetre-level positional accuracy. All three flights were operated with a side and forward overlap of 75% and 80%, respectively, and a flight altitude of 60 m. Invariant panels were also placed within the study area and imaged during the flights. These were subsequently used for radiometric calibration. These panels were used to normalise for variations in atmosphere and solar illumination across the three image acquisition dates.

Table 2.1. Habitat types found within Irish dune systems and corresponding habitat codes

Habitat type and code	Present within the study area
Annex I	
1210 – Annual vegetation of drift lines[a]	✓
1220 – Perennial vegetation of stony banks[a]	×
2110 – Embryonic shifting dunes	✓
2120 – Shifting dunes along the shoreline with *Ammophila arenaria* (white dunes)	✓
2130 – Fixed coastal dunes with herbaceous vegetation (grey dunes)[b]	✓
2140 – Decalcified fixed dunes with *Empetrum nigrum*[b]	×
2150 – Atlantic decalcified fixed dunes (*Calluno-Ulicetea*)[b]	×
2170 – Dunes with *Salix repens* ssp. *argentea* (*Salicion arenariea*)	✓
21A0 – Machair[b]	×
2190 – Humid dune slacks	✓
Fossitt	
CD4 – Dune scrub and woodland	✓
ED1 – Exposed sand	✓
ED3 – Recolonising bare ground	✓
LS1 – Shingle and gravel shores	✓
LS2 – Sandy shores	✓

[a]Habitats associated with dune systems.

[b]Priority habitats.

Source: EC (2013) and Fossitt (2000).

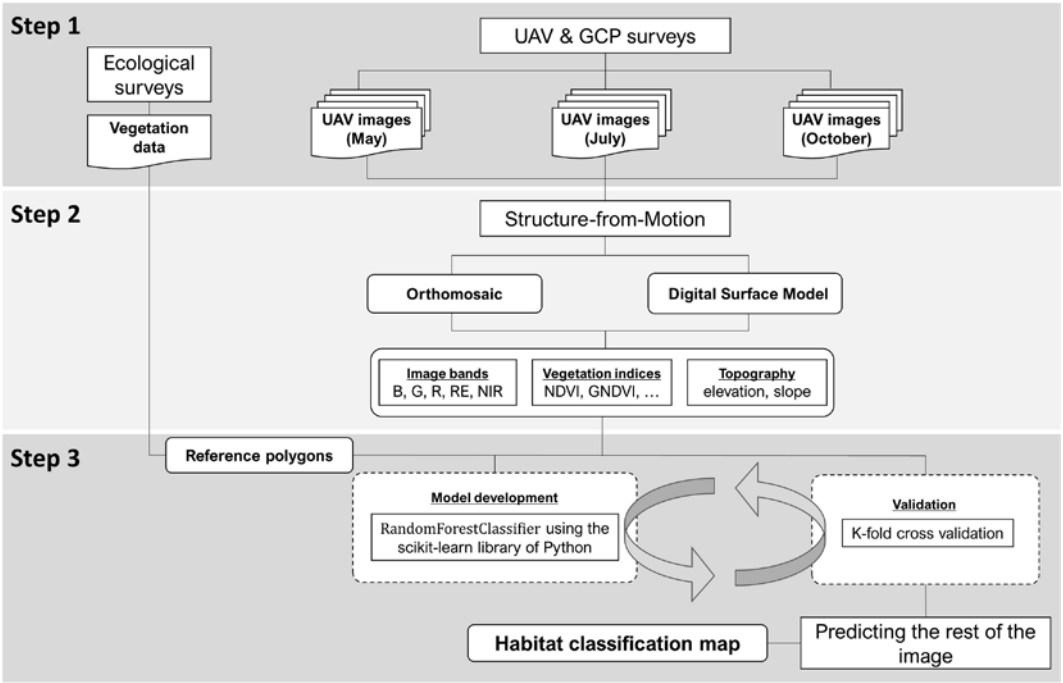

Figure 2.2. Methodology workflow in using multitemporal high-resolution UAV imagery to characterise different habitat types. B, blue band; G, green band; GNDVI, green normalised difference vegetation index; NDVI, normalised difference vegetation index; NIR, near-infrared band; R, red band; RE, red edge band. Reproduced from Cruz *et al*. (2023a); licensed under CC BY 4.0 (https://creativecommons.org/licenses/by/4.0/).

Reference data collection. Extensive ecological field surveys were carried out by experienced ecologists to collect ground truth data (i.e. reference points representing the actual location of a habitat type) to train the model and validate the results. The ecologists used the GNSS device to record the coordinates of the data points. Each point was located at the centre of an area of relatively homogeneous habitat cover. The radius of this area around each point, typically 1–10 m, was recorded by the ecologists based on their expert opinion of its spatial extent (Figure 2.3a,b). Each point also included a record of habitat codes based on Annex I and Fossitt classification systems and was photographed in the north-view direction; a consistent aspect assisted ecologists if a point needed to be located again on the ground.

Reference points were first collected in the week following the first UAV survey to prevent disturbance to the site. Further site visits coordinated with the second and third UAV surveys facilitated the addition of more points and the assessment of any significant vegetation changes from the previous survey. After verifying that no change in habitat types occurred within the growing season, which would be expected within Irish dune systems, the point data collected from all field campaigns were combined into a single set ($n = 418$) and used to classify all acquired UAV images. The point data were converted into polygons using the radius recorded in the field (Figure 2.3b and c). Both the remote sensing analyst and the ecologists visually inspected the collected field data (i.e. polygons) on the screen to ensure that there was no overlap and to verify that they were aligned with the correct habitats as seen on the UAV image. Owing to time constraints related to field-based data collection, 198 additional reference polygons were labelled on screen by the ecologists and remote sensing analyst to supplement those classes that had an insufficient number of field-collected samples.

Step 2: image pre-processing

Structure from motion. A DSM and an orthomosaic were created for each set of image acquisition using the structure-from-motion-based processing chain in Pix4DMapper (v. 4.3.33). The processing involves keypoint (i.e. distinct features in an image, usually of high contrast) extraction, keypoint matching between images, camera model correction, geolocation based on the global positioning system (GPS) flight

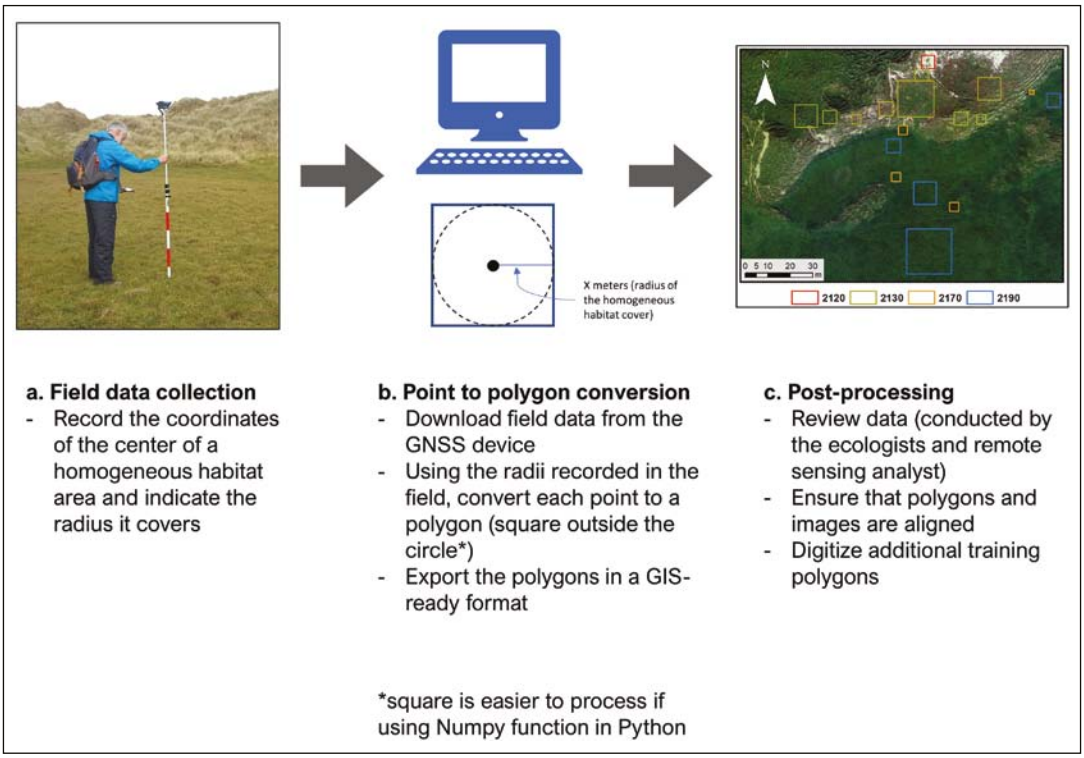

Figure 2.3. Diagram of the reference data collection and processing steps. GIS, geographic information system. Reproduced from Cruz *et al.* (2023a); licensed under CC BY 4.0 (https://creativecommons.org/licenses/by/4.0/).

trajectories and the GCPs deployed on-site, and dense point cloud generation. The point cloud was used to derive the DSM.

Feature extraction. Feature extraction is a technique whereby raw raster images are used to generate new features or variables that provide more information to help discriminate different classes. Sixteen raster layers were generated from the photogrammetric products for each field campaign. These layers were grouped into two datasets comprising spectral and topographic variables (Table 2.2). The spectral variables were derived from the orthomosaic and consist of five radiometrically calibrated surface reflectance bands, the first principal component analysis (PCA) band and eight vegetation indices. In contrast, topographic variables such as elevation and slope were derived from the DSM.

The reference data polygons (various sizes) were used to extract pixels from each variable in Table 2.2. This study used a 17-pixel non-overlapping sliding kernel (equivalent to 1 m × 1 m on the ground) to divide each reference polygon into several equal-sized sub-polygons. The mean of the pixel values within each sub-polygon was calculated for every raster layer. The resulting mean pixel values and the corresponding polygon labels constituted the final reference dataset. This approach of using a sliding averaging kernel reduces issues around reflectance-based adjacency effects and erroneous values due to geometric misalignment when using individual pixel values.

Step 3: modelling and validation

Several classification models were generated using the supervised RF algorithm to investigate the effect of vegetation phenology and topographic information on the classification accuracy. The input for each model varied depending on combinations of variables (spectral variables only, RF_S; spectral and topographic variables, RF_{ST}) and the number of field campaigns. In total, there were 14 data combinations subjected to the RF algorithm (Table 2.3). In this study, the RF algorithm was implemented in Python 3.7 using the Scikit-learn library (Pedregosa *et al*., 2011). The parameters used for each model were $M\_var = \sqrt{M}$ for the number of variables at each split, where M is the total number of variables, and $N\_tree = 500$ trees (Gislason *et al*., 2006).

The RF technique was applied to each dataset to classify the four coastal dune Annex I habitats – 2120, 2130, 2170 and 2190 – and five Fossitt habitats. The other two Annex I habitats (1210 and 2110) were not included in the classification, as they occur in small, isolated patches and only 13 reference points were collected, and this would result in a severely imbalanced training set and, therefore, a biased model (Khoshgoftaar *et al*., 2007). To evaluate the model performance, the accuracy was estimated using k-fold cross-validation. This method estimates model performance by partitioning the data into k subsets, training the model k times using $k-1$ subsets for training and the remaining subset for validation each time, and averaging the performance metrics across all k trials (Berrar, 2019). Five folds were used here, i.e. the model training and validation process was repeated five times. The average and standard error values were calculated from each k-fold model. The final model to predict the class labels of the entire study area used all the training data. The model performance for each class was also evaluated

Table 2.2. List of variables used in the study

Spectral variables	
Blue band (B)	Modified soil-adjusted vegetation index 2 (MSAVI2)
Green band (G)	Normalised difference red edge index (NDRE)
Red band (R)	Normalised difference vegetation index (NDVI)
Red edge band (RE)	Normalised difference water index (NDWI)
Near-infrared band (NIR)	Simple ratio index (SR)
Enhanced vegetation index (EVI)	Principal component 1 (PC1)
Enhanced vegetation index 2 (EVI2)	
Green normalised difference vegetation index (GNDVI)	
Topographic variables	
Elevation	Slope

Table 2.3. Datasets used in training models

	Field campaign			Variable	
Dataset	**May (M)**	**July (J)**	**October (O)**	**Spectral only (RF_S)**	**Spectral and topographic (RF_{ST})**
M_RF_S	✓			✓	
J_RF_S		✓		✓	
O_RF_S			✓	✓	
MJ_RF_S	✓	✓		✓	
JO_RF_S		✓	✓	✓	
MO_RF_S	✓		✓	✓	
MJO_RF_S	✓	✓	✓	✓	
M_RF_{ST}	✓				✓
J_RF_{ST}		✓			✓
O_RF_{ST}			✓		✓
MJ_RF_{ST}	✓	✓			✓
JO_RF_{ST}		✓	✓		✓
MO_RF_{ST}	✓		✓		✓
MJO_RF_{ST}	✓	✓	✓		✓

M, J, O, field campaign month.

using confusion matrices and estimating derived evaluation metrics known as precision, recall and F1-score (Muller and Guido, 2017). Precision is the fraction of correct predictions for each class, and recall is the fraction of true labels that were correctly classified. F1-score is a single value that reports the overall accuracy, taking both recall and precision into consideration. It is the harmonic mean (weighted) of recall and precision values.

2.2.3 Temporal analysis of coastal dune habitats

Two tests were prepared to determine which time period is optimal, in terms of classification accuracy, for image acquisition for this coastal dune habitat mapping. The first test (Test 1) was applied to the M_RF_{ST}, J_RF_{ST} and O_RF_{ST} training models. For each of these models, data from the image dates that were not used in the training were combined to generate the test dataset. So the M_RF_{ST} model was evaluated with the combined July and October data. The generated test dataset was randomly resampled 1000 times to create 1000 different test datasets. In other words, the M_RF_{ST} model was evaluated using 1000 test datasets, which generated 1000 accuracy values. Next, the J_RF_{ST} model was evaluated using the combination of the May and October data. Finally, the O_RF_{ST} model was evaluated using the combined May and July data. Therefore, each of these models had 1000 accuracy values. For the second test (Test 2), each model was reproduced but this time with only 80% of the data (sub-polygons). The remaining 20% from each of the three campaigns were pooled and used to generate the test dataset. In this way, each model was assessed using the same test dataset. Similarly to Test 1, the test dataset was randomly resampled 1000 times to create 1000 different test datasets. These 1000 test datasets were used to evaluate each Test 2 model. The mean and standard error were computed for each of the models from Test 1 and Test 2.

2.3 Results

2.3.1 Acquisitions and variables used in the classification

The results obtained in *k*-fold validation are presented in Table 2.4. The mean accuracy values of all models were above 80%, with MJO_RF_{ST} showing the best performance (94.26%) and O_RF_S the worst (84.09%). The computed standard error showed that mean accuracy based on $k=5$ had low variability across the data. The models that used spectral variables only (RF_S) achieved a higher level of accuracy when the data from two or more field campaigns were combined. This pattern was also seen in the results from the

Table 2.4. *k* = 5 cross-validation mean accuracy and standard error values for models obtained for each dataset

	Accuracy based on five-fold cross-validation method			Accuracy based on five-fold cross-validation method	
Dataset	Mean	SE	Dataset	Mean	SE
M_RF_S	84.58	0.58	M_RF_{ST}	91.35	0.45
J_RF_S	84.81	0.42	J_RF_{ST}	92.57	0.52
O_RF_S	84.09	1.22	O_RF_{ST}	91.68	1.06
MJ_RF_S	88.48	1.17	MJ_RF_{ST}	93.49	0.52
MO_RF_S	90.85	0.48	MO_RF_{ST}	93.93	0.33
JO_RF_S	89.76	1.14	JO_RF_{ST}	92.54	1.13
MJO_RF_S	92.37	0.26	MJO_RF_{ST}	94.26	0.44

The datasets considered are described in Table 2.3. Values are percentages (%).
SE, standard error.

models using both spectral and topographic variables (RF_{ST}), with just one exception: JO_RF_{ST}, which had a slightly lower accuracy (92.54%) than J_RF_{ST} (92.57%). All the models that used both the spectral and topographic variables (RF_{ST}) had a mean accuracy that exceeded 90%, with the highest level of accuracy acquired, for MJO_RF_{ST}, being 94.26% and the lowest, for M_RF_{ST}, being 91.35%. When comparing the RF_{ST} models with the corresponding RF_S models, the addition of topographic data always improved mean accuracy. The accuracy increase ranged from 2% to 8%, depending on the number of image sets considered in the model. The increase in accuracy for single image models was greater (M, +6.77%; J, +7.76%; O, +7.59%) than the multiple image models (MJ, +5.01%; MO, +3.08%; JO, +2.78%; MJO, +1.89%). In other words, the more image sets considered in the model, the smaller the benefit of including the topographic variables.

The model performance for each habitat, as presented by the confusion matrices and recall, precision and F1-score values, differed between datasets. Overall, all models were able to predict most of the four Annex I dune habitats correctly (F1-score > 0.75). Misclassifications among Annex I habitats primarily occurred between 2170 and 2190. One possible reason for the misclassification is that 2170 and 2190 can often contain similar plant communities, and they are even categorised as a single habitat type in the Irish Fossitt classification system (Fossitt, 2000). Habitat 2120 was also misclassified as ED1 and ED3, probably owing to large areas of exposed sand in all three habitats. When topographic variables are included in the models, the F1-scores increase for most of the habitat types, with some classes reaching F1-scores > 0.90. In general, both marine littoral sediments, LS1 and LS2, showed the highest F1-score values at ≥ 0.96. In contrast, degraded versions of Annex I habitats exposed sand (ED1) and recolonising bare ground (ED3) had the lowest F1-score values for all the models.

During the growing season, different months were identified as optimal for discriminating the habitats. Both 2120 and 2170 could be best differentiated in July, as the F1-scores of 0.91 and 0.90, respectively, were slightly higher than the F1-scores for May and October. In contrast, October was the best time to identify 2130. Finally, 2190 achieved the same F1-score (0.92) across all acquisition dates (Table 2.5). These results show that there is no optimum acquisition period that can be used to discriminate all Annex I habitat types.

2.3.2 Temporal analysis of dune habitats

The RF-based models trained with data from the same site from May, July or October (Test 1) each achieved mean accuracies of above 70% (Table 2.6). However, the accuracy of the model trained on the July data was higher than that of the models trained on the May or October data. The results of Test 2 followed the same trend as those of Test 1. The J_RF_{ST} model had the highest performance, followed by O_RF_{ST} and M_RF_{ST} (Table 2.6). These results suggest that the best month for image acquisition was found to be the middle of the growing season for coastal dune vegetation.

Table 2.5. Per-class precision (P) and recall (R) values, and F1-scores (F1) obtained for models from each dataset

	May			July			October			May–July			May–Oct			July–Oct			May–July–Oct		
Habitat	R	P	F1	R	P	F1	R	P	F1	R	P	F1	R	P	F1	R	P	F1	R	P	F1
Spectral variables only (RF_S)																					
2120	0.88	0.77	0.82	0.84	0.77	0.80	0.90	0.80	0.85	0.87	0.80	0.84	0.95	0.84	0.89	0.94	0.82	0.87	0.96	0.85	0.90
2130	0.78	0.77	0.78	0.81	0.78	0.80	0.67	0.72	0.69	0.88	0.82	0.85	0.88	0.84	0.86	0.85	0.82	0.83	0.90	0.86	0.88
2170	0.79	0.78	0.79	0.77	0.80	0.79	0.79	0.75	0.76	0.87	0.85	0.86	0.90	0.87	0.88	0.87	0.87	0.87	0.92	0.90	0.91
2190	0.84	0.80	0.82	0.77	0.77	0.77	0.79	0.75	0.77	0.85	0.89	0.87	0.88	0.91	0.90	0.84	0.84	0.84	0.88	0.93	0.91
CD4	0.88	0.92	0.90	0.95	0.94	0.94	0.97	0.97	0.97	0.93	0.95	0.94	0.97	0.98	0.97	0.98	0.98	0.98	0.98	0.98	0.98
ED1	0.64	0.95	0.76	0.63	0.86	0.73	0.51	0.79	0.62	0.70	0.95	0.81	0.64	0.84	0.73	0.46	0.93	0.61	0.70	0.95	0.81
ED3	0.38	0.60	0.46	0.53	0.66	0.59	0.57	0.82	0.67	0.50	0.65	0.56	0.54	0.82	0.65	0.69	0.89	0.78	0.64	0.89	0.74
LS1	0.99	0.97	0.98	0.97	0.99	0.98	0.96	0.98	0.97	0.99	0.99	0.99	1.00	0.98	0.99	0.99	0.99	0.99	1.00	0.99	0.99
LS2	0.97	0.97	0.97	0.98	0.95	0.96	0.99	0.94	0.96	0.99	0.96	0.97	0.99	0.98	0.98	0.99	0.96	0.98	0.99	0.97	0.98
Spectral and topographic variables (RF_{ST})																					
2120	0.97	0.84	0.90	0.96	0.86	0.91	0.95	0.82	0.88	0.98	0.86	0.92	0.98	0.87	0.92	0.96	0.83	0.89	0.98	0.87	0.92
2130	0.88	0.85	0.87	0.90	0.87	0.88	0.90	0.89	0.90	0.93	0.87	0.90	0.92	0.90	0.91	0.90	0.88	0.89	0.93	0.88	0.90
2170	0.89	0.86	0.88	0.90	0.91	0.90	0.87	0.87	0.87	0.92	0.92	0.92	0.93	0.92	0.93	0.91	0.91	0.91	0.93	0.94	0.94
2190	0.91	0.92	0.92	0.92	0.92	0.92	0.92	0.92	0.92	0.92	0.96	0.94	0.93	0.94	0.94	0.92	0.92	0.92	0.93	0.94	0.94
CD4	0.93	0.95	0.94	0.96	0.96	0.96	0.97	0.98	0.98	0.95	0.96	0.96	0.98	0.98	0.98	0.98	0.98	0.98	0.98	0.98	0.98
ED1	0.64	0.95	0.76	0.63	0.96	0.76	0.63	0.86	0.73	0.70	0.97	0.81	0.64	0.98	0.78	0.51	0.91	0.65	0.70	0.97	0.81
ED3	0.64	0.99	0.78	0.72	0.91	0.80	0.67	0.93	0.78	0.68	0.95	0.79	0.75	0.98	0.85	0.71	0.96	0.82	0.72	0.98	0.83
LS1	0.99	0.97	0.98	0.99	0.99	0.99	0.97	0.98	0.98	0.99	1.00	0.99	0.99	0.98	0.98	0.99	0.99	0.99	0.99	0.99	0.99
LS2	0.98	0.98	0.98	1.00	0.98	0.99	0.99	0.97	0.98	1.00	0.98	0.99	0.99	0.98	0.98	1.00	0.98	0.99	0.99	0.98	0.99

The habitat codes are described in Table 2.1.

Table 2.6. Summary table showing the mean and standard error values for each model evaluated on the Test 1 and Test 2 datasets

	Test 1		Test 2	
Model	**Mean**	**SE**	**Mean**	**SE**
M_RF_{ST}	0.742	0.00026	0.788	0.00026
J_RF_{ST}	0.809	0.00021	0.860	0.00023
$O\_R_{FS}T$	0.747	0.00024	0.829	0.00025

SE, standard error.

The mean accuracies obtained from all models evaluated using Test 1 data ranged from 0.74 to 0.81, which was slightly lower than the accuracy range when Test 2 was used (from 0.78 to 0.86) (Table 2.6). This result could be due to Test 2 models being tested with a dataset that included samples from the same month as the data used to train the model.

2.3.3 Distribution and extent of dune habitat types

The computed area of the different habitat types, as classified by RF models based on three single image acquisitions, is shown in Figure 2.4. The study site was dominated by Annex I habitat 2130, which covers almost 60% of the total area. This was followed by the 2170 and 2190 habitats, which covered about 12–15% of the area. Habitat 2120 covered around 5–6% of the area. All Fossitt habitats (i.e. CD4, ED1, ED3, LS1 and LS2) corresponded to the smallest area proportions within the study area and accounted for less than 10% of the total area. Proportions of habitats did not differ markedly between models.

The spatial classification output for July is shown in Figure 2.4. Habitat 2130 (grey dunes) occupied more than half of the study area. Habitat 2190 (dune slacks) was mostly surrounded by habitat 2170 (dunes with *Salix repens*). Habitat 2120 (dunes with *Ammophila arenaria*) was generally located parallel to the shore, alongside LS1 and LS2 habitats. Scrub composed of the invasive species sea buckthorn (*Hippophae rhamnoides*) was classified as habitat CD4 on the east side of the study site. The presence of human disturbance (beach access paths) can also be observed in the coastal dune environment.

2.4 Discussion

This study focused on automatic classification of coastal dune habitats using UAV imagery and the RF algorithm. It was designed to assess the impact that temporally acquired UAV-derived spectral and topographic data has on classification accuracy. The results show that the inclusion of topographic information (elevation and slope) contributes to

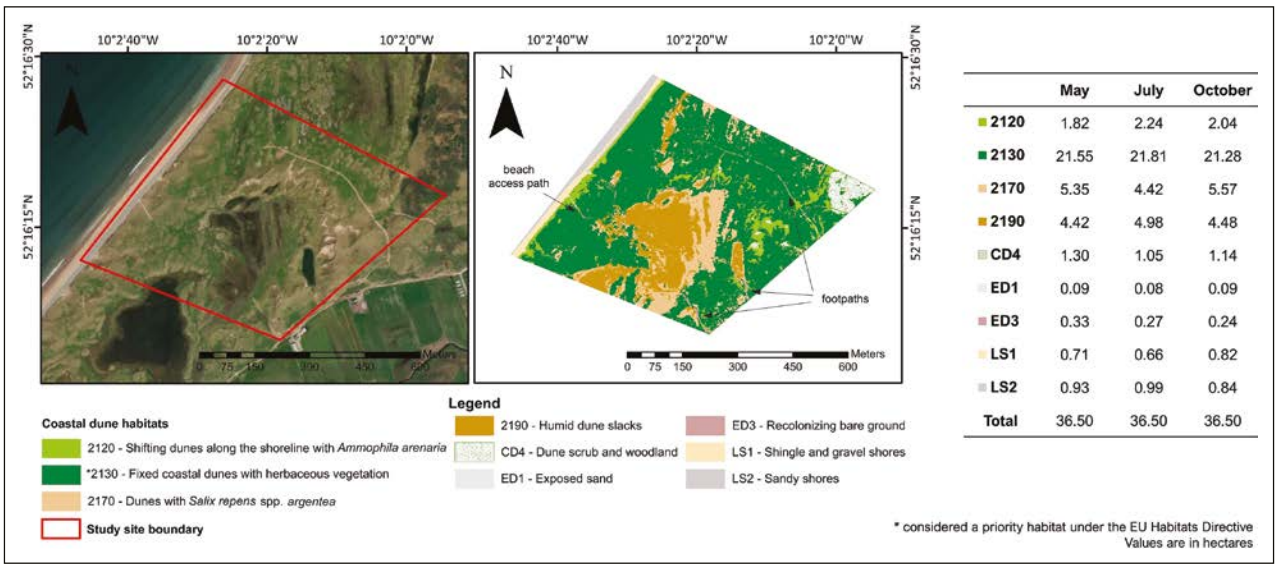

	May	July	October
2120	1.82	2.24	2.04
2130	21.55	21.81	21.28
2170	5.35	4.42	5.57
2190	4.42	4.98	4.48
CD4	1.30	1.05	1.14
ED1	0.09	0.08	0.09
ED3	0.33	0.27	0.24
LS1	0.71	0.66	0.82
LS2	0.93	0.99	0.84
Total	36.50	36.50	36.50

Figure 2.4. Supervised RF classification map of coastal dune habitats in the Magharees, County Kerry. Area in hectares calculated for each habitat type classified using UAV images acquired at three time points within the vegetation-growing season. Reproduced from Cruz *et al.* (2023a); licensed under CC BY 4.0 (https://creativecommons.org/licenses/by/4.0/).

increased accuracy for all models (Table 2.4). The reason for this could be that the addition of topographic data improves the classification of coastal dune habitats by discriminating between Annex I habitats 2170 and 2190. Habitat 2190 is predominantly located at the lowest elevation at the study site and on flat terrain. Habitat 2170 is located in areas at slightly higher elevations. The value of using topographic information for mapping vegetation and other habitats in improving classification accuracy has also been noted in previous studies using other remote sensing data (e.g. Marcinkowska-Ochtyra *et al*., 2019; Scholefield *et al*., 2019; Yousefi Lalimi *et al*., 2017). This result suggests good potential for using UAVs for habitat mapping, as topographic information can be obtained during the photogrammetric processing of the images with a high level (±0.75 m) of vertical accuracy.

The highest level of accuracy was achieved when both spectral and topographic variables from the three time periods were combined in the model. In the RF_S model category (i.e. models using spectral variables only), the accuracy was higher when data from two or more acquisition periods were used (e.g. M_RF_S: 84.58% vs MJO_RF_S: 92.37%). In contrast, the RF_{ST} models (i.e. models using both spectral and topographic variables) only showed a slight increase in accuracy when more temporal data were used (e.g. M_RF_{ST}: 91.35% vs MJO_RF_{ST}: 94.26%). In other words, a single acquisition of spectral and topographic data is deemed to be sufficient to classify coastal dune habitats and has a similar level of accuracy to models using data from multiple periods. From a practical point of view, the fusion of spectral and topographic data acquired from a single period within the growing season could be used instead of using multitemporal data, as it gives accuracies of >91%.

Considering the time and operational costs associated with acquiring and processing UAV data, it is important to identify the optimal time period for data collection. This study shows that July is the optimum time period for data acquisition at this site. However, both May and October also yielded high levels of accuracy, suggesting that an acquisition at any time in these 6 months will yield good results. These findings have an important practical application to the time period for future data collection over coastal dune sites. Given the potential impact of climate change on this environment, the optimal period may change over time; however, this can be reassessed with the methodology used in this study. The use of UAV surveys to acquire centimetre-resolution images is currently limited to small areas – typically a few square kilometres – owing to factors such as the flight speed, legally required proximity of operators to UAVs and battery life. This limitation might make UAV surveys impractical for operational use in regular habitats or vegetation mapping at regional or national scales. While UAV-based mapping is often conducted at a local scale, it could be extended to mapping at a larger scale when combined with satellite imagery (Kattenborn *et al*., 2019b). Nevertheless, UAV technology is continuously developing, and its range is increasing. The emergence of new remote sensing platforms could provide novel avenues for addressing the current challenge of UAVs in terms of spatial areal coverage without compromising the spatial image resolution.

Two habitat types covering small areas were excluded in this analysis, as there was an insufficient number of reference samples collected in the field. Since these habitat types are small and occur in patches, a relatively intensive survey would be needed to collect sufficient samples for the models. The development of methods related to how to deal with these proportionally small habitats is ongoing. With increased technological advances, both for computer processing power and for remote sensing platforms, there are opportunities to explore the application of deep learning algorithms in other areas. Moreover, the calculation of different texture features from the imagery could be used to allow the representation of vegetation structure within habitats (Wood *et al*., 2012). These data, combined with image bands, vegetation indices and three-dimensional information of the habitats, could further enhance classification accuracy. The addition of texture features in the classification was demonstrated by previous habitat and vegetation mapping studies (Fraser *et al*., 2016; Gonçalves *et al*., 2016). It is also worth emphasising that other factors, e.g. spatial resolution, algorithm selection and training data size, may improve the classification results obtained in this study. Future studies are encouraged to test the influence of these factors on classification accuracy.

This study has demonstrated the advantage of using UAVs by providing a high-resolution habitat map (6 cm spatial resolution) showing the degradation caused by both natural and human disturbance and the

presence of invasive species. The methodology used in this study has the potential for use in classifying other habitat types. Ecologists and other monitoring experts also see opportunities to integrate UAV remote sensing with the traditional field methods for targeted surveillance monitoring of habitats (e.g. detection of the extent and direction of change of the habitat location and status) and for monitoring over larger areas (Anderson and Gaston, 2013; Cruzan *et al*., 2016). This means that UAV data and analysis can detect hotspots of change, facilitating targeted field visits (Mücher and Hazeu, 2021).

2.5 Conclusion

This chapter demonstrates the use of the combined multitemporal UAV data and RF classifier as a tool for automatic characterisation of different coastal dune habitats. The results show a range of accuracies in the models, from 84% to 94%. Integration of spectral and topographic information derived from the three sets of images delivered the highest accuracy model (94.26%). The classification results also suggest that the middle period of the growing season is better than the early and late seasons for image acquisitions. This approach used a low-cost multispectral UAV system to accurately classify coastal dune habitats. It therefore has the potential to be applied in the classification of other habitat types. The high level of accuracies obtained in this study highlight the potential applications of UAV data in other vegetation-related remote sensing applications, including mapping of invasive species and other plant species characterisation.

3 Improving the Mapping of Coastal Invasive Species Using Unoccupied Aerial Vehicle Imagery and Deep Learning

3.1 Introduction

Invasive alien species (IASs) are organisms found in an environment outside their natural range that can cause negative impacts on this new environment (IUCN, 2000). They are considered among the major drivers of global biodiversity loss, as they can alter ecosystem functions and services and cause species richness decline (Mollot *et al*., 2017). The adverse impacts of IASs have been recognised by international organisations such as the International Union for Conservation of Nature (IUCN, 2000) and the EU through the EU Regulation on the prevention and management of the introduction and spread of IASs (EU, 2014). In Ireland's most recent HD report, the presence of IASs is one of the major threats to and pressures on habitats, affecting more than 40% of all reported habitats (NPWS, 2019). Furthermore, the estimated cost of IASs to the Irish economy was €202 million in 2013 (Kelly *et al*., 2013).

In general, the assessment of IASs requires accurate maps to monitor their location and expansion over time. These maps can also be used to identify hotspots where management efforts can be focused, as well as to measure the success of control programmes. The information is commonly obtained through traditional ground-based field surveys, which can be costly and spatially restricted and involve considerable time and effort. Furthermore, the rate of IAS introductions is increasing globally, which can limit the potential of using manual methods alone for large-scale monitoring (Seebens *et al*., 2017). Consequently, an alternative is needed: a technique that is more efficient and repeatable to improve the capturing and monitoring of the spatial distribution of these IASs.

Spartina anglica C. E. Hubb (*Sporobolus anglicus* (C. E. Hubb.) P. M. Peterson and Saarela), also known as common cordgrass, is an IAS commonly found in saltmarsh and mudflat habitats in Ireland (Stokes *et al*., 2006). First introduced in Cork Harbour to bind and stabilise sediment, it has subsequently spread to other locations on the Irish coast. This perennial grass spreads by seed dispersal or vegetatively by rhizomes, which can form extensive meadows (Nehring and Adsersen, 2006). It invades and displaces HD Annex I habitats, including tidal mudflats and sandflats, Atlantic salt meadows and *Salicornia* beds (NPWS, 2019). This reduces feeding habitats for birds (Stokes *et al*., 2006). Monitoring the location and extent of *S. anglica* is an important step in assessing its rate of expansion (Brophy *et al*., 2019).

Advances in mapping technology, such as remote sensing, offer a potential solution to monitoring *S. anglica* (Huang and Asner, 2009). Medium-resolution satellite imagery, typically > 10 m/pixel, has been used to detect *S. anglica* covering large areas (Li *et al*., 2010; Zuo *et al*., 2012). However, it is too coarse for detailed mapping, such as delineating *S. anglica* when mixed with native species or detecting expansion in the form of small clonal patches. Early detection of *S. anglica* expansion is considered the best approach to prevent further spread, to minimise the cost of controlling the plant and to increase the success of eradicating it (Brophy *et al*., 2019). Mapping small patches of *S. anglica* requires sub-metre spatial resolution imagery. Another important limitation when using satellite imagery is cloud cover. Countries with high levels of cloud cover, such as Ireland, will benefit less from using optical satellite imagery for monitoring (Connolly, 2018). Hence, UAVs are suitable platforms for acquiring high-resolution imagery appropriate for mapping *S. anglica* patches.

Previous studies on mapping *S. anglica* used traditional machine learning classifiers such as RF (Proença *et al*., 2019; Van Beijma *et al*., 2014). This classifier can process a large number of explanatory features that have been manually extracted (handcrafted) (Belgiu and Drăgut, 2016). However, choosing relevant features can be time-consuming

and involves expert knowledge of the characteristics of the plant species. Deep learning can eliminate the need for these pre-specified handcrafted features (Li *et al*., 2018). Deep learning is a subfield of machine learning that aims to learn complex patterns from large amounts of data and automatically extract high-level features from these data rather than manually select them (Goodfellow *et al*., 2016; Li *et al*., 2018). This makes it a more robust method for image processing. Semantic segmentation is an image-processing technique that aims to assign a semantic label to every pixel in the image (Yu *et al*., 2018), and has gained significant attention because of its application of deep learning in many computer vision tasks, such as in self-driving cars (Sharma *et al*., 2019) and medical image diagnoses (Ahmed *et al*., 2020). This technique is also becoming popular for processing remote sensing data for many environmental applications, such as vegetation mapping (Balado *et al*., 2021; Kattenborn *et al*., 2019a; Osco *et al*., 2021). In the context of IASs, semantic segmentation could be a foundation for applications such as food security and habitat degradation monitoring. However, owing to the need to account for factors such as variable field conditions and plant growth stages, accurate segmentation of plant species presents a challenge in deep learning.

In many cases, deep learning requires large amounts of labelled training data to produce a robust model (Li *et al*., 2018). The acquisition and building of manually labelled datasets can require considerable effort, cost and time. These requirements can be prohibitive; therefore, a deep learning approach may not always appear feasible. Data augmentation and semi-supervised learning (SSL) are techniques that can reduce the reliance on large amounts of labelled data. Data augmentation does this by applying transformations to the existing data, thus increasing the amount and diversity of labelled data. Common augmentation techniques involve geometric transformations, including flips, rotations, translations and cropping. More advanced techniques for augmenting data, including colour space modifications, have recently been developed (Shorten and Khoshgoftaar, 2019). In SSL, both labelled and unlabelled data are used to train a model instead of solely labelled data. Pseudo-labelling (Lee, 2013) is an approach to SSL that deals with unlabelled data. It uses a model initially trained on labelled data to make predictions for unlabelled data. These newly labelled data are integrated with those previously labelled and the model is retrained. This process is then iterated. Since it is tedious and expensive in terms of cost and time to label images for segmentation tasks but cheap to gather unlabelled data, the model takes advantage of both the labelled and unlabelled data. However, deep learning studies that have investigated the benefits of augmentation and pseudo-labelling techniques have mostly been related to medical images (Chlap *et al*., 2021; Mao *et al*., 2022) and other natural images of common objects (Perez and Wang, 2017; Zheng *et al*., 2020). The effectiveness of applying these techniques to UAV-acquired images for mapping invasive species to improve accuracy and prevent overfitting, hence improving transferability, has not yet been fully explored.

This study develops an automatic segmentation model for mapping *S. anglica* using UAV images. The aims of this study are (1) to select an effective segmentation network structure by comparing the performance differences of three network hyperparameters, namely model architecture, encoder backbone and input image patch size; (2) to propose a method of combining data augmentation and pseudo-labelling techniques for image segmentation of UAV-acquired images; (3) to assess the performance of the proposed method; and (4) to evaluate the performance of the final segmentation model on a dataset acquired using a different sensor. The aim is that, by using this approach, the mapping and monitoring of *S. anglica* and other invasive species can be substantially automated.

3.2 Materials and Methods

The methodology is divided into four stages: data collection, data preparation, model development and selection, and model evaluation. The first stage consists of acquiring UAV images and field data, and the second stage is transforming these datasets into a format suitable for training a deep learning model. The third stage includes examining the effects of applying different modifications (patch size, architecture, pre-trained model, augmentation technique and pseudo-labelling) to the model to facilitate the model selection. The fourth stage evaluates the final model to see its generalisation performance when applied to new and unseen data.

3.2.1 Study area

North Bull Island is a wedge-shaped, low-lying coastal "barrier island" located in the northern part of Dublin Bay on the east coast of Ireland (Figure 3.1) (Mathew *et al*., 2019). It is part of the United Nations Educational, Scientific and Cultural Organization (UNESCO)-designated Dublin Bay Biosphere Reserve and the North Dublin Bay SAC (SAC code 000206, approximately 1474 ha in area) site of the Natura 2000 network. This SAC includes four saltmarsh habitats listed under Annex I of the EU HD (NPWS, 2013c). However, *S. anglica* is also present, forming extensive meadows and smaller patches.

In this study, two areas of interest were chosen to assess how well the method would perform in delineating *S. anglica*. These two study sites were found on the sheltered (western) side of North Bull Island within the saltmarsh habitat. The first site ($Site_{train}$) was chosen for model training and selection, while the second site ($Site_{test}$) was for model evaluation. This way, there was no overlap between model training and evaluation datasets, to avoid any bias in predictions.

3.2.2 Data collection

Field data

Extensive field surveys were conducted by an experienced ecologist to record locations of *S. anglica* point samples using an Emlid Reach RS+ GNSS device (https://emlid.com/reachrs/), which provided positions with centimetre-level accuracy. Each point was located at the centre of a homogeneous area of *S. anglica* cover. The radius of this area around each point, typically 1–10 m, was estimated and recorded by the ecologist. The point data were then converted into polygons using the recorded radii. These polygons were used to guide the preparation of reference data (labels) in section 3.2.3.

Unoccupied aerial vehicle images

Three field campaigns, two for $Site_{train}$ and one for $Site_{test}$, were conducted to acquire high-resolution (5 cm) UAV imagery. For $Site_{train}$, both flights – in August 2019 and October 2021 – used a MicaSense Altum multispectral sensor with five spectral bands: blue, green, red, red edge and near-infrared

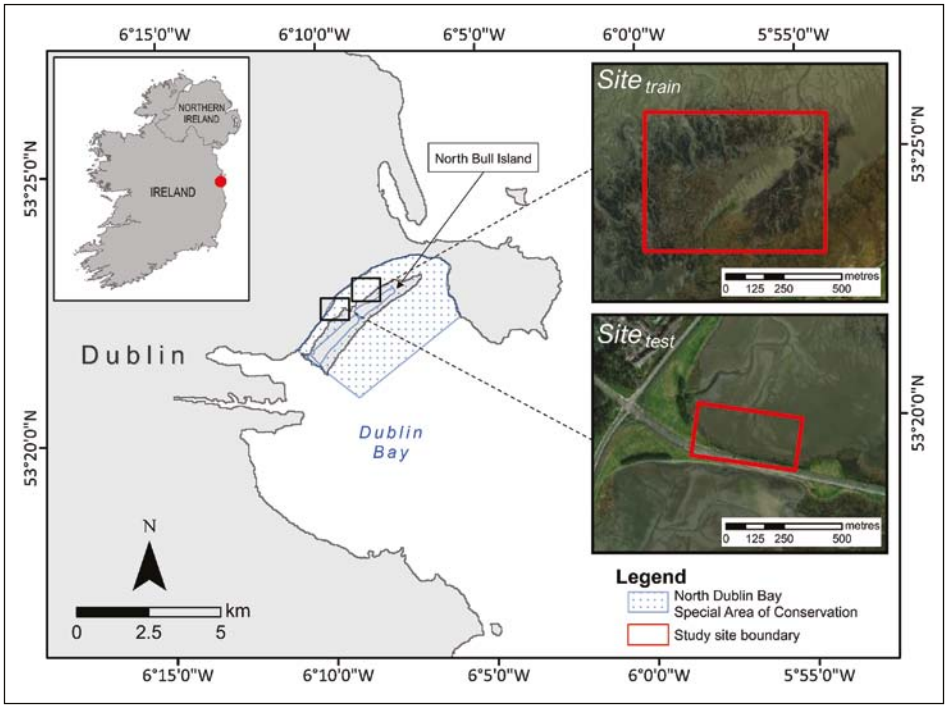

Figure 3.1. Map location of the study area on North Bull Island, Ireland (left), and close-ups of the training and test study sites (right). Reproduced from Cruz *et al.* (2023b); licensed under CC BY 4.0 (https://creativecommons.org/licenses/by/4.0/).

(MicaSense, 2019). For $Site_{test}$, a digital camera DJI Zenmuse P1 (dji.com/ie/zenmuse-p1/specs) was used to acquire imagery in October 2022. Owing to different acquisition days and different camera sensors used, there were variations in the captured images in terms of the appearance and colour of the vegetation (Figure 3.2).

Each set of UAV imagery was processed using the structure-from-motion technique in Pix4D software (Pix4D, Switzerland, version 4.3.33) to generate an orthomosaic. The processing involves keypoint extraction, keypoint matching between images, camera model optimisation, geolocation based on GPS flight trajectories and dense point cloud generation. For this study, only red, green and blue (RGB) image bands were utilised in the modelling because RGB images are relatively easy to acquire using cheap hardware and would therefore represent a more financially viable option for invasive plant managers. The $Site_{train}$ orthomosaics were subdivided into three sets: train, validation and unlabelled. The train and validation sets were used to facilitate the deep learning training process, while the unlabelled set was for the pseudo-labelling (see section 3.3.2). On the other hand, the $Site_{test}$ orthomosaic was used to evaluate the generalisation performance of the final model (test set). The study used different sensors; hence, the ability of the model to generalise across sensors was tested.

3.2.3 Data preparation

The reference data (labels) were prepared by manually delineating *S. anglica* boundaries (in the form of polygons) in a geographic information system (GIS) environment. This delineation was based on the acquired field data and used image interpretation. The image pixels belonging to *S. anglica* were assigned a value of 1, whereas pixels representing the background (e.g. exposed mud, macroalgae and other plant communities) were assigned a value of 0. Thus, the input for the modelling was a binary-labelled image with *S. anglica* as one class and the background as the second class. This labelling was done for the train, validation and test sets.

3.2.4 Training parameters and evaluation metric

Segmentation was implemented using the Segmentation models library of Python 3.7 based on Keras 2.9 and TensorFlow 2.9 (Yakubovskiy, 2019). The training phase involved passing the image patches into a deep learning network over a certain number of model iterations (epochs). Here, all models were trained in 100 epochs. The goal was to improve the result per epoch by optimising model weights. The model weights were only considered and saved if the loss value was lower than the value derived in the previous epoch. The Adam algorithm

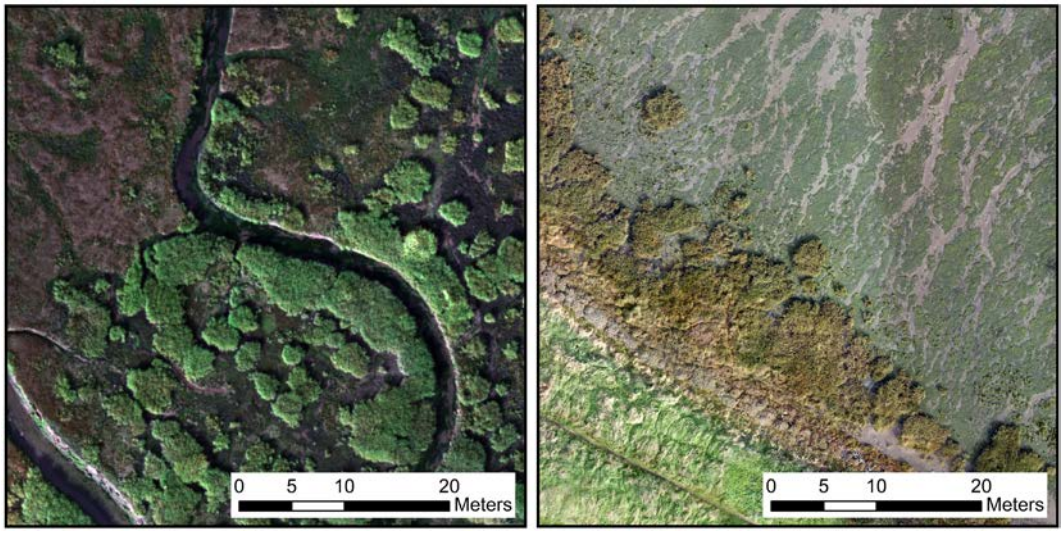

Figure 3.2. Comparison between the UAV images taken at $Site_{train}$ (left) and $Site_{test}$ (right). Reproduced from Cruz *et al*. (2023b); licensed under CC BY 4.0 (https://creativecommons.org/licenses/by/4.0/).

(Kingma and Ba, 2015), with a learning rate of 10^{-4}, was used in optimisation. Binary focal loss (Lin *et al*., 2018) was selected as the loss function. Given the binary classification problem (absence of *S. anglica* = 0, presence of *S. anglica* = 1), the final layer activation was set to a sigmoid function. We used 50% as the threshold to transform the results into a binary classification image (0–50%, class 0; 50.01–100%, class 1). All computations were performed on a local workstation using a CUDA-compatible graphics processing unit (GPU) with 12 GB of GDDR6 memory (NVIDIA GeForce RTX 3060).

For model comparison and selection, we used the Jaccard index, also known as the Intersection over Union (IOU) metric. The Jaccard index (Jaccard, 1908) is a well-known statistic used to measure the spatial similarity between two sample sets. This index is computed by dividing the area of overlap between the model-predicted image and the labelled image (predicted and labelled) by the area of union between them (predicted or labelled): IOU = (area of overlap) / (area of union). The value ranges from 0 to 1, where 0 indicates no overlap between the two, and 1 indicates a complete overlap. This means that the higher the IOU score, the better the model is. The mean Intersection over Union (mIOU) score was computed for each class by averaging all IOU scores of that class.

3.3 Experiments

3.3.1 Image patch size and network structure

Image patch size. The labelled train image was split into sub-images, called patches, using a sliding kernel of 50% overlap. In this way, we created more training patches. Similarly, the labelled validation image was divided into patches but with no overlap. This experiment aimed to test the effect of image patch size on the model performance. Hence, we prepared two sets of patches of sizes 128 × 128 and 256 × 256 pixels. As expected, fewer patches were generated with the larger patch size.

Model architecture and backbone. A general semantic segmentation network structure consists of an encoder and a decoder. An encoder is used to extract features from an image by downsampling, while a decoder is used to upsample the extracted features to their original image dimension. In this study, three encoder–decoder model architectures were implemented – U-Net (Ronneberger *et al*., 2015), LinkNet (Chaurasia and Culurciello, 2018) and Feature Pyramid Network (FPN) (Lin *et al*., 2017) – to determine the model network structure to be used in segmentation. For the feature encoder backbones, we considered 10 existing pre-trained models initialised with ImageNet weights (Deng *et al*., 2009) (Table 3.1). Furthermore, each network structure was trained on the two image patch sizes: 128 × 128 and 256 × 256 pixels. Hence, 60 models were trained and compared in this section. Using mIOU as the evaluation metric, this experiment showed that the U-Net architecture with Inception-v3 as its backbone (U-Net_Inception-v3) and trained on 128-pixel × 128-pixel image patches offered the best model performance. This will be further detailed in section 3.4.1. Consequently, we used U-Net_Inception-v3 in all the subsequent processing.

3.3.2 Data augmentation and pseudo-labelling

Data augmentation. The train image patches were subjected to augmentation techniques using the Albumentations library (Buslaev *et al*., 2020) in Python. These techniques were grouped into two categories: position and colour space augmentations. In the first group, position augmentation, the orientation of the features on the image is altered. In this case, a rotation scheme was used. Rotation is a suitable augmentation technique for UAV images, as they can be viewed from any orientation. To avoid border and resampling artefacts due to arbitrary rotation angles, an image patch (Figure 3.3a) was rotated around its centre using multiples of 90° (90°, 180° or 270°) (Figure 3.3b–d). This transformation also required corresponding rotational changes to the labels. The second group, colour space augmentation, allows random changes in the brightness, hue and saturation of an image by applying the colour jitter technique (Figure 3.3e–h).

Table 3.1. List of encoder backbones used in this study

Encoder backbone	
VGG (VGG-16, VGG-19)	DenseNet-121
ResNet (ResNet-50, ResNet-101, ResNet-152)	Inception-v3
ResNeXt (ResNeXt-50, ResNeXt-101)	Inception-ResNet-v2

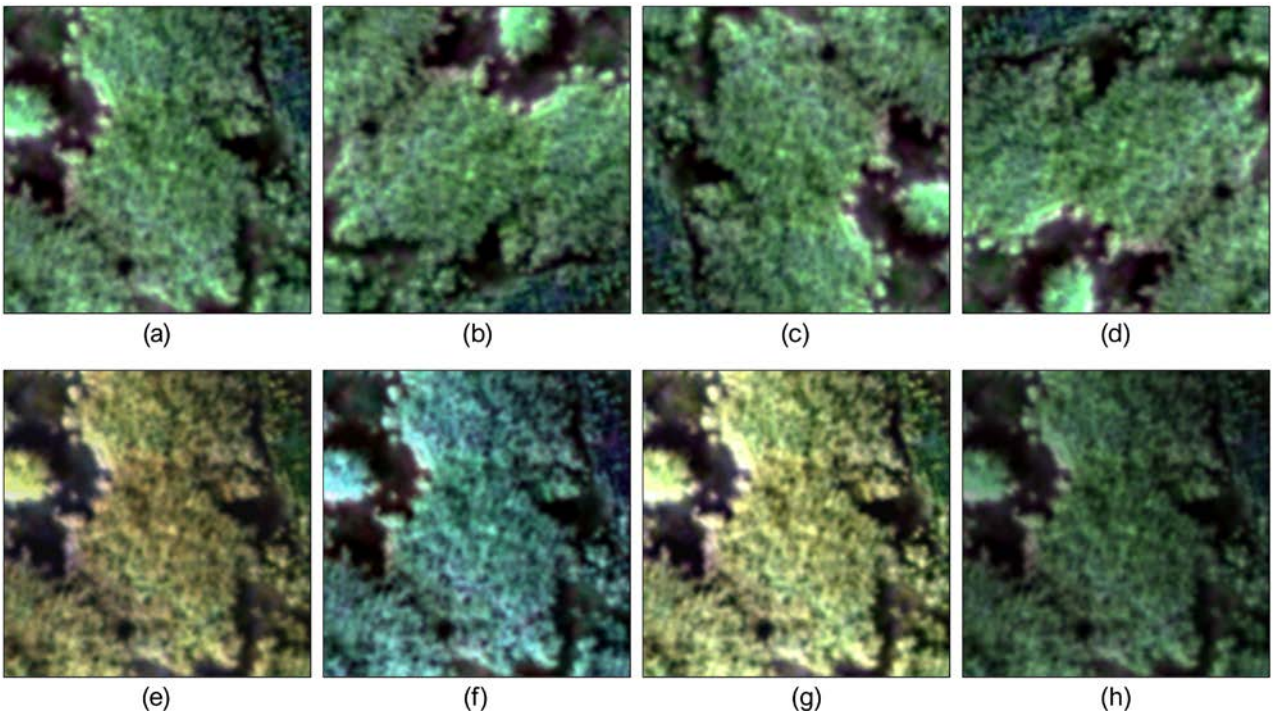

Figure 3.3. Original image patch (a) and generated images after multiples of 90° rotation (b–d) and colour jitter (e–h) augmentations were applied. Reproduced from Cruz *et al.* (2023b); licensed under CC BY 4.0 (https://creativecommons.org/licenses/by/4.0/).

The purpose of colour jitter is to simulate images acquired in different natural lighting conditions and at different acquisition dates, which will affect the appearance and colour of the vegetation. In contrast to the first group, this technique does not require any changes to the labels, as there is no geometric change as there would be with a rotation.

Pseudo-labelling. There were 28,564 unlabelled patches of 128 pixels × 128 pixels generated for this study. The model trained using the augmented data was used to predict the labels (pseudo-labels) of all pixels of each unlabelled patch (Figure 3.4). The labelled dataset was then expanded based on the confidence of these pseudo-labels. To improve the overall performance of the final model, we used a threshold to select only those pseudo-labels that the model was very confident about. Since the model output predicted probabilities of the presence of *S. anglica* with values from 0 to 1, all predictions with $Pr\,(y > 0.95) + Pr\,(y > 0.05) > 0.90$ were selected and added to the new training set, and the remaining were designated as unlabelled data. The model was then retrained with the new training set consisting of the labelled data and the selected subset of pseudo-labelled data. This new model was then used to predict the remaining unlabelled dataset. This process was repeated until 95% of the unlabelled samples passed the threshold, and was then used to retrain the model.

For the experiments involving pseudo-labels, we slightly modified the validation set by splitting off samples ($n = 100$) from the test set and adding them to the validation set, resulting in a new set of validation data ($validation_{aug\_pseudo}$ set). This was done because the domain gap (different sensor, different site and seasonal variation) between the original validation set and the test set meant that optimising hyperparameters for the original validation set may result in a model that does not generalise well to domain variations. Including validation samples from the target domain allows for a model with better generalisation characteristics to be selected. Note that the remaining test set did not contain any of the samples that were split off for validation. The final model derived from the previous section was evaluated on the test set. To investigate the contribution of data augmentation and pseudo-labelling to the overall model performance on the test set, we ran the same experiment, but this time with no data augmentation or pseudo-labelling implemented on the original train data.

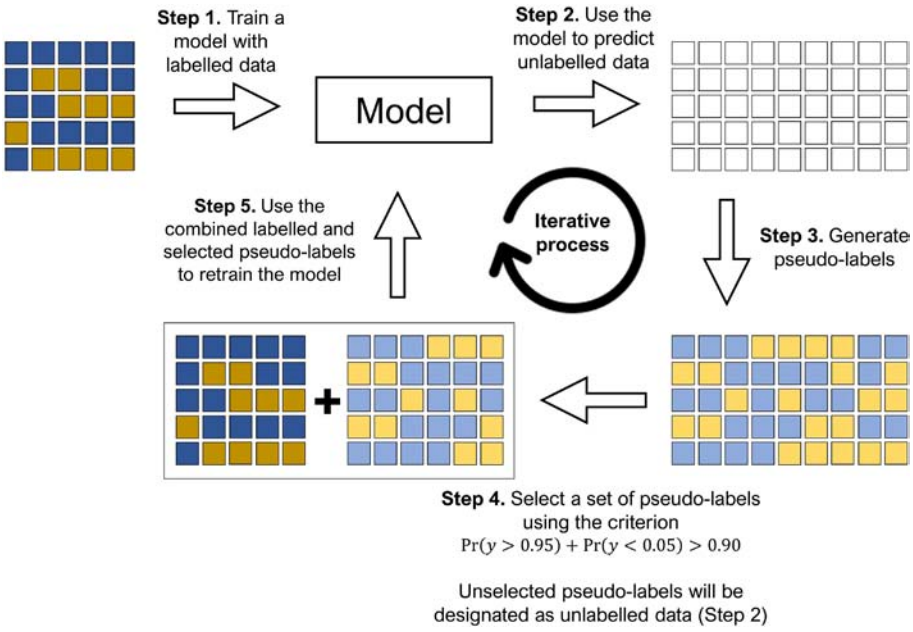

Figure 3.4. The pseudo-labelling process. Reproduced from Cruz *et al*. (2023b); licensed under CC BY 4.0 (https://creativecommons.org/licenses/by/4.0/).

3.4 Results

3.4.1 Performance comparison between architectures and backbones using different patch sizes

Comparing all the models produced in section 3.3.1, U-Net_Inception-v3 applied on the 128-pixel × 128-pixel image patches yielded the highest mIOU score, of 0.832. This was followed by the LinkNet_Inception-v3 model applied on the 128-pixel × 128-pixel image patches, which had a slightly lower mIOU score of 0.830. In general, no pattern was observed in which a specific image patch size led to better model performance. This means that patch sizes of 128 × 128 and 256 × 256 pixels, where 1 pixel = 5 cm, can be used to both recognise and capture contextual information about *S. anglica* on the images. Instead, the model performance varied depending on the architecture and encoder backbone used.

Aside from mIOU scores, training speed varied among models, ranging from approximately 25 minutes to almost 3 hours. Overall, in the cases of both patch sizes, the U-Net and LinkNet models were trained at similar speeds, whereas the FPN models were the slowest to be trained. Regarding the backbones used, ResNeXt-101 was the slowest to train, followed by ResNeXt-50, ResNet-152 and Inception-ResNet-v2. The remaining backbones (VGG-16, VGG-19, ResNet-50, ResNet-101, DenseNet-121, Inception-v3) were trained at similar speeds, each approximately three times faster than the ResNeXt-101 training speed. Furthermore, models trained on 128-pixel × 128-pixel image patches were consistently slower to train than those trained on the 256-pixel × 256-pixel image patches, possibly because of the difference in the total number of resulting image patches, as described in section 3.3.1.

Applying the trained model to a new set of patch-based images was extremely fast and could produce segmented results in less than a second. Comparing all the models, the two VGG backbones exhibited the fastest inference speeds. The U-Net and LinkNet models usually offered faster inference speeds than the FPN models, although the difference was marginal. Despite the 128-pixel × 128-pixel image patches comprising only one-quarter as many pixels as the 256-pixel × 256-pixel image patches, they were less than four times as fast.

3.4.2 Data augmentation and pseudo-labelling

Figure 3.5 shows the performance comparison between models with and without applying data augmentation and pseudo-labelling techniques. The baseline model (without data augmentation and pseudo-labels) achieved a 0.761 mIOU score

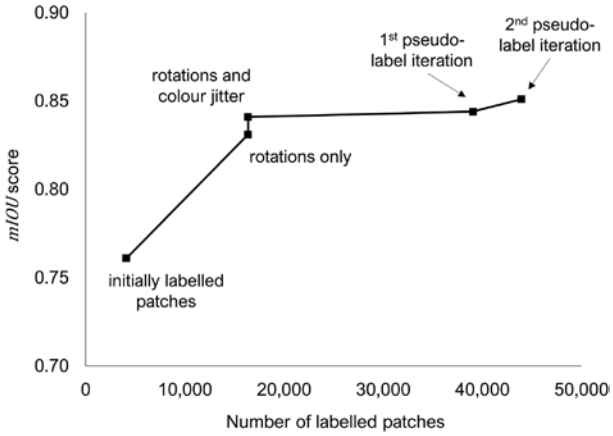

Figure 3.5. Number of labelled patches used to train a model and its corresponding performance represented by mIOU score. Reproduced from Cruz *et al*. (2023b); licensed under CC BY 4.0 (https://creativecommons.org/licenses/by/4.0/).

on validation$_{aug_pseudo}$ data. Applying data augmentation techniques to the initially labelled data improved the model performance, with an increase of 0.070 when using rotations only and a further increase of 0.010 when colour jitter augmentation was applied to the rotated images. Augmentation increased the number of labelled patches four-fold, from 4092 to 16,368 (+12,276). Pseudo-labelling also contributed to the performance improvement of the model. After iteratively retraining the model with augmented labelled data and unlabelled data with pseudo-labels, its performance slightly improved from 0.841 to 0.851 (Figure 3.5). However, this modest improvement required the addition of a further 27,570 pseudo-labelled training patches.

3.4.3 Evaluation of the model on test data

The mIOU score when the final model was applied to test data was 0.712 (Table 3.2). Results also showed a total mIOU score decrease of 0.158 in the model performance when we eliminated both the augmentation and pseudo-labelling techniques in the process (Table 3.2). Figure 3.6 shows sample test images and the comparison between their reference labels and the labels predicted by the model.

3.5 Discussion

Our study demonstrates that deep learning-based segmentation can accurately map the distribution

Table 3.2. Model performance when data augmentation and pseudo-labelling techniques were removed in the process

	Test data	
Scenario	**mIOU**	**mIOU Δ**
Final model on the test set	0.712	–
Model with data augmentation but without pseudo-labelled data	0.698	–0.014
Model without data augmentation and pseudo-labelled data	0.554	–0.158

of *S. anglica* in UAV imagery. The results are in line with previous studies that have shown the potential of deep learning for high-resolution mapping of invasive species using UAV imagery (Gonçalves *et al*., 2022; James and Bradshaw, 2020; Qian *et al*., 2020).

The U-Net_Inception-v3 model was selected based on its performance (highest mIOU score of 0.832) and training speed (approximately 34 minutes for 100 epochs on a GPU). It offered the best balance between training speed and accuracy. However, this model exhibited an average inference speed of 61.19 ms per input image – 17.94 ms slower than the model with the fastest inference speed (LinkNet_VGG-16). The difference in inference speed between the two models is very small; this may not be a problem in most monitoring programmes. While LinkNet_VGG-16 had the fastest inference speed, 43.25 ms, its mIOU score (0.692) was 0.14 lower than that of U-Net_Inception-v3. Monitoring of an invasive species requires a model with good segmentation results so that the model can accurately determine the spatial extent and rate of expansion of that species.

The application of augmentation and pseudo-labelling techniques helped improve model robustness by increasing the diversity of the training data. The integration of these techniques by James and Bradshaw (2020) enhanced vegetation mapping. These techniques are advantageous, as manual delineation of irregular plant canopies on the imagery is tedious. According to our analysis, after applying data augmentation, there was a substantial increase in the mIOU score; however, when a large amount of unlabelled data was subsequently included, there was only a slight improvement in the model performance (Figure 3.5). This result could be due to a large amount of variance added to the training data by applying data augmentation techniques. For remote

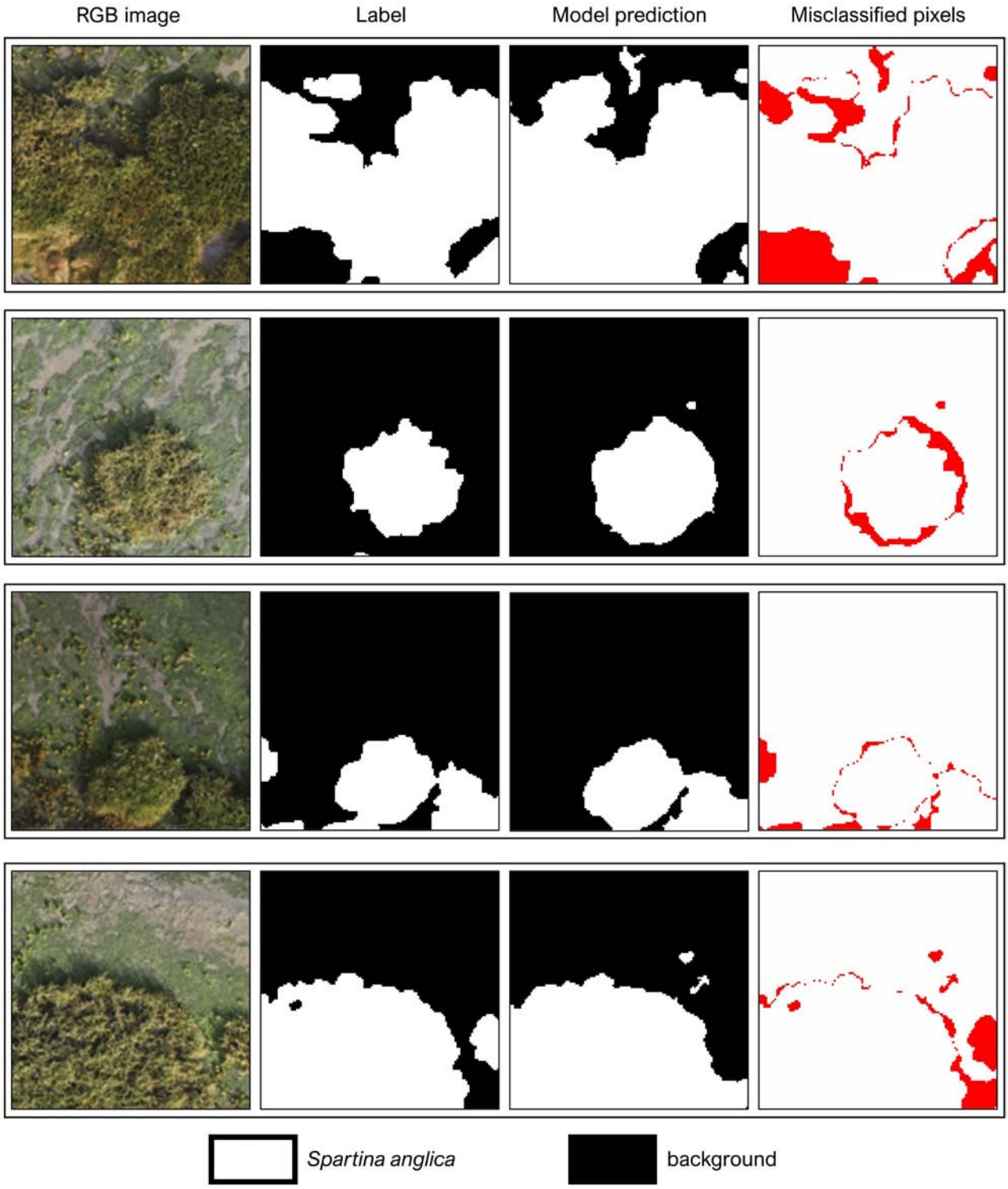

Figure 3.6. Sample RGB test images and their corresponding segmentation reference labels and model predictions, with an image indicating incorrectly classified pixels (red). Reproduced from Cruz *et al*. (2023b); licensed under CC BY 4.0 (https://creativecommons.org/licenses/by/4.0/).

sensing, however, acquiring RGB images using low-cost UAVs to generate unlabelled data is relatively simple. Hence, pseudo-labelling can have an important practical significance in improving the segmentation performance, as domain-specific labelled samples may be limited.

In general, the time of the year when the image is acquired can affect the model performance.

Plant colouration and morphology will change with the different seasons of the year. *S. anglica* changes from mid-green during the growing season to pale brown during the winter as it dies back. Variation in sunlight levels at the time of UAV surveys will also affect the brightness of the captured images. Aiming to assess the transferability of the model, we acquired a new set of images and performed the prediction under different conditions, i.e. different cameras, different sites and different times of the year. Hence, variations in illumination and differences in vegetation appearance were observed when comparing the images used in model training and testing. Despite this different scenario, the final model still achieved good results, with an mIOU score of 0.712.

Inaccuracies in the segmentation could be due to the location of the training and test datasets and potential errors in the delineation of *S. anglica* boundaries. The train images were acquired from a site where areas dominated by *S. anglica* were intermixed with *Salicornia* beds. The test images were acquired from a site where areas dominated by *S. anglica* adjoined Atlantic salt meadows dominated by common saltmarsh grass (*Puccinellia maritima*) and sea purslane (*Atriplex portulacoides*). It is likely that some *S. anglica* patches were not correctly segmented owing to variations in species composition surrounding *S. anglica* between the training and test sites. Even though the features of *S. anglica* on high-resolution UAV imagery are quite distinct, performing manual delineation by image interpretation can be subjective and introduce positional errors. This can happen along the edges of plant canopies where image pixels are spectrally mixed with other plants or other environmental background noise, such as mud. In this study, the chance of incorrect segmentation increased along the edges of *S. anglica* (see Figure 3.6). These inaccuracies might affect the training process, thus lowering the predictive accuracy.

A requirement of the presented methodology is a computer that supports the workload associated with deep learning. Computational resources and dataset size both impact the time it takes to train a model. The increasing amount of available remote sensing data means that the demand for computing resources to train models in a reasonable time is also increasing (Chi *et al*., 2016). Therefore, there is a need for the use of GPUs, which can process multiple computations simultaneously, as these can significantly speed up deep learning operations. As these models are retrained with more datasets and applied to larger spatial extents, there may be a need for either cloud-based services (e.g. Google Colaboratory (Carneiro *et al*., 2018)) or national centres for high-performance computing (e.g. European High Performance Computing Joint Undertaking), which can provide access to computing resources for deep learning projects to accelerate training and inference speeds with minimal computing resources from the users.

In Ireland, *S. anglica* is found in many coastal counties and can grow on mudflats and saltmarshes. Saltmarshes occur in a range of geomorphological contexts: estuaries, bays, fringes, sandflats and lagoons (Curtis and Sheehy Skeffington, 1998). Considering this variation in situations where *S. anglica* can establish, there are opportunities to explore updating our model to generalise well with other locations when more data become available.

The techniques used here provided robust results; however, the model's accuracy could be improved further. Future studies can consider using more extensive combinations of augmentation techniques and more domain adaptation techniques, which can potentially improve the generalisation ability of a deep learning model. Also, future studies can explore using weighted cross entropy with weights reducing for image pixels nearer to the boundaries of plant canopies (James and Bradshaw, 2019). Furthermore, the high-resolution *S. anglica* extent map generated from UAV imagery using the methodology presented can serve as training data for satellite image-based models to map on a regional or national scale (Kattenborn *et al*., 2019b).

3.6 Conclusion

Developing baseline data on the current extent of invasive species, as well as timely and effective monitoring of their expansion, is crucial for biodiversity conservation and the sustainable management of habitats. Advances in UAV remote sensing and deep learning have provided a huge potential for accurately mapping these invasive species. The results of this study show that the choice of model network structure and the use of techniques that can enhance the size and quality of training data are important decisions when creating robust deep learning models

for mapping invasive species. This study aimed to improve the method for mapping the spatial distribution of *S. anglica* invading saltmarsh habitats by using deep learning-based semantic segmentation applied to high-resolution UAV imagery. The results indicated that the U-Net architecture with Inception-v3 as the encoder backbone trained on 128-pixel × 128-pixel image patches was the best model in terms of model performance. Applying data augmentation to the initially labelled data increased the mIOU score by 0.08, with a further small improvement of 0.01 after adding pseudo-labels. These techniques improved model robustness. The final model evaluated on a separate test dataset achieved an mIOU score of 0.712, indicating good generalisation ability. For practical purposes, the segmentation model developed in the study can be utilised for spatiotemporal mapping of *S. anglica* distribution. These high-resolution maps are useful for understanding the pattern and rate of *S. anglica* invasion and potentially for evaluating the effectiveness of control efforts. The proposed methodology is transferable and can be adapted for mapping other invasive species.

4 Mapping of Temperate Upland Habitats Using High-resolution Satellite Imagery and Machine Learning

4.1 Introduction

Uplands comprise a range of extensive, mostly semi-natural habitats, including blanket bogs, heaths, fens, grasslands and those associated with exposed rocks and scree (Perrin *et al*., 2009). These habitats are protected in the EU under the HD (EU, 1992). They provide important services, such as carbon sequestration and storage, biodiversity support, flood mitigation and water quality regulation (Bonn *et al*., 2008). However, they are also highly vulnerable to climate change and to increasing pressures and threats from anthropogenic stressors, mainly due to land use changes (Connolly, 2018; Crowle and McCormack, 2009; Perrin *et al*., 2017; Young *et al*., 2005). Examples include unsustainable agricultural practices, extensive afforestation, wind farm development and scrub encroachment. These stressors can lead to habitat fragmentation and widespread degradation, causing these habitats to lose their capacity to deliver such services (Connolly, 2018; Perrin *et al*., 2009). In the most recent *State of Nature in the EU* report, only 15% of the habitats in the EU were in favourable condition, with blanket bogs showing a deteriorating trend (European Environment Agency, 2020).

The alarming decline in habitat conditions within the EU has been recognised by the European Commission through the proposed Nature Restoration Law (EC, 2022). This law will require EU Member States to develop and implement restoration measures for degraded ecosystems and habitats, such as drained bogs. Each Member State must also monitor and report its progress in implementing the law (European Council, 2023). Comprehensive mapping is fundamental for executing this legal requirement, as it can provide baseline data, such as the location and extent of habitats, and can be used to monitor and track their condition over time as well as to support restoration programmes. Common methods to map habitats include ground-based field surveys or interpretation from aerial imagery (Smith *et al*., 2011). However, the vast, remote and rugged terrain of upland habitats may limit the frequency of manual field surveys to conduct mapping of these habitats, as there are issues with resource availability (i.e. limited time and high cost) (Buchanan *et al*., 2005; Müller and Brandl, 2009). Using aerial imagery to delineate habitat boundaries – in the form of polygons – can also be challenging, as upland habitats are typically composed of complex vegetation mosaics, making it difficult to represent habitat types as separate polygons (O'Connell *et al*., 2014; Perrin *et al*., 2009). A complementary approach to addressing these mapping challenges should be considered, particularly with the increased need for accurate, timely and broad-scale spatial information on these protected habitats.

Remote sensing is a promising approach to mapping and monitoring habitats and vegetation communities within them (Corbane *et al*., 2015; Mücher and Hazeu, 2021; Nagendra *et al*., 2013). Specifically, optical imagery acquired by satellites has been used for mapping upland habitats (Barrett *et al*., 2016; Connolly, 2018; Mehner *et al*., 2004; O'Connell *et al*., 2014). The spatial extent that a single satellite image can cover (e.g. 100 km × 100 km for a Sentinel-2 image (Drusch *et al*., 2012)) is a significant advantage, particularly in upland habitats, as they can be extensive (JNCC, 2015). Moreover, satellite remote sensing technologies have significantly improved over the last decade (Cantrell *et al*., 2021; Gleyzes *et al*., 2012; Kim *et al*., 2022). They now provide imagery at higher spatial, spectral and temporal resolutions than previously available (i.e. spatial resolution of a few metres with less than a week's revisit time), creating opportunities for detailed botanical mapping of upland habitats (Ingle *et al*., 2023). Previous studies have demonstrated that higher spatial resolution imagery (< 5 m) can improve

classification accuracy. However, these studies were mainly focused on general land cover classes wherein spectral characteristics can be quite distinct (Boyle *et al*., 2014; Fisher *et al*., 2017). The impact of image spatial resolution on classifying spectrally similar habitats, such as in uplands, has not been fully explored.

Most upland habitat mapping studies have used the conventional hard or crisp classification technique (Barrett *et al*., 2016; Mehner *et al*., 2004). This technique involves a classifier making a definitive decision on which class a pixel belongs to (most likely to the dominant class). Each pixel is assumed to be pure; hence, it is associated only with a single class (Fisher, 1997). However, information in a satellite image pixel often relates to multiple classes. As some habitats are often intermixed, the crisp classification technique may mean that information about other classes will be omitted (Lucas *et al*., 2007). Moreover, the technique can result in abrupt transitions between habitats in the maps, which poorly describe the continuous nature of upland habitats. Upland habitats rarely have sharp boundaries. They are mainly heterogeneous, occurring in complex mosaics (Gatis *et al*., 2022; O'Connell *et al*., 2014). A soft or fuzzy classification technique can be used to address the challenge of mapping transitional boundaries in the uplands. In contrast to the crisp classification technique, fuzzy classification allows each image pixel to be described by the probabilities of occurrence of all classes being considered (Foody, 1996). In other words, instead of classifying individual pixels into mutually exclusive classes, the fuzzy classification provides information on the probability that a certain class is present in every pixel. This technique can allow the representation of mixed and gradual transitions that often exist between habitats in complex environments such as uplands (Feilhauer *et al*., 2021). Moreover, the area computed from class probabilities can also be more accurate and closer to the actual area of that class (Sales *et al*., 2022).

RF is a widely used machine learning algorithm for classifying habitat and vegetation because of its robustness and excellent results (Amani *et al*., 2017; Cruz *et al*., 2023a; van Iersel *et al*., 2018). RF (Breiman, 2001) is an ensemble learning algorithm made up of decision trees, wherein each tree makes its own class prediction. The final class prediction has the most votes over all these trees (i.e. majority voting). RF can also provide information on class probabilities (Malley *et al*., 2012). This attribute of RF, which has been used in previous satellite-based remote sensing studies (O'Connell *et al*., 2015; Raab *et al*., 2018; Sales *et al*., 2022), could be explored for classifying upland habitats.

This study aimed to utilise a combination of machine learning and high-resolution satellite imagery to map complex upland habitats. Specifically, our aims were the following: (1) to determine the impact of spatial resolution on classification accuracy, (2) to compare crisp and fuzzy classification approaches using the RF algorithm for mapping upland habitats and (3) to apply RF-based models to map and describe the spatial distributions of habitats at two studied Irish upland sites.

4.2 Materials and Methods

4.2.1 Study sites

Two Irish upland sites, one in the Wicklow Mountains and one in the Slieve Mish Mountains, were selected for this study (Figure 4.1). Both sites are designated as SACs, part of the Natura 2000 network (NPWS, 2016, 2017), the world's largest network of protected sites covering the most valuable yet threatened habitats and species in the EU territory (Evans, 2012). The two sites are dominated by three upland habitats protected under the HD (those listed under Annex I): wet heath, dry heath and blanket bog (the EU HD codes are 4010, 4030 and 7130, respectively)[1] (Perrin *et al*., 2014a, 2017). The study focused on classifying these three Annex I upland habitats. Other common habitats present at each site were also classified, as some of them represent disturbance on uplands, such as the eroding blanket bog and the presence of dense bracken.

The first site (WM) is in the Wicklow Mountains, located south of County Dublin. WM covers an area of ~1020 ha, which is just over 3% of the entire Wicklow Mountains SAC extent. This site is a good example of a mountain blanket bog in eastern Ireland, consisting of deep peat with depths ranging from 1 to 6 m (Holden and Connolly, 2011). The second studied site

1 Refer to Table 4.1 for the complete list of habitats used in the study.

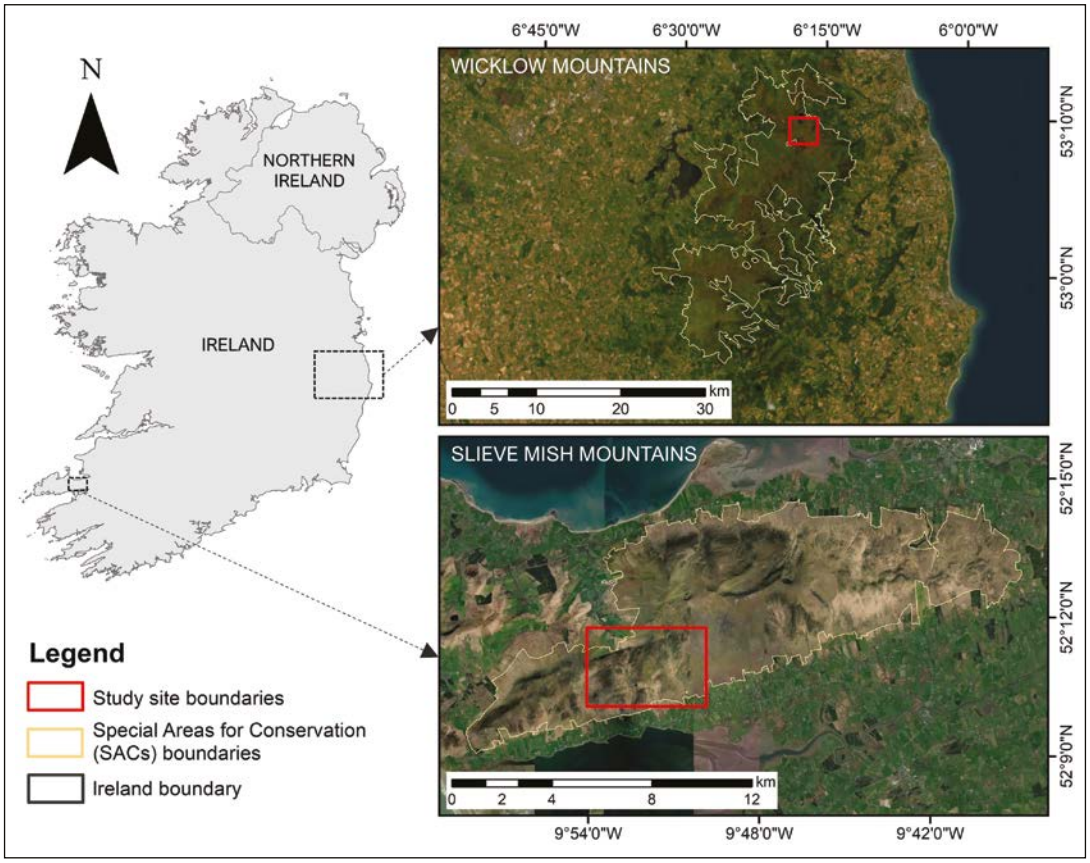

Figure 4.1. Inset maps showing the locations of the two study sites, Wicklow Mountains (top right) and Slieve Mish Mountains (bottom right), and the boundaries of the SAC covering each site. Reproduced from Cruz *et al*. (2024); licensed under CC BY 4.0 (https://creativecommons.org/licenses/by/4.0/).

(SM) is in Slieve Mish Mountains SAC, located on the eastern side of the Dingle Peninsula in County Kerry. SM extends to an area of approximately 1500 ha, about 15% of the Slieve Mish Mountains SAC extent, which is 9790 ha (Perrin *et al*., 2014a).

4.2.2 General methodology

High-resolution (2-m) Pleiades satellite imagery and digital terrain models (DTMs) were obtained for both sites. Several raster layers, or variables, were generated for each site using the obtained datasets to describe the characteristics of each habitat. These variables were resampled from the original 2-m resolution to 4-m, 6-m, 8-m and 10-m resolutions, generating five sets of variables. A reference dataset was used to train and evaluate an RF-based classification model for each set. The trained model was then applied to produce spatially continuous crisp and fuzzy classified images within the study site. Figure 4.2 provides an overview of the workflow.

Datasets

Pleiades satellite imagery and digital terrain model. Cloud-free Pleiades images for each site were downloaded from the Sentinel Hub EO Browser through the European Space Agency sponsorship programme (sentinel-hub.com/Network-of-Resources/). The downloaded images for the SM and WM sites were captured on 15 April 2020 and 8 May 2022, respectively, which closely aligns with the collection period of field datasets. Both images have a spatial resolution of 2 m and consist of four spectral bands on the following wavelengths: blue (430–550 nm), green (490–610 nm), red (600–720 nm) and near-infrared (750–950 nm). The downloaded images had already been orthorectified and projected on the Universal Transverse Mercator Zone 29 North coordinate system. DTMs for both sites were also obtained and reprojected to the same coordinate system as the Pleiades images.

To ensure the classification focused only on the upland area, the image extents for both sites were modified

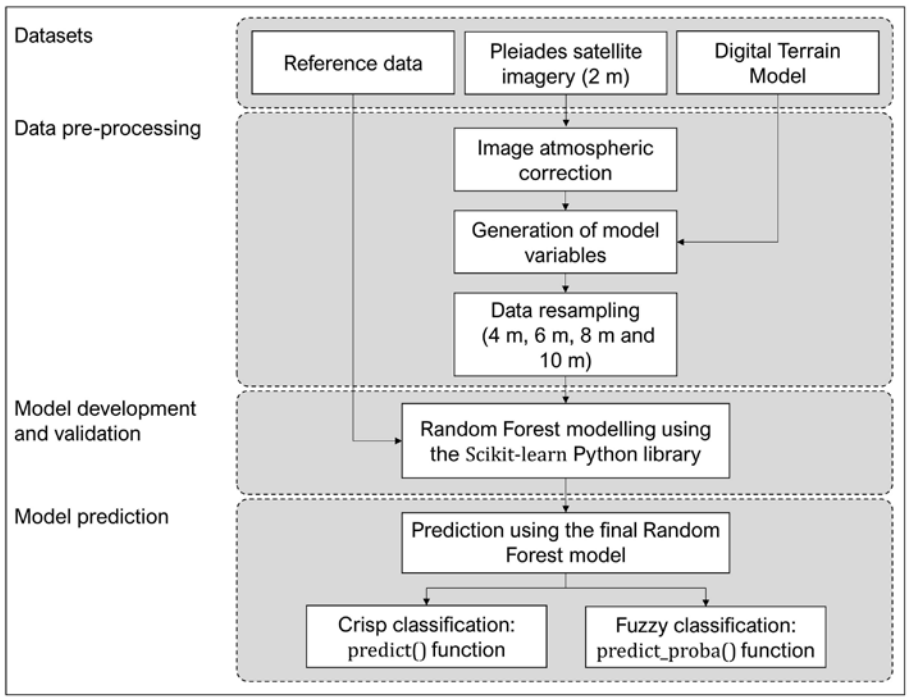

Figure 4.2. The workflow illustrating the processing performed in the study. Reproduced from Cruz *et al.* (2024); licensed under CC BY 4.0 (https://creativecommons.org/licenses/by/4.0/).

to align with the boundary used in the national survey of Irish upland habitats (Perrin *et al*., 2014b). This boundary was based on the definition of upland habitats by Perrin *et al*. (2009), i.e. any unenclosed land areas found at altitudes above 150 m and contiguous areas of related habitats below this value. The downloaded image for the SM site was clipped using the boundary. No clipping was necessary for the WM site image, as its extent was already within the boundary.

Reference dataset. For this study, a reference dataset was used that consisted of data collected both in the field and through on-screen digitisation. In the field, the ecologists used GNSS receivers (centimetre-level accuracy) to record the location of a habitat, represented by a point. To ensure the recording of the correct coordinates of a point within a particular habitat, each point was measured at the centre of an area of a relatively homogeneous habitat cover. Ecologists also recorded the corresponding Annex I habitat name and photographed it in the north-view direction. If a point was not an Annex I habitat, the Fossitt habitat classification scheme was used to label it. Fossitt (2000) provides a standard guide for habitat identification in Ireland. The field data points were then visually inspected on the screen by the remote sensing analyst to ensure they aligned with the correct habitats, as seen on the satellite image. A similar process was applied to the additional points added in a GIS environment to supplement the field data. This process consisted of manual and subjective interpretation of the satellite image by the remote sensing analyst guided by the data from previous field surveys (Perrin *et al*., 2014a, 2017). These previous survey data consisted of polygons with records of approximate percentages of the constituent habitat types. Hence, the additional points were based on those polygons mostly comprising a single habitat (>98%). Tables 4.1 and 4.2 provide the list of habitats considered for each study site and the corresponding codes. To account for the shaded areas in the image

Table 4.1. List of habitats for each study site

Study site	Habitats
WM	Wet heath (4010), dry heath (4030), blanket bog (7130), grasslands/fens (GS3, GS4, PF2, PF3), bracken (HD1), eroding blanket bog (PB5), artificial surfaces (BL3), watercourses/bodies (3160), shadow
SM	Wet heath (4010), dry heath (4030), blanket bog (7130), grasslands/fens (GS3, GS4, PF1, PF2), artificial surfaces (including exposed rocks) (8110, BL3), watercourses/bodies (3160, FP2, FW4), shadow

Table 4.2. Habitat type and corresponding EU HD/Fossit code

Habitat type and code
Annex I
3160: Acid oligotrophic lake
4010: Northern Atlantic wet heaths with *Erica tetralix*
4030: European dry heaths
7130: Blanket bogs (* if active bog)
8110: Siliceous scree of the montane to snow levels
Fossitt (2000)
BL3: Building and artificial surfaces
FP2: Non-calcareous springs
FW1: Eroding/upland rivers
FW4: Drainage ditches
GS3: Dry-humid acid grassland
GS4: Wet grassland
HD1: Dense bracken
PB5: Eroding blanket bog
PF1: Rich fen and flush
PF2: Poor fen and flush

caused by tree canopy and steep slopes, we added a pseudo-habitat "shadow" to the lists (Table 4.1).

Data pre-processing

Generation of atmospherically corrected surface reflectance data. Each pixel in a single band of the satellite imagery was represented by the top-of-atmosphere reflectance scaled by 10,000. Hence, we divided each pixel value by 10,000 to rescale them to floating-point values 0.0 to 1.0, consistent with the range of reflectance. To correct the image for the influence of the atmosphere, we undertook the dark object subtraction method. This is a simple atmospheric correction method wherein the assumption is that the darkest pixels (e.g. deep water, shadow) would have zero reflectance, if not for the effects of the atmosphere on the image (Chavez, 1988). Here, the pixel values within the 10th percentile in a single band were averaged, and the result was then subtracted from all pixel values from that band. This process was repeated for all the bands of the satellite imagery, resulting in an atmospherically corrected image.

Variable preparation. For each study site, variables were prepared to be used as input for the modelling. Individual atmospherically corrected image bands were included, as they can provide information in the visible and near-infrared regions of the image. Various vegetation indices were generated, as they have been found to perform well in assessing vegetation cover and are extensively used for mapping habitats and vegetation communities (Bendig *et al*., 2015; Bhatnagar *et al*., 2020; Cruz *et al*., 2023a; Suo *et al*., 2019). A further variable related to PCA was also developed. PCA is a technique that reduces data dimensionality by creating new, uncorrelated variables known as the principal components (Jolliffe, 2002). Here, the first principal component band, having an eigenvalue of more than 75%, was extracted, as it contains most of the information from the original data. In addition, four textural variables (mean, contrast, variance and correlation) were derived based on the grey-level co-occurrence matrix (Haralick *et al*., 1973) of each image band. Specifically, these variables were computed over a 5 × 5 neighbourhood. Previous remote sensing studies have shown that the inclusion of textural variables in the classification improves accuracy, as they can describe spatial patterns and variations of the features within a band (Barrett *et al*., 2016; Kattenborn *et al*., 2019b). Finally, elevation and slope were also generated, as they describe the site topography, and can be determinants of habitat distribution (Cruz *et al*., 2023a; Scholefield *et al*., 2019; Zuleta *et al*., 2018). Overall, 33 variables were considered in the study (Table 4.3).

Image resampling. To determine the impact of spatial resolution on the classification accuracy, all variables were resampled from the original 2-m spatial resolution to 4-, 6-, 8- and 10-m resolutions (Figure 4.3). This created five datasets for each site. Ten metres was selected as the lowest resampled resolution because freely accessible Sentinel-2 satellite images have this spatial resolution for the visible and near-infrared bands. This way, the accuracy difference between a high spatial resolution commercial satellite image and a free medium-resolution satellite image can be assessed.

The resampling technique was based on averaging the pixel values within the new pixel size. This technique, however, could result in multiple field data points falling within a single pixel of the coarser image. Hence, we reviewed their locations on the 10-m-resolution image to ensure that there was no more than one point within a pixel.

Table 4.3. List of variables used in the study

Spectral variables	
Blue band (B)	Atmospherically resistant vegetation index (ARVI)
Green band (G)	Green normalised difference vegetation index (GNDVI)
Red band (R)	Red green blue vegetation index (RGBVI)
Near-infrared band (NIR)	Modified green red vegetation index (MGRVI)
Simple ratio index (SR)	Optimised soil-adjusted vegetation index (OSAVI)
Normalised difference vegetation index (NDVI)	Principal component 1 (PC1)
Enhanced vegetation index (EVI)	
Normalised difference water index (NDWI)	
Modified soil-adjusted vegetation index 2 (MSAVI2)	
Textural variables	
Mean, contrast, variance and correlation (computed for B, G, R and NIR)	
Topographic variables	
Elevation	Slope

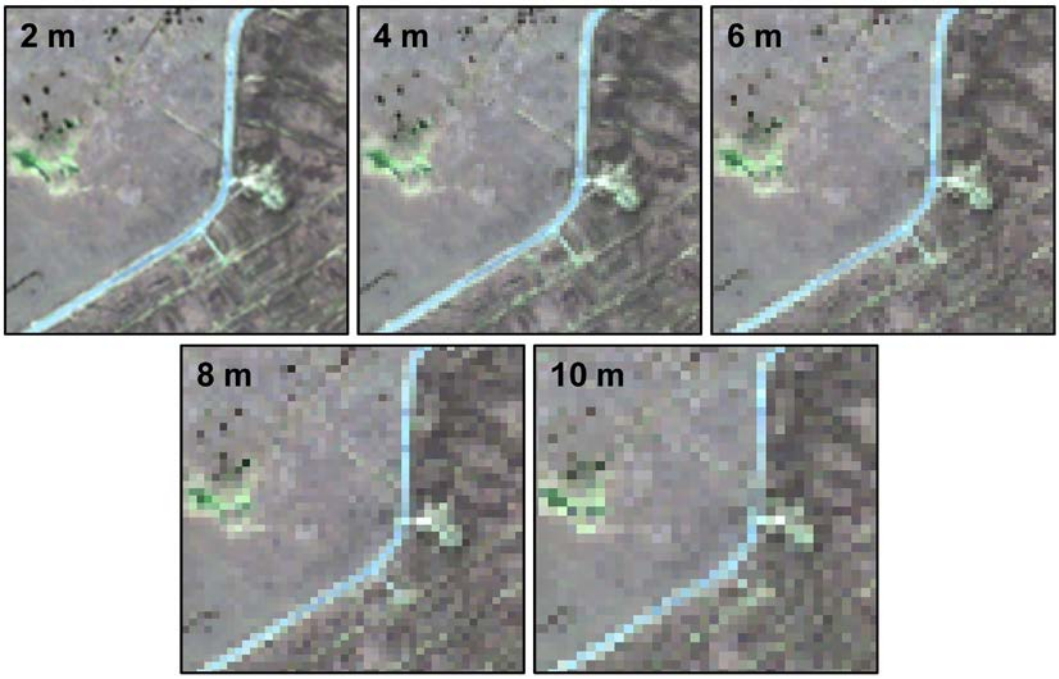

Figure 4.3. Resampled images (original 2-m resolution pixel size to 4-, 6-, 8- and 10-m resolutions). Reproduced from Cruz *et al.* (2024); licensed under CC BY 4.0 (https://creativecommons.org/licenses/by/4.0/).

Model development and validation

The Scikit-learn Python library (Pedregosa *et al.*, 2011) was used to implement the RF technique. This technique was applied to each dataset (i.e. variables of different spatial resolutions) to create a habitat classification model. Thus, five models were developed for each site. Each model was evaluated using the *k*-fold cross-validation method. In this method, the points were randomly divided into *k* subsets or folds of approximately equal size. Each fold was used to evaluate the model, which was trained on the remaining $k-1$ folds; this process was repeated until all folds were used in the validation (Berrar, 2019). Five folds were used in this study, which means that the model training and validation process was repeated five times. The average and standard error of the accuracy scores were then computed across these

five folds. The final model to predict the pixel labels for the entire study site used all the points. In addition, the relative importance of variables for each model was analysed based on mean decrease in impurity (Breiman *et al*., 1984).

Model prediction

Using the final model developed for each site, we generated two predictions: habitat predictions (crisp) and habitat probability predictions (fuzzy). The predict() function in Scikit-learn was used to return the predicted class for each pixel, i.e. the class with the highest probability across all the decision trees, generating a single image with row and column dimensions similar to the input satellite image. The predict_proba() function was used to return a vector of class probabilities within the interval [0,1] for each pixel, which was computed by averaging the class-predicted probabilities of all the decision trees. This latter function generates multiple images where each image represents the probabilities for a different habitat considered by the model (i.e. one image for each habitat).

To help visualise the spatial confidence of the classification associated with probabilities, we used entropy. In machine learning, entropy is defined as a measure of purity in a dataset (Shannon, 1948). It is computed by:

$$E(p) = -\sum_{n=1}^{c} p_i log_2 p_i,$$

where p is the probabilities obtained from the fuzzy classification. The value of entropy is inversely proportional to the confidence in the prediction. In other words, the entropy value is low for high-confidence predictions (peaky probability distribution), and the entropy value is high for low-confidence predictions (flat probability distribution). For example, if two pixels have probability predictions of (0.05, 0.90, 0.05) and (0.35, 0.40, 0.25), it can be considered that the first pixel was predicted with a higher level of confidence, i.e. having lower a entropy value, than the second pixel.

4.3 Results

4.3.1 Effect of spatial resolution on mapping upland habitats

Table 4.4 summarises the results obtained by the five-fold cross-validation method for WM and SM models trained at five different spatial resolutions. Overall, the models trained using a higher spatial resolution dataset generally achieved better performance. For both sites, the models trained on 2-m-resolution datasets had the highest mean accuracy (WM_2m, 80.34%; SM_2m, 79.64%), followed by models trained on 4-m-resolution datasets (WM_4m and SM_4m) with an accuracy of 77–79%. Furthermore, there was a decrease in accuracy of about 4–7% when the coarser 10-m-resolution datasets were used for model training compared with when the 2-m-resolution datasets were used. However, this trend of higher spatial resolution datasets leading to better classification accuracy was not always the case. For example, the coarser resolution-based WM_8m model achieved a higher accuracy (75.94%) than the WM_6m model (73.71%). Similarly, the SM_10m model performed better than the SM_8m model (75.44% vs 73.83%).

The contributions of each input variable to the model predictions are summarised in Figure 4.4. In general, spectral variables consistently showed higher importance for both sites, while textural variables presented lower importance values. It can be observed that the importance of variables varied depending

Table 4.4. Five-fold cross-validation mean accuracy and standard error results for WM and SM models

Wicklow Mountains site			Slieve Mish Mountains site		
Model	**Mean accuracy (%)**	**SE**	**Model**	**Mean accuracy (%)**	**SE**
WM_2m	80.34	3.78	SM_2m	79.64	5.43
WM_4m	77.47	3.21	SM_4m	78.78	5.15
WM_6m	73.71	3.92	SM_6m	77.81	6.34
WM_8m	75.94	2.10	SM_8m	73.83	6.25
WM_10m	73.55	1.95	SM_10m	75.44	7.61

SE, standard error.

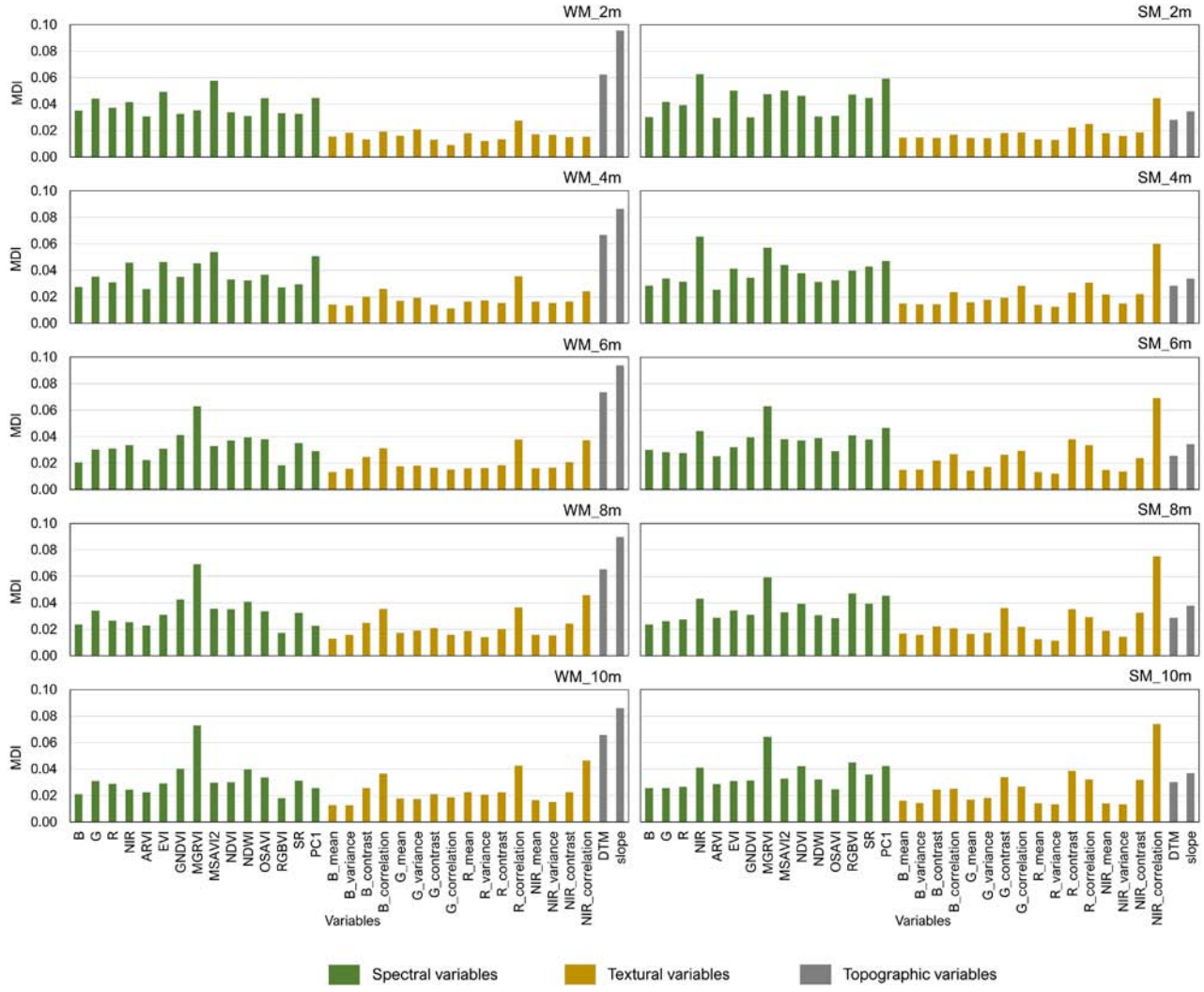

Figure 4.4. Variable importance scores for WM and SM models at different spatial resolutions. The *x*-axes display the input variables analysed in the study, while the *y*-axes represent the variable importance scores calculated using mean decrease in impurity. Reproduced from Cruz *et al*. (2024); licensed under CC BY 4.0 (https://creativecommons.org/licenses/by/4.0/).

on the spatial resolution of the datasets used in the modelling. For example, the importance of textural variables increased gradually as the spatial resolution coarsened, whereas, for spectral variables, their importance values slightly decreased with lower spatial resolutions. Elevation and slope variables showed almost the same importance values across spatial resolutions.

Models for each site exhibited different important variables. The elevation and slope, representing the topography of the site, were often ranked as the most important variables in relation to the WM models. Conversely, the modified green red vegetation index and near-infrared correlation textural variable were the most important variables in the majority of the SM models (Figure 4.4). Figure 4.5 shows the crisp RF-based classified images of a part of the WM site to compare the impact of using different spatial resolution datasets on model outputs. Overall, classification results across the five spatial resolutions demonstrated comparable patterns of habitat distributions, with greater spatial detail in the 2-m-classified image. These details, however, differed depending on the spatial resolution used. For example, the size of mapped water bodies within the encircled section of Figure 4.5 increased when using lower spatial resolutions. Similar trends were observed for patches of eroding blanket bogs.

Figure 4.6 displays the areal proportions of habitats as classified using different resolutions for the WM and SM sites. No significant differences were observed in the areal proportions between the different habitats.

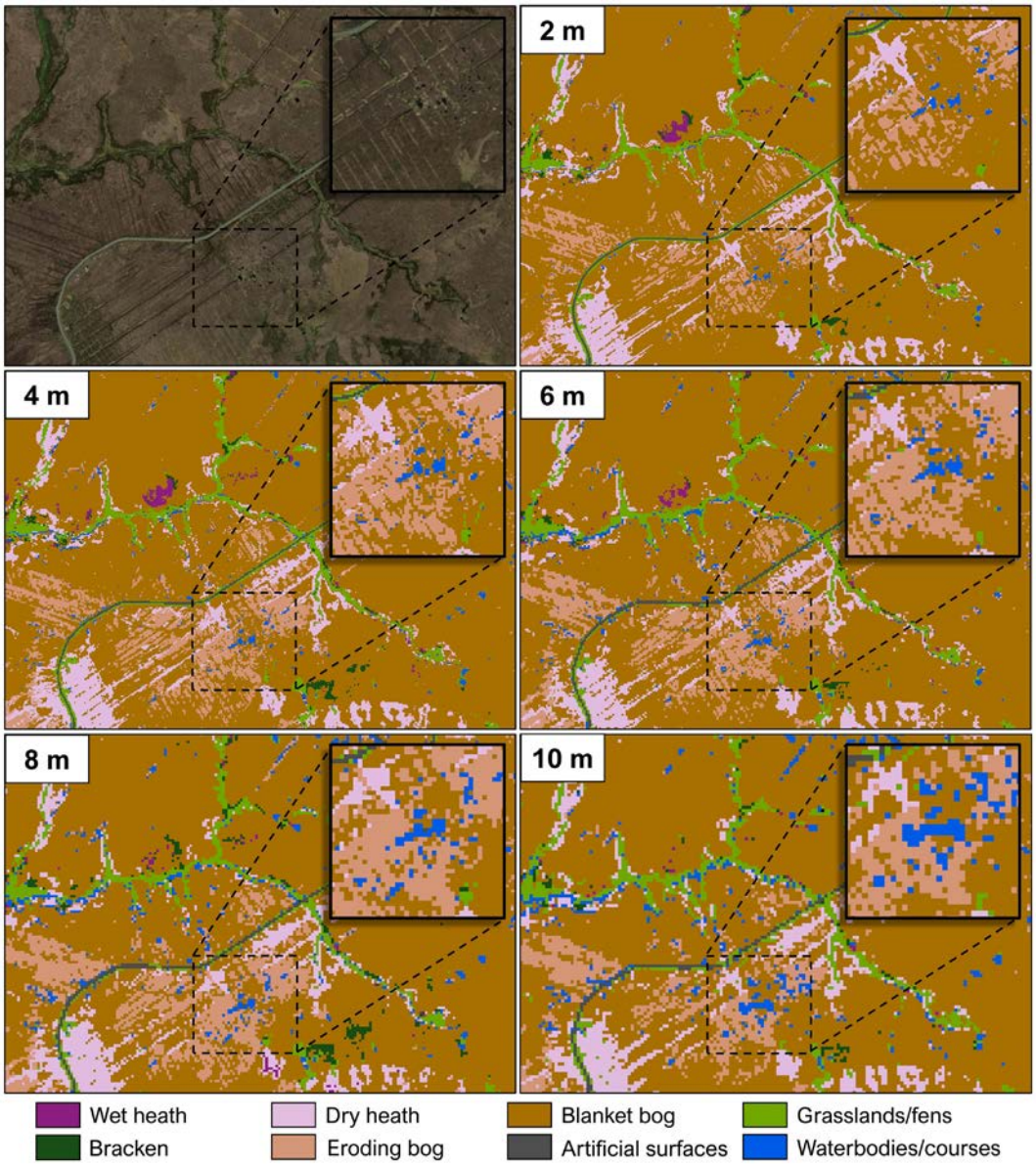

Figure 4.5. Crisp classification results over a portion of the WM site (top left) based on five spatial resolutions (2–10 m). The inset squares illustrate larger water bodies with lower spatial resolution. Reproduced from Cruz *et al.* (2024); licensed under CC BY 4.0 (https://creativecommons.org/licenses/by/4.0/).

However, it can be observed that habitats with the smallest proportions generally increased in size with lower spatial resolutions.

4.3.2 Model predictions

Figure 4.7 shows the crisp and fuzzy classification results over a portion of the WM site (Figure 4.7a). In the crisp classification result (Figure 4.7b), each pixel was characterised by a single habitat type. In contrast, the fuzzy classification results (Figure 4.7c–k) represented the probability of each habitat being present on each pixel, i.e. there was one greyscale image for every habitat type. Hence, the number of output fuzzy images corresponds to the number of habitats considered in the modelling. The white pixels in the image indicate areas where a particular habitat was predicted to be 100% present in that pixel. For example, blanket bog (Figure 4.7e) and grasslands/fens and flushes (Figure 4.7f) were some of the habitats that were distinctly separated from their surroundings. In contrast, black pixels represent those areas where a habitat was predicted with 0% probability, indicating its absence in that pixel. Grey pixels, therefore, denote predictions that fall between 0.0 and 1.0. These predictions could suggest areas

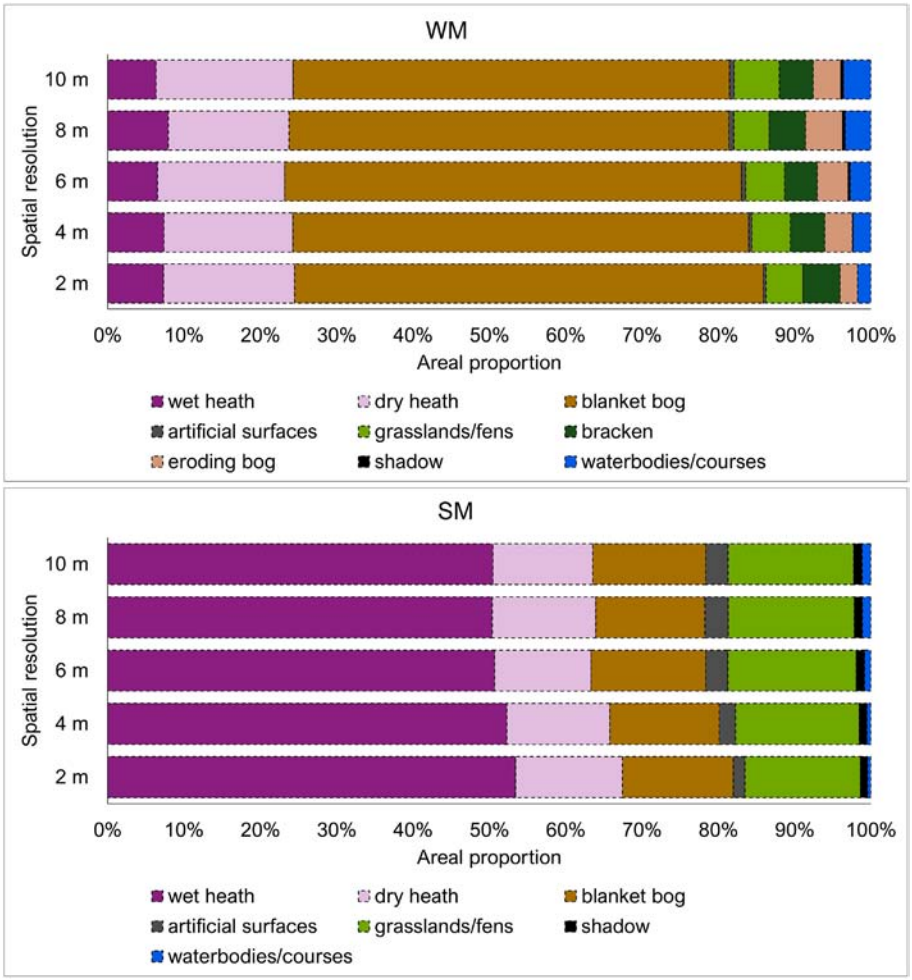

Figure 4.6. Areal proportion for each habitat from the model classification results for WM and SM sites. Reproduced from Cruz *et al.* (2024); licensed under CC BY 4.0 (https://creativecommons.org/licenses/by/4.0/).

of mixed habitats. The total of all the probabilities in a pixel adds up to 1.0. The complete crisp and fuzzy classification results for WM and SM sites can be found in Cruz *et al*. (2024).

4.3.3 Distribution and extent of upland habitats

The WM site (Figure 4.8a) was dominated by blanket bogs, covering almost 60% of the site. This habitat was most extensive on a relatively flat or gently sloping higher altitude part of the site (Figure 4.8b and c). Large areas of wet heath and dry heath were found on the hillsides, where the terrain was characterised by steep slopes (Figure 4.8b and c). In these areas, mosaics of dense bracken and grasslands/fens were also present. Eroding blanket bog areas were located near the roads (i.e. classified as artificial surfaces) and often occurred in straight parallel lines, intermixed with dry heath. The site was also characterised by a big lake in the north and several small bog pools around the centre of the map; both were classified as water bodies/courses (Figure 4.8c).

The colour scale of the entropy image (Figure 4.8d) indicates the level of certainty in the classification, i.e. light pixels being more confident and dark pixels being less confident. The areas mapped as blanket bogs and as other common features that are spectrally distinct, such as water bodies and roads, were classified with a high level of certainty, as observed by the light colour on the map (Figure 4.8d). However, most wet heath or dry heath areas were classified with less certainty.

The SM site (Figure 4.9a) was covered by about 50% wet heath. This habitat was mainly located at lower altitudes of the site and where the slope was less steep. As the altitude increased and the slope

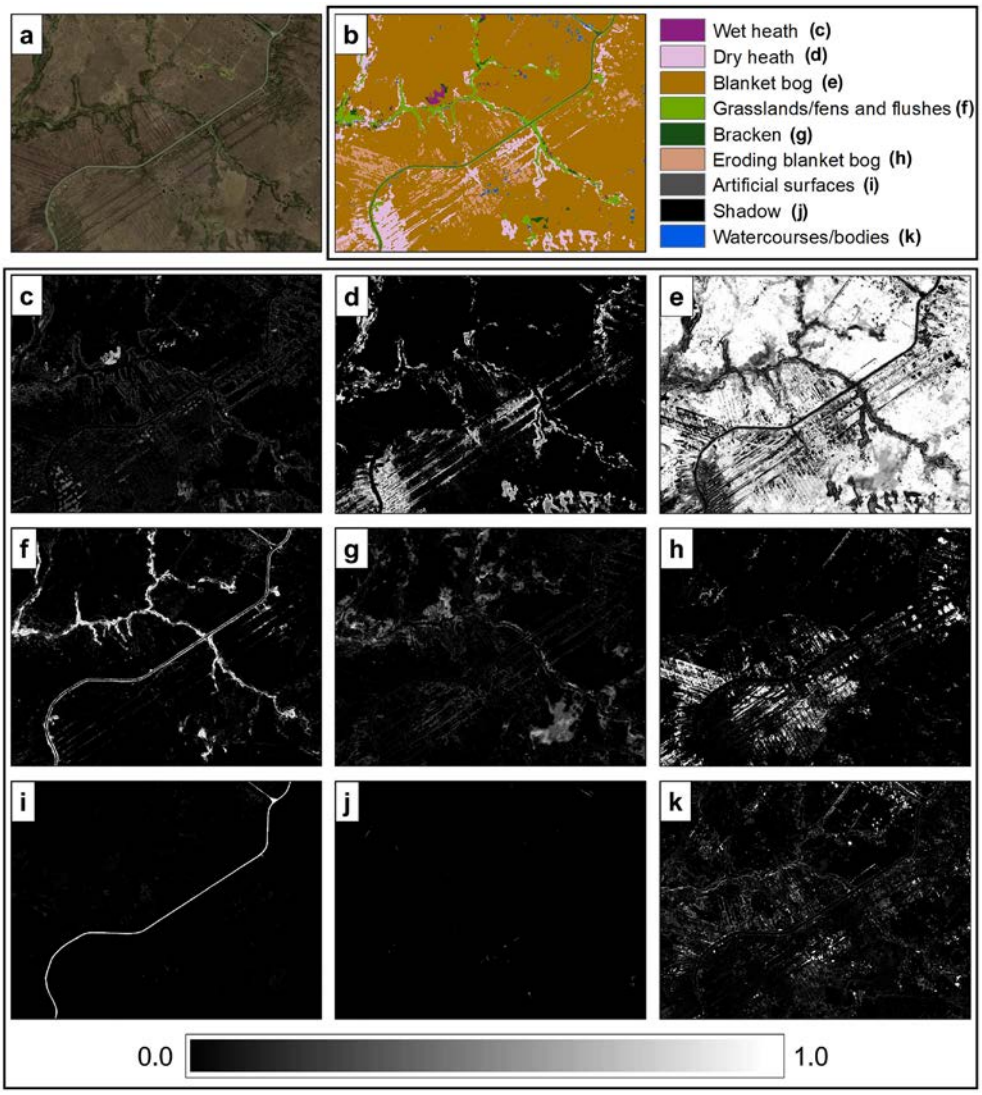

Figure 4.7. The WM site (a) and the corresponding crisp (b) and fuzzy (c–k) classification results. The colour scale at the bottom represents the probability of each habitat being present in every pixel. Reproduced from Cruz *et al.* (2024); licensed under CC BY 4.0 (https://creativecommons.org/licenses/by/4.0/).

gradually became steep, the wet heath habitat transitioned into mosaics of blanket bogs, dry heath and grasslands/fens (Figure 4.9b and c). Patches of exposed rocks/scree were scattered across the site. The site was also crossed by narrow watercourses. Shadow was recorded in the north-western part of the SM site owing to the quite steep slope obscuring the actual habitat. The entropy image (Figure 4.9d) showed that the dominant cover (wet heath) areas were classified with a high level of certainty, i.e. low entropy. In contrast, dry heath and blanket bog were the areas mapped with less certainty, illustrating ambiguity in the prediction, possibly owing to these habitats occurring in mosaics.

4.4 Discussion

This study demonstrates the potential of using high-resolution Pleiades satellite imagery and RF machine learning to accurately map upland habitats in two designated upland sites. The spatial distribution maps produced using the developed RF models provide essential information on the extent and location of protected habitats, as well as on the degraded versions of blanket bogs. The methodology was designed to evaluate the impact of varying image spatial resolutions on classification accuracy. Our results showed that using finer spatial resolution data generally leads to improved classification accuracy, consistent with other satellite-based remote sensing

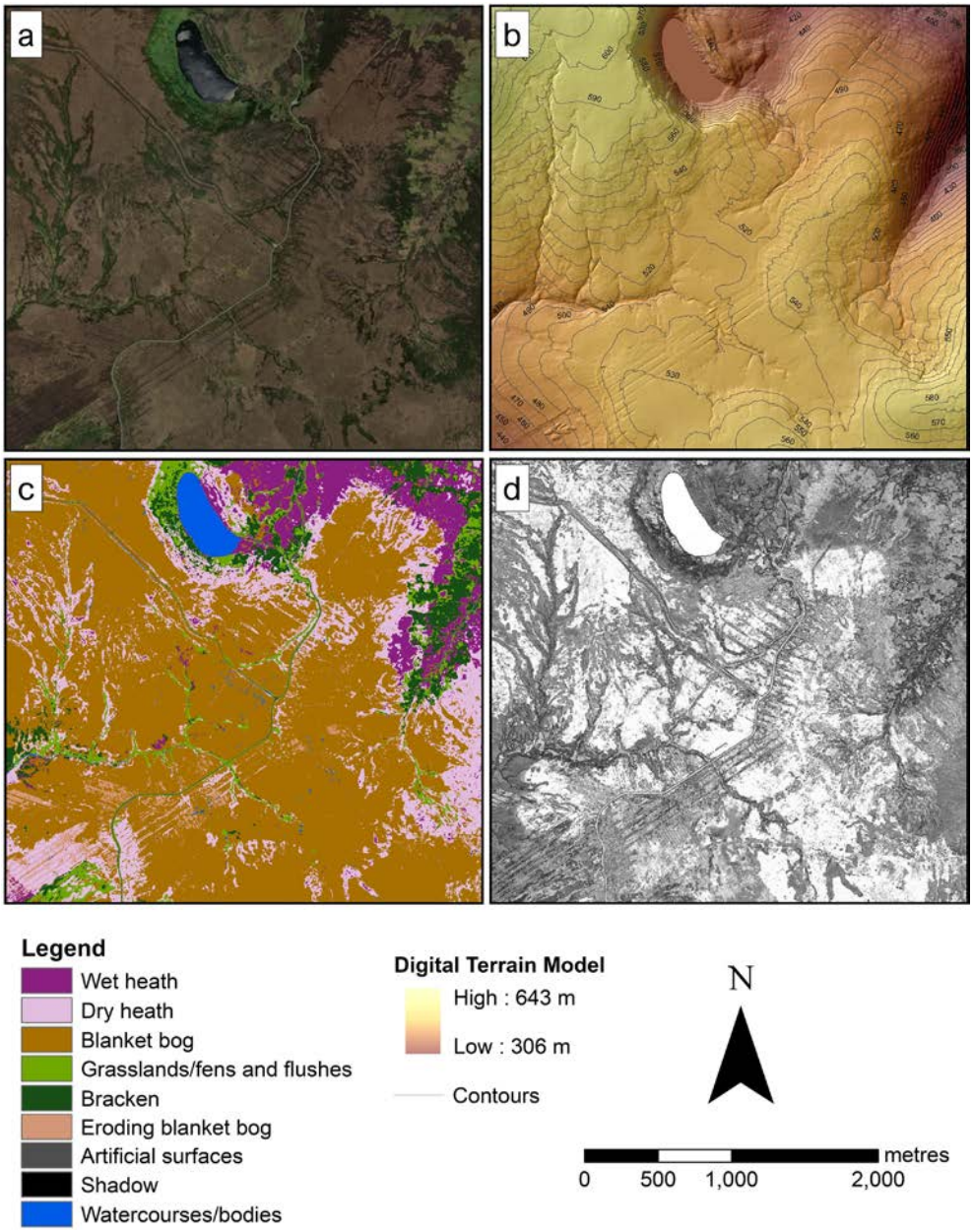

Figure 4.8. Basemap (a) and the DTM (b) of the WM site, and the corresponding crisp classification result (c) and entropy image (d) for the 2-m-resolution model. The shades in (d) represent the level of certainty, with lighter shades being more certain and darker shades being less certain. Reproduced from Cruz *et al*. (2024); licensed under CC BY 4.0 (https://creativecommons.org/licenses/by/4.0/).

studies (Boyle *et al*., 2014; Dorji and Fearns, 2017; Fisher *et al*., 2017). The observed differences between the area of each habitat, depending on what spatial resolution was used in the modelling (see Figure 4.6), could be explained by the lower spatial resolution imagery overestimating and underestimating different habitats. In our study, habitats that occurred as small patches, such as bog pools, were highly influenced by an overestimation of area, while dominant habitats, such as blanket bogs and heath, were affected by an underestimation of area when a lower spatial resolution image was used (see Figures 4.5 and 4.6). This finding has implications when using freely available satellite imagery, such as Sentinel-2 and Landsat-8, for assessing highly heterogeneous or fragmented landscapes. A coarse-resolution image may under- or overestimate the actual size of different habitats.

While our results showed only slight differences in the computed area when mapping with different spatial resolutions (Δ_{ave} = 14.7 ha between the 2-m- and 10-m-resolution images), this may lead to a more

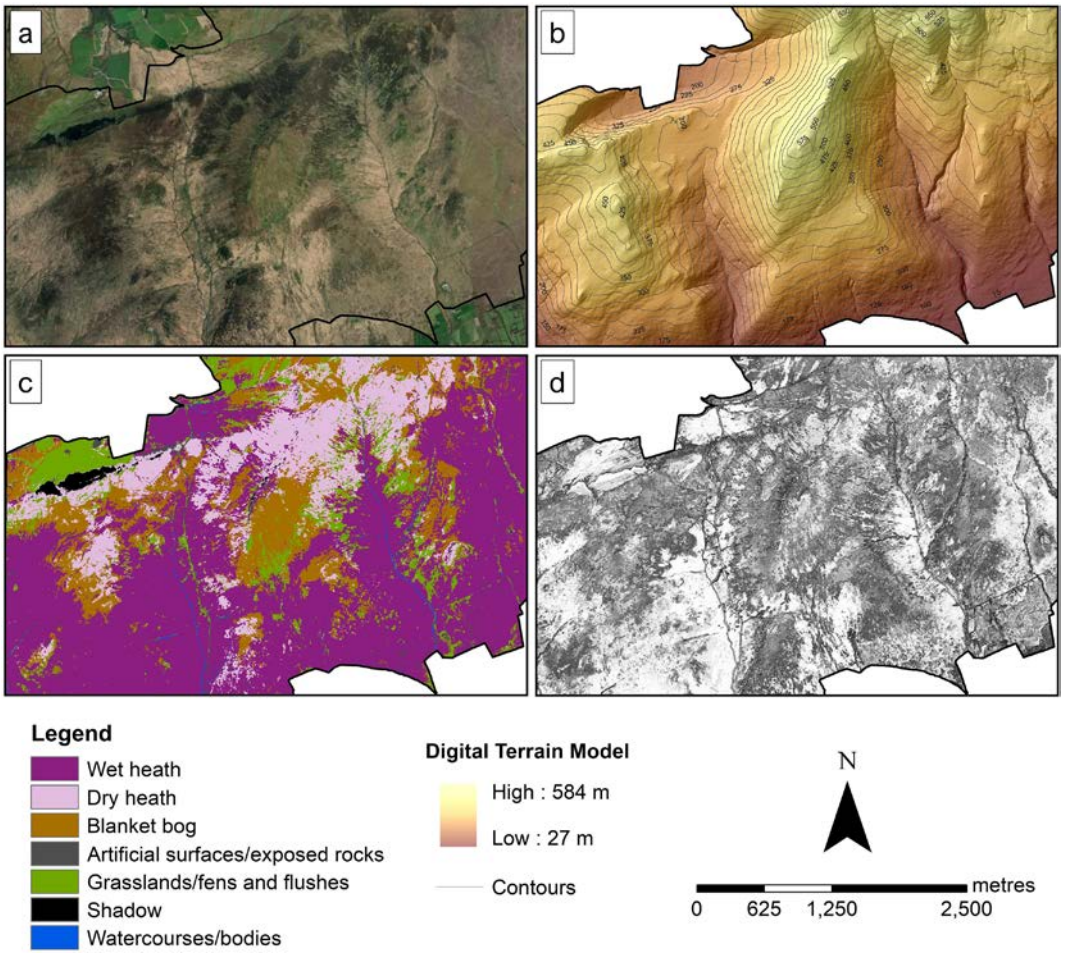

Figure 4.9. The basemap (a) and the DTM (b) of SM, and the corresponding crisp classification result (c) and entropy image (d) for the 2-m-resolution model. The shades in (d) represent the level of certainty, with lighter shades being more certain and darker shades being less certain. Reproduced from Cruz *et al.* (2024); licensed under CC BY 4.0 (https://creativecommons.org/licenses/by/4.0/).

significant difference if the mapping is conducted on a regional scale. This variation in habitat areas may lead to inaccurate assessments and reporting of the actual habitat status (Hernando *et al*., 2017). Therefore, it is important to consider using an image with a fixed spatial resolution when monitoring habitats with remote sensing to ensure reliability in reporting spatial extents and accurately measuring the change over time. Reporting the spatial resolution of the data used in the analysis is also crucial.

Our study also compared two RF mapping techniques in classifying upland habitats: crisp and fuzzy. Both techniques can map the general distribution of upland habitats at the WM and SM sites. In the crisp classification technique, the distribution of upland habitats is presented as a single map. However, this technique (i.e. assigning one habitat per pixel) may oversimplify the typical complex distributions of upland habitats observed in the field, especially when using images of lower spatial resolutions (Figure 4.5). In the fuzzy classification technique, the distribution of habitats is presented in multiple maps, providing rich information (probabilities of habitat occurrence per pixel) about the habitat composition and patterns (Figure 4.7c–k). The technique can also be applied to detect transition zones between habitats. These zones are observed as the spatial transition in the probability of a habitat from high to low, and, in the same area, an inverse pattern of probability change (i.e. from low to high) is exhibited by another habitat (Feilhauer *et al*., 2021). The study of de Klerk *et al*. (2018) also used probability maps to further describe and categorise transition zones – depending on their widths – as sharp, moderate and slow transitions. While these zones can be mapped as separate classes using the crisp technique, this may result in many classes, making it difficult to interpret the map (Feilhauer *et al*., 2021).

Our study also demonstrated the use of entropy images as a measure to estimate confidence predictions. Previous studies have also proposed other measures, such as confusion indices and RGB colour blend images, for estimating confidence in predictions generated from fuzzy classification (Duff *et al*., 2014; Feilhauer *et al*., 2021; Zlinszky and Kania, 2016). Understanding a set of fuzzy maps may not be straightforward, especially for non-specialist users; therefore, most fuzzy maps are converted to a single crisp classified map (Zlinszky and Kania, 2016). While conservation managers may prefer using crisp classification maps because they are generally easy to interpret, they can also benefit from entropy images. These images can be used to identify areas on the crisp classified map that are most likely occupied by mosaics of habitats and not just by a single habitat that the crisp classified map indicates. This could suggest that using entropy images can have a more practical significance when mapping with freely accessible satellite images (e.g. Landsat-8 and Sentinel-2), as their coarse spatial resolutions would mean that a single pixel most likely covers more than one habitat. Also, areas on the map with higher entropy values are considered less accurate than areas with lower entropy values; further assessment of these less accurate areas is recommended, especially if they were previously assessed with lower entropy values, i.e. considered highly accurate. Therefore, this finding suggests that presenting habitat distribution with a crisp classified map can be supplemented with the corresponding entropy image, as the latter provides additional information about the confidence in predictions.

Our results highlighted that small or narrow patches were clearly mapped in higher spatial resolution imagery. Detecting small but important features on the map may help better assess the habitat condition. For example, eroding blanket bogs, which are often characterised by a network of channels occurring in linear patterns (Fossitt, 2000), were visibly delineated on the WM_2m map (Figure 4.8c). Missed detection of small-sized degradation may lead to false conclusions on the habitat status. Moreover, the information on locations of these eroding bogs (i.e. mapped closer to the road) may indicate that bogs closer to the road are more vulnerable to anthropogenic activities, such as drainage and turf cutting, than those located far from the road. In the report of Perrin *et al*. (2017), a lot of the eroding of bogs at the WM site is the result of peat extraction by hand and using sausage machines. Therefore, creating detailed and accurate maps has an important implication for conservation and can be used to propose recommendations, e.g. bogs closer to the road require special attention for protection, as the soil carbon loss in these areas may be significant.

Overall, while there is a high cost involved in acquiring higher resolution satellite data, the detailed information they can provide is of utmost importance in habitat conservation, particularly in spatially extensive, heterogeneously complex landscapes. The crisp and fuzzy mapping approaches presented here can also be used to represent the natural complexity of the spatial distribution of upland habitats. Future studies can explore applying these approaches for mapping uplands more extensively, as well as mapping dynamic habitats, such as coastal areas, and those with spectrally similar vegetation communities, such as grasslands.

4.5 Conclusion

Our study used high-resolution satellite imagery and RF machine learning to map upland habitats. Using higher spatial resolution imagery generally improves mapping accuracy. In the two upland sites we studied, the highest accuracy maps were obtained (WM site, 80.34%; SM site, 79.64%) with the 2-m-resolution datasets. These maps provide information on the spatial distribution of habitats in great detail. Coarser spatial resolution datasets, however, resulted in a reduction of the accuracy and a slight overestimation of area for narrow and small-sized habitats. Therefore, a higher spatial resolution dataset is preferred if mapping habitats in a more heterogeneous landscape. Our study also demonstrated the use of crisp and fuzzy classification techniques in mapping upland habitats. Crisp classification results in a single habitat map, which is relatively easy to interpret. Fuzzy classification delivers probability maps for each habitat considered in the modelling. While these maps may be more difficult to interpret, they can represent the typical complex mosaics and gradual transitions of upland habitats as observed in the field. They can also be used to describe spatial confidence in the classification through computing the entropy. Using fuzzy classified maps has the potential to improve our understanding of nature's fuzzy patterns.

5 Conclusions and Recommendations

The following are the main conclusions that can be drawn from this research.

- High-resolution UAV data (images and DSMs), combined with field-based data, can effectively and accurately map the distributions of Annex I habitats and degradation and presence of invasive species using the RF machine learning algorithm.
- Applying methods to assess changes in seasonal vegetation colour is crucial in producing robust and accurate habitat distribution maps. This can be done by modelling to determine which period of the growing season is the optimum period for habitat classification, i.e. when spectral differences between vegetation are more enhanced, or by using data augmentation techniques of deep learning to simulate the colour of the target plant species at any period of the year or time of the day.
- Augmentation and pseudo-labelling techniques can be used to increase the amount and diversity of training data, resulting in more robust classification models.
- Deep learning can offer a more efficient way of tracking invasive species, facilitating timely and targeted implementation of intervention measures.
- The combination of satellite imagery and fuzzy classification based on the RF algorithm has shown promising results for mapping complex mosaics of habitats in uplands where the deployment of UAVs may be challenging.
- There is no one-size-fits-all mapping methodology for habitat monitoring. An integration of methods can deal with different scenarios and diverse application areas.
- The high-resolution data machine learning approach can provide quantitative information for assessing highly valued habitats. Although the research focuses on specific habitats at selected sites, the approaches presented here are fully adaptable and reproducible to mapping different habitats and plant species. These technologies have the potential to be a vital source of valuable information, and they can be operationalised and integrated into existing monitoring initiatives.

There are limitations related to data acquisition and processing. These limitations indicate significant areas for future work. In the broader context of habitat mapping with remote sensing and machine learning, examples of areas for future work are outlined below.

5.1 Model Transferability

One of the key recommendations of iHabiMap is the transferability of machine learning models, i.e. the ability of a model to use previously obtained knowledge and apply this to a new task. In general, most models are used to perform a single task and may not perform well for future tasks, unless a large amount of training data specific to the task is available. In habitat mapping and monitoring, transferability can be characterised as the ability of a model trained on a particular site or at a specific period to be applied to different sites or periods (Tuanmu *et al*., 2011). Future work is encouraged to improve both the spatial and temporal transferability of trained models.

5.2 Testing of the Presented Methodologies on Images Acquired by Occupied Airborne Platforms (i.e. Aircraft)

iHabiMap focused on developing habitat mapping methodologies using high-resolution images acquired by UAVs and commercial satellite platforms. Aerial data are also important, as they are the intermediate platform between satellites and UAV platforms in terms of spatial extent, flexibility and endurance in data acquisition (Matese *et al*., 2015). Aircraft can mount a wide range of sensors for acquiring high spatial resolution data. Aircraft surveys can be flexible, and thus key phenological stages of vegetation can also be targeted. They can cover significantly larger areas than UAVs. Further work is needed to explore the

applicability of models to multispectral images and elevation models obtained from aircraft.

5.3 Using Data Acquired by Unoccupied Aerial Vehicle-mounted Hyperspectral Camera and Light Detection and Radiation

A recent technological innovation is the development of UAV platforms that can carry more sophisticated sensors, such as hyperspectral cameras and LiDAR (light detection and ranging) equipment. A hyperspectral camera is a sensor that can acquire images of hundreds of narrow and contiguous spectral bands. The information from these bands can allow for detecting subtle spectral differences between vegetation types. LiDAR is a type of remote sensing that measures laser pulses, which can provide detailed information on the structure and height of vegetation. This information may improve the modelling for monitoring, especially for botanically complex environments such as semi-natural grasslands or woodlands. As technologies continue to progress, the methodologies are also expected to be updated accordingly.

5.4 Collaboration among Remote Sensing Analysts, Ecologists and Conservation Managers

Habitat mapping using remote sensing and machine learning technologies requires extensive knowledge from domain experts in ecology. iHabiMap is a product of much dialogue between ecologists, remote sensing experts and machine learning experts. It shows the significance of interdisciplinary dialogue. Ecologists' knowledge is crucial for collecting high-quality field data for the training and evaluation of models. This type of collaboration is essential to produce accurate and reliable models for habitat-monitoring efforts.

Further collaboration between experts is needed for more specific applications of these technologies in habitat and biodiversity conservation. These include assessing functional plant traits, producing essential biodiversity variables and modelling the impact of natural and anthropogenic factors on habitats.

iHabiMap Outputs

Peer-reviewed publications:

Cruz, C., Perrin, P.M., Martin, J.R., O'Connell, J., McGuinness, K. and Connolly, J., 2024. Mapping of temperate upland habitats using high-resolution satellite imagery and machine learning. *Environmental Monitoring and Assessment*, 196(9). https://doi.org/10.1007/s10661-024-12998-0

Cruz, C., McGuinness, K., O'Connell, J., Perrin, P., Martin, J. and Connolly, J., 2023. Improving deep learning-based mapping of coastal invasive species from UAV imagery. *International Journal of Remote Sensing* 44: 5712–5735. https://doi.org/10.1080/01431161.2023.2251186

Cruz, C., O'Connell, J., McGuinness, K., Martin, J., Perrin, P. and Connolly, J., 2023. Assessing the effectiveness of UAV data to accurately map coastal dune habitats. *European Journal of Remote Sensing* 56(1): 2191870. https://doi.org/10.1080/22797254.2023.2191870

Conference presentations:

Cruz, C., O'Connell, J., Martin, J., Perrin, P. and Connolly, J., 2024. Drones and machine learning for habitat monitoring. Paper presented at the European Geosciences Union General Assembly, Vienna, 14 to 19 April.

Cruz, C., McGuinness, K., Perrin, P.M., O'Connell, J., Martin, J.R. and Connolly, J., 2023. Improving deep learning-based mapping of coastal invasive species from UAV imagery. Paper presented at the Remote Sensing and Photogrammetry Society Conference, Keyworth, 5 to 6 September.

Connolly, J., Habib, W., Cruz, C. and Gilet, L., 2023. A multi-scale geospatial assessment of peatlands in Ireland. Paper presented at the RE3 Conference, Quebec, 9 to 16 June.

Cruz, C. and Connolly, J., 2023. Mapping Irish habitat types using drones and machine learning. Paper presented at Environ 2023, Atlantic University, Letterkenny, Co. Donegal, 3 to 5 April.

Cruz, C., O'Connell, J., McGuiness, K., Martin, J.R., Perrin, P.M. and Connolly, J, 2022. Drones and machine learning for accurate and fine-grained mapping of Irish habitat types. Paper presented at the 14th Irish Earth Observation Symposium, Technological University Dublin, 3 to 4 November.

O'Connell, J., Chavan, C., Cruz, C., Connolly, J., McGuinness, K., Martin, J.R. and Perrin, P.M., 2022. Challenges in the use of EO and machine learning in the monitoring of natural habitats. Paper presented at the 14th Irish Earth Observation Symposium, Technological University Dublin, 3 to 4 November.

Cruz, C., O'Connell, J., McGuiness, K., Martin, J.R., Perrin, P.M. and Connolly, J., 2022. Can UAVs be used as an effective tool to capture the spatial distributions of habitat types? Paper presented at the XXIV International Society for Photogrammetry and Remote Sensing Congress, Nice, 6 to 11 June.

Cruz, C., Connolly, J., Martin, J.R., McGuinness, K., O'Connell, J. and Perrin, P.M., 2021. UAV-based approach for fine-scale mapping of habitats. Paper presented at the Conference of Irish Geographers, Trinity College Dublin, 18 to 21 May.

Cruz, C., McGuinness, K., O'Connell, J., Martin, J.R., Perrin, P.M. and Connolly, J., 2021. Habitat mapping in coastal dunes using random forest classification of UAV images. Paper presented at the European Geosciences Union General Assembly, online, 19 to 30 April. https://doi.org/10.5194/egusphere-egu21-6301

Cruz, C., O'Connell, J., McGuinness, K., Martin, J.R., Perrin, P.M. and Connolly, J., 2020. Habitat mapping, assessment and monitoring using high-resolution imagery. Paper presented at the 5thAnnual Insight Student Conference, National University of Ireland, Galway, 12 February.

Cruz, C., O'Connell, J., McGuinness, K., Martin, J., Perrin, P. and Connolly, J., 2019. iHabiMap: habitat mapping, monitoring and assessment using high-resolution imagery. Paper presented at the 13th Irish Earth Observation Symposium, National University of Ireland Galway, 5 to 6 November. Available online: https://doras.dcu.ie/24004/ (accessed 8 October 2024).

PhD thesis:

Cruz, C., 2024. High-resolution remote sensing data and machine learning approaches for mapping and monitoring habitats. PhD Thesis. Trinity College Dublin, Ireland. Available online: http://hdl.handle.net/2262/108437 (accessed 12 November 2024).

References

Ahmed, L., Iqbal, M.M., Aldabbas, H., Khalid, S., Saleem, Y. and Saeed, S., 2020. Images data practices for semantic segmentation of breast cancer using deep neural network. *Journal of Ambient Intelligence and Humanized Computing* 14: 15227–15243. https://doi.org/10.1007/s12652-020-01680-1

Amani, M., Salehi, B., Mahdavi, S., Granger, J.E., Brisco, B. and Hanson, A., 2017. Wetland classification using multi-source and multi-temporal optical remote sensing data in Newfoundland and Labrador, Canada. *Canadian Journal of Remote Sensing* 43(4): 360–373. https://doi.org/10.1080/07038992.2017.1346468

Anderson, K. and Gaston, K.J., 2013. Lightweight unmanned aerial vehicles will revolutionize spatial ecology. *Frontiers in Ecology and the Environment* 11(3): 138–146. https://doi.org/10.1890/120150

Assmann, J.J., Kerby, J.T., Cunliffe, A.M. and Myers-Smith, I.H., 2019. Vegetation monitoring using multispectral sensors – best practices and lessons learned from high latitudes. *Journal of Unmanned Vehicle Systems* 7(1): 54–75. https://doi.org/10.1139/juvs-2018-0018

Balado, J., Olabarria, C., Martínez-Sánchez, J., Rodríguez-Pérez, J.R. and Pedro, A., 2021. Semantic segmentation of major macroalgae in coastal environments using high-resolution ground imagery and deep learning. *International Journal of Remote Sensing* 42(5): 1785–1800. https://doi.org/10.1080/01431161.2020.1842543

Barbier, E.B., Hacker, S.D., Kennedy, C., Koch, E.W., Stier, A.C. and Silliman, B.R., 2011. The value of estuarine and coastal ecosystem services. *Ecological Monographs* 81(2): 169–193. https://doi.org/10.1890/10-1510.1

Barrett, B., Raab, C., Cawkwell, F. and Green, S., 2016. Upland vegetation mapping using random forests with optical and radar satellite data. *Remote Sensing in Ecology and Conservation* 2(4): 212–231. https://doi.org/10.1002/rse2.32

Belcore, E., Pittarello, M., Lingua, A.M. and Lonati, M., 2021. Mapping riparian habitats of Natura 2000 network (91E0*, 3240) at individual tree level using UAV multi-temporal and multi-spectral data. *Remote Sensing* 13: 1756. https://doi.org/10.3390/rs13091756

Belgiu, M. and Drăgut, L., 2016. Random forest in remote sensing: a review of applications and future directions. *ISPRS Journal of Photogrammetry and Remote Sensing* 114: 24–31. https://doi.org/10.1016/j.isprsjprs.2016.01.011

Bendig, J., Yu, K., Aasen, H., Bolten, A., Bennertz, S., Broscheit, J., Gnyp, M.L. and Bareth, G., 2015. Combining UAV-based plant height from crop surface models, visible, and near infrared vegetation indices for biomass monitoring in barley. *International Journal of Applied Earth Observation and Geoinformation* 39: 79–87. https://doi.org/10.1016/j.jag.2015.02.012

Berrar, D., 2019. Cross-validation. *Encyclopedia of Bioinformatics and Computational Biology* 1: 542–545. https://doi.org/10.1016/B978-0-12-809633-8.20349-X

Bhatnagar, S., Gill, L., Regan, S., Naughton, O., Johnston, P., Waldren, S. and Ghosh, B., 2020. Mapping vegetation communities inside wetlands using Sentinel-2 imagery in Ireland. *International Journal of Applied Earth Observation and Geoinformation* 88: 102083. https://doi.org/10.1016/j.jag.2020.102083

Bonn, A., Rebane, M. and Reid, C., 2008. Ecosystem services: a new rationale for conservation of upland environments. In Bonn, A., Allott, T., Hubacek, K. and Stewart, J. (eds), *Drivers of Environmental Change in Uplands*. First edition. Routledge, London, pp. 448–474. https://doi.org/10.4324/9780203886724

Boyle, S.A., Kennedy, C.M., Torres, J., Colman, K., Pérez-Estigarribia, P.E. and De La Sancha, N.U., 2014. High-resolution satellite imagery is an important yet underutilized resource in conservation biology. *PLOS ONE* 9(1): e86908. https://doi.org/10.1371/journal.pone.0086908

Breiman, L., 2001. Random forests. *Machine Learning* 45: 5–32. https://doi.org/10.1023/A:1010933404324

Breiman, L., Friedman, J.H., Olshen, R.A. and Stone, C.J., 1984. *Classification and Regression Trees*. CRC Press, New York.

Brophy, J.T., Perrin, P.M., Penk, M.R., Devaney, F.M. and Leyden, K.J., 2019. *Saltmarsh Monitoring Project 2017–2018*. National Parks and Wildlife Service, Dublin. Available online: http://hdl.handle.net/2262/89539 (accessed 8 October 2024).

Buchanan, G., Pearce-Higgins, J., Grant, M., Robertson, D. and Waterhouse, T., 2005. Characterization of moorland vegetation and the prediction of bird abundance using remote sensing. *Journal of Biogeography* 32(4): 697–707. https://doi.org/10.1111/j.1365-2699.2004.01187.x

Buslaev, A., Iglovikov, V.I., Khvedchenya, E., Parinov, A., Druzhinin, M. and Kalinin, A.A., 2020. Albumentations: fast and flexible image augmentations. *Information* 11(2): 125. https://doi.org/10.3390/info11020125

Cantrell, S.J., Christopherson, J.B., Anderson, C., Stensaas, G.L., Ramaseri Chandra, S.N., Kim, M. and Park, S., 2021. *System Characterization Report on the WorldView-3 Imager Version 1.1, October 2021*. U.S. Geological Survey Open-File Report 2021-1030-I, U.S. Geological Survey, Reston, VA. https://doi.org/10.3133/ofr20211030I

Carneiro, T., Da Nobrega, R.V.M., Nepomuceno, T., Bian, G.-B., De Albuquerque, V.H.C. and Filho, P.P.R., 2018. Performance analysis of Google Colaboratory as a tool for accelerating deep learning applications. *IEEE Access* 6: 61677–61685. https://doi.org/10.1109/ACCESS.2018.2874767

Chaurasia, A. and Culurciello, E., 2018. LinkNet: exploiting encoder representations for efficient semantic segmentation. *Proceedings of the IEEE Visual Communications and Image Processing Conference*, St. Petersburg, FL, 10 to 13 December, pp. 1–4. https://doi.org/10.1109/VCIP.2017.8305148

Chavez, P.S., 1988. An improved dark-object subtraction technique for atmospheric scattering correction of multispectral data. *Remote Sensing of Environment* 24(3): 459–479. https://doi.org/10.1016/0034-4257(88)90019-3

Chi, M., Plaza, A., Benediktsson, J.A., Sun, Z., Shen, J. and Zhu, Y., 2016. Big data for remote sensing: challenges and opportunities. *Proceedings of the IEEE* 104(11): 2207–2219. https://doi.org/10.1109/JPROC.2016.2598228

Chlap, P., Min, H., Vandenberg, N., Dowling, J., Holloway, L. and Haworth, A., 2021. A review of medical image data augmentation techniques for deep learning applications. *Journal of Medical Imaging and Radiation Oncology* 65(5): 545–563. https://doi.org/10.1111/1754-9485.13261

Connolly, J., 2018. Mapping land use on Irish peatlands using medium resolution satellite imagery. *Irish Geography* 51(2): 187–204. https://doi.org/10.55650/igj.2018.1371

Corbane, C., Lang, S., Pipkins, K., Alleaume, S., Deshayes, M., García Millán, V.E., Strasser, T., Vanden Borre, J., Toon, S. and Michael, F., 2015. Remote sensing for mapping natural habitats and their conservation status – new opportunities and challenges. *International Journal of Applied Earth Observation and Geoinformation* 37: 7–16. https://doi.org/10.1016/j.jag.2014.11.005

Crowle, A. and McCormack, F., 2009. Condition of upland terrestrial habitats. In Bonn, A., Allott, T., Hubacek, K. and Stewart, J. (eds), *Drivers of Environmental Change in Uplands*. Routledge, London, pp. 156–170.

Cruz, C., 2024. High-resolution remote sensing data and machine learning approaches for mapping and monitoring habitats. PhD Thesis. Trinity College Dublin, Ireland. Available online: http://hdl.handle.net/2262/108437 (accessed 12 November 2024).

Cruz, C., O'Connell, J., McGuinness, K., Martin, J.R., Perrin, P.M. and Connolly, J., 2023a. Assessing the effectiveness of UAV data for accurate coastal dune habitat mapping. *European Journal of Remote Sensing* 56(1): 2191870. https://doi.org/10.1080/22797254.2023.2191870

Cruz, C., McGuinness, K., Perrin, P.M., O'Connell, J., Martin, J.R. and Connolly, J., 2023b. Improving the mapping of coastal invasive species using UAV imagery and deep learning. *International Journal of Remote Sensing*, 44(18): 5713–5735. https://doi.org/10.1080/01431161.2023.2251186

Cruz, C., Perrin, P.M., Martin, J.R., O'Connell, J., McGuinness, K. and Connolly, J., 2024. Mapping of temperate upland habitats using high-resolution satellite imagery and machine learning. *Environmental Monitoring and Assessment* 196(9). https://doi.org/10.1007/s10661-024-12998-0

Cruzan, M.B., Weinstein, B.G., Grasty, M.R., Kohrn, B.F., Hendrickson, E.C., Arredondo, T.M. and Thompson, P.G., 2016. Small unmanned aerial vehicles (micro-UAVs, drones) in plant ecology. *Applications in Plant Sciences* 4(9): 1600041. https://doi.org/10.3732/apps.1600041

Curtis, T.G.F. and Sheehy Skeffington, M.J., 1998. The salt marshes of Ireland: an inventory and account of their geographical variation. *Biology and Environment: Proceedings of the Royal Irish Academy* 98B(2): 87–104.

de Klerk, H.M., Burgess, N.D. and Visser, V., 2018. Probabilistic description of vegetation ecotones using remote sensing. *Ecological Informatics* 46: 125–132. https://doi.org/10.1016/j.ecoinf.2018.06.001

Delaney, A., Devaney, F.M., Martin, J.M. and Barron, S.J., 2013. *Monitoring Survey of Annex I Sand Dune Habitats in Ireland*. Irish Wildlife Manuals No. 75. National Parks and Wildlife Service, Dublin, Ireland.

Deng, J., Dong, W., Socher, R., Li, L.-J., Li, K. and Fei-Fei, L., 2009. ImageNet: a large-scale hierarchical image database. *Proceedings of the 2009 IEEE Conference on Computer Vision and Pattern Recognition*, Miami, FL, 20 to 25 June, pp. 248–255. https://doi.org/10.1109/CVPR.2009.5206848

Doody, J.P., 2013. *Sand Dune Conservation, Management and Restoration*. Springer, New York. Available online: https://doi.org/10.1007/978-94-007-4731-9.

Dorji, P. and Fearns, P., 2017. Impact of the spatial resolution of satellite remote sensing sensors in the quantification of total suspended sediment concentration: a case study in turbid waters of northern Western Australia. *PLOS ONE* 12(4): e0175042. https://doi.org/10.1371/journal.pone.0175042

Drusch, M., Del Bello, U., Carlier, S., Colin, O., Fernandez, V., Gascon, F., Hoersch, B., Isola, C., Laberinti, P., Martimort, P., Meygret, A., Spoto, F., Sy, O., Marchese, F. and Bargellini, P., 2012. Sentinel-2: ESA's optical high-resolution mission for GMES operational services. *Remote Sensing of Environment* 120: 25–36. https://doi.org/10.1016/j.rse.2011.11.026

Duff, T.J., Bell, T.L. and York, A., 2014. Recognising fuzzy vegetation pattern: the spatial prediction of floristically defined fuzzy communities using species distribution modelling methods. *Journal of Vegetation Science* 25(2): 323–337. https://doi.org/10.1111/jvs.12092

EC (European Commission), 2011. Communication from the Commission to the European Parliament, the Council, the European Economic and Social Committee and the Committee of the Regions "Our life insurance, our natural capital: an EU Biodiversity Strategy to 2020". COM(2011) 244 final, 3.5.2011, Brussels.

EC (European Commission), 2013. *Interpretation Manual of European Union Habitats,* version EUR 28. European Commission, Brussels. Available online: http://ec.europa.eu/environment/nature/legislation/habitatsdirective/docs/Int_Manual_EU28.pdf (accessed 28 March 2023).

EC (European Commission), 2020. Communication from the Commission to the European Parliament, the Council, the European Economic and Social Committee and the Committee of the Regions "EU Biodiversity Strategy for 2030 bringing back nature into our lives". COM(2020) 380 final, 20.5.2020, Brussels. Available online: https://eur-lex.europa.eu/legal-content/EN/TXT/?uri=celex%3A52020DC0380 (accessed 8 October 2024).

EC (European Commission), 2022. Communication from the Commission to the European Parliament, the Council, the European Economic and Social Committee and the Committee of the Regions "Proposal for a Regulation of the European Parliament and of the Council on nature restoration". COM(2022) 304 final, 22.6.2022, Brussels. Available online: https://eur-lex.europa.eu/legal-content/EN/TXT/HTML/?uri=CELEX:52022PC0304&from=EN (accessed 8 October 2024).

Eisenbeiss, H., 2009. UAV photogrammetry. DSc Thesis. ETH Zurich, Switzerland. https://doi.org/10.3929/ethz-a-005939264

EPA (Environmental Protection Agency), 2020. *Ireland's Environment – An Integrated Assessment 2020*. EPA, Johnstown Castle, Ireland.

Ettritch, G., Bunting, P., Jones, G. and Hardy, A., 2018. Monitoring the coastal zone using earth observation: application of linear spectral unmixing to coastal dune systems in Wales. *Remote Sensing in Ecology and Conservation* 4(4): 303–319. https://doi.org/10.1002/rse2.79

European Council, 2023. Nature restoration: Council and Parliament reach agreement on new rules to restore and preserve degraded habitats in the EU. Available online: https://www.consilium.europa.eu/en/press/press-releases/2023/11/09/nature-restoration-council-and-parliament-reach-agreement-on-new-rules-to-restore-and-preserve-degraded-habitats-in-the-eu/ (accessed 25 September 2024).

European Environment Agency, 2020. *State of Nature in the EU: Results from Reporting under the Nature Directives 2013–2018*. EEA, Copenhagen, Denmark. https://doi.org/10.2800/705440

EU (European Union), 1992. Directive 92/43/EEC of the European Parliament and of the Council of 21 May 1992 on the conservation of natural habitats and of wild fauna and flora. OJ L 206, 22.7.1992, p. 7–50.

EU (European Union), 2014. Regulation (EU) No 1143/2014 of the European Parliament and the Council of 22 October 2014 on the prevention and management of the introduction and spread of invasive alien species. OJ L 317, 4.11.2014, p. 35–55. Available online: http://data.europa.eu/eli/reg/2014/1143/oj (accessed 8 October 2024).

EU (European Union), 2022. Decision (EU) 2022/591 of the European Parliament and of the Council of 6 April 2022 on a General Union Environment Action Programme to 2030. OJ L 114, 12.4.2022, p. 22–36. Available online: https://eur-lex.europa.eu/legal-content/EN/TXT/HTML/?uri=CELEX:32022D0591 (accessed 8 October 2024).

Evans, D., 2012. Building the European Union's Natura 2000 network. *Nature Conservation* 1: 11–26. https://doi.org/10.3897/natureconservation.1.1808

Fawagreh, K., Gaber, M.M. and Elyan, E., 2014. Random forests: from early developments to recent advancements. *Systems Science and Control Engineering* 2(1): 602–609. https://doi.org/10.1080/21642583.2014.956265

Feilhauer, H., Zlinszky, A., Kania, A., Foody, G.M., Doktor, D., Lausch, A. and Schmidtlein, S., 2021. Let your maps be fuzzy! — Class probabilities and floristic gradients as alternatives to crisp mapping for remote sensing of vegetation. *Remote Sensing in Ecology and Conservation* 7(2): 292–305. https://doi.org/10.1002/rse2.188

Fisher, P., 1997. The pixel: a snare and a delusion. *International Journal of Remote Sensing* 18(3): 679–685. https://doi.org/10.1080/014311697219015

Fisher, J., Acosta, E.A., Dennedy-Frank, P.J., Kroeger, T. and Boucher, T.M., 2017. Impact of satellite imagery spatial resolution on land use classification accuracy and modeled water quality. *Remote Sensing in Ecology and Conservation* 4(2): 137–149. https://doi.org/10.1002/rse2.61

Foody, G.M., 1996. Fuzzy modelling of vegetation from remotely sensed imagery. *Ecological Modelling* 85: 3–12. https://doi.org/10.1016/0304-3800(95)00012-7

Fossitt, J.A., 2000. *A Guide to Habitats in Ireland*. The Heritage Council, Dublin.

Fraser, R.H., Olthof, I., Lantz, T.C. and Schmitt, C., 2016. UAV photogrammetry for mapping vegetation in the low-Arctic. *Arctic Science* 2(3): 79–102. https://doi.org/10.1139/as-2016-0008

Gatis, N., Carless, D., Luscombe, D.J., Brazier, R.E. and Anderson, K., 2022. An operational land cover and land cover change toolbox processing open-source data. *Ecological Solutions and Evidence* 3: e12162. https://doi.org/10.1002/2688-8319.12162

Gislason, P.O., Benediktsson, J.A. and Sveinsson, J.R., 2006. Random forests for land cover classification. *Pattern Recognition Letters* 27(4): 294–300.

Gleyzes, M.A., Perret, L. and Kubik, P., 2012. Pleiades system architecture and main performances. *International Archives of the Photogrammetry, Remote Sensing and Spatial Information Sciences* XXXIX-B1: 537–542. https://doi.org/10.5194/isprsarchives-xxxix-b1-537-2012

Gonçalves, J., Henriques, R., Alves, P., Sousa-Silva, R., Monteiro, A.T., Lomba, Â., Marcos, B. and Honrado, J., 2016. Evaluating an unmanned aerial vehicle-based approach for assessing habitat extent and condition in fine-scale early successional mountain mosaics. *Applied Vegetation Science* 19(1): 132–146. https://doi.org/10.1111/avsc.12204

Gonçalves, C., Santana, P., Brandão, T. and Guedes, M., 2022. Automatic detection of *Acacia longifolia* invasive species based on UAV-acquired aerial imagery. *Information Processing in Agriculture* 9(2): 276–287. https://doi.org/10.1016/j.inpa.2021.04.007

Goodfellow, I., Bengio, Y. and Courville, A., 2016. *Deep Learning*. MIT Press, Cambridge, MA. Available online: http://www.deeplearningbook.org/ (accessed 25 September 2024).

Han, L., Yang, G., Dai, H., Xu, B., Yang, H., Feng, H., Li, Z. and Yang, X., 2019. Modeling maize above-ground biomass based on machine learning approaches using UAV remote-sensing data. *Plant Methods* 15: 10. https://doi.org/10.1186/s13007-019-0394-z

Haralick, R.M., Shanmugam, K. and Dinstein, I., 1973. Textural features for image classification. *IEEE Transactions on Systems, Man and Cybernetics* SMC-3: 610–621. https://doi.org/10.1109/TSMC.1973.4309314

Hernando, A., Velázquez, J., Valbuena, R., Legrand, M. and García-Abril, A., 2017. Influence of the resolution of forest cover maps in evaluating fragmentation and connectivity to assess habitat conservation status. *Ecological Indicators* 79, 295–302. https://doi.org/10.1016/j.ecolind.2017.04.031

Holden, N.M. and Connolly, J., 2011. Estimating the carbon stock of a blanket peat region using a peat depth inference model. *Catena* 86(2): 75–85. https://doi.org/10.1016/j.catena.2011.02.002

Huang, C. and Asner, G.P., 2009. Applications of remote sensing to alien invasive plant studies. *Sensors* 9(6): 4869–4889. https://doi.org/10.3390/s90604869

Ingle, R., Habib, W., Connolly, J., Mccorry, M., Barry, S. and Saunders, M., 2023. Upscaling methane fluxes from peatlands across a drainage gradient in Ireland using PlanetScope imagery and machine learning tools. *Scientific Reports* 13(11997): 1–11. https://doi.org/10.1038/s41598-023-38470-6

IUCN (International Union for the Conservation of Nature), 2000. *IUCN Guidelines for the Prevention of Biodiversity Loss Caused by Alien Invasive Species*. IUCN, Gland, Switzerland. Available online: https://portals.iucn.org/library/efiles/documents/Rep-2000-052.pdf (accessed 25 September 2024).

Jaccard, P., 1908. Nouvelles recherches sur la distribution florale. *Bulletin de la Société Vaudoise des Sciences Naturelles* 44: 223–270.

James, K. and Bradshaw, K., 2019. Segmenting objects with indistinct edges, with application to aerial imagery of vegetation. *Proceedings of the South African Institute of Computer Scientists and Information Technologists 2019 Conference*, New York, 17 to 18 September. https://doi.org/10.1145/3351108.3351124

James, K. and Bradshaw, K., 2020. Detecting plant species in the field with deep learning and drone technology. *Methods in Ecology and Evolution* 11(11): 1509–1519. https://doi.org/10.1111/2041-210X.13473

Jensen, J.R., 2014. *Remote Sensing of the Environment: An Earth Resource Perspective*. Second edition. Pearson Education Limited, Upper Saddle River, NJ.

JNCC (Joint Nature Conservation Committee), 2015. *UK Terrestrial and Freshwater Habitat Types: Upland Habitat Descriptions*. JNCC, Peterborough, UK. Available online: https://data.jncc.gov.uk/data/b0b5e833-7300-4234-8ae5-bdbf326e854c/habitat-types-uplands.pdf (accessed 25 September 2024).

Jolliffe, I.T., 2002. *Principal Component Analysis*. Second edition. Springer, New York. https://doi.org/10.1007/b98835

Kattenborn, T., Eichel, J. and Fassnacht, F.E., 2019a. Convolutional neural networks enable efficient, accurate and fine-grained segmentation of plant species and communities from high-resolution UAV imagery. *Scientific Reports* 9: 17656. https://doi.org/10.1038/s41598-019-53797-9

Kattenborn, T., Lopatin, J., Förster, M., Braun, A.C. and Fassnacht, F.E., 2019b. UAV data as alternative to field sampling to map woody invasive species based on combined Sentinel-1 and Sentinel-2 data. *Remote Sensing of Environment* 227: 61–73. https://doi.org/10.1016/j.rse.2019.03.025

Kelly, J., Tosh, D., Dale, K. and Jackson, A., 2013. *The Economic Cost of Invasive and Non-Native Species in Ireland and Northern Ireland*. Northern Ireland Environment Agency, Belfast, and National Parks and Wildlife Service, Dublin.

Khoshgoftaar, T.M., Golawala, M. and Van Hulse, J., 2007. An empirical study of learning from imbalanced data using random forest. Paper presented at the 19th IEEE International Conference on Tools with Artificial Intelligence, Patras, Greece, 29 to 31 October, pp. 310–317. https://doi.org/10.1109/ICTAI.2007.46

Kim, M., Park, S., Anderson, C. and Stensaas, G.L., 2022. *System Characterization Report on Planet's SuperDove*. *U.S. Geological Survey Open-File Report 2021–1030–F*. U.S. Geological Survey, Reston, VA. https://doi.org/10.3133/ofr20211030F

Kingma, D.P. and Ba, J.L., 2015. Adam: a method for stochastic optimization. *Proceedings of the 3rd International Conference on Learning Representations*, San Diego, CA, 7 to 9 May. https://doi.org/10.48550/arXiv.1412.6980

Lee, D.-H., 2013. Pseudo-label: the simple and efficient semi-supervised learning method for deep neural networks. *Paper presented at the ICML 2013 Workshop on Challenges in Representation Learning*, Atlanta, GA, 21 June.

Li, J., Gao, S. and Wang, Y., 2010. Invading cord grass vegetation changes analyzed from Landsat-TM imageries: a case study from the Wanggang area, Jiangsu coast, eastern China. *Acta Oceanologica Sinica* 29(3): 26–37. https://doi.org/10.1007/s13131-010-0034-y

Li, Y., Zhang, H., Xue, X., Jiang, Y. and Shen, Q., 2018. Deep learning for remote sensing image classification: a survey. *Wiley Interdisciplinary Reviews: Data Mining and Knowledge Discovery* 8(6): 1–17. https://doi.org/10.1002/widm.1264

Lin, T.-Y., Dollar, P., Girshick, R., He, K., Hariharan, B. and Belongie, S., 2017. Feature pyramid networks for object detection. *Proceedings of the 2017 IEEE Conference on Computer Vision and Pattern Recognition*, Honolulu, HI, 21 to 26 July, pp. 936–944. https://doi.org/10.1109/CVPR.2017.106

Lin, T.-Y., Goyal, P., Girshick, R., He, K. and Dollar, P., 2018. Focal loss for dense object detection. *IEEE Transactions on Pattern Analysis and Machine Intelligence* 42(2): 2980–2988. https://doi.org/10.1109/TPAMI.2018.2858826

Lu, B. and He, Y., 2017. Species classification using unmanned aerial vehicle (UAV)-acquired high spatial resolution imagery in a heterogeneous grassland. *ISPRS Journal of Photogrammetry and Remote Sensing* 128: 73–85. https://doi.org/10.1016/j.isprsjprs.2017.03.011

Lucas, R., Rowlands, A., Brown, A., Keyworth, S. and Bunting, P., 2007. Rule-based classification of multi-temporal satellite imagery for habitat and agricultural land cover mapping. *ISPRS Journal of Photogrammetry and Remote Sensing* 62(3): 165–185. https://doi.org/10.1016/j.isprsjprs.2007.03.003

Mack, E.L., Firbank, L.G., Bellamy, P.E., Hinsley, S.A. and Veitch, N., 1997. The comparison of remotely sensed and ground-based habitat area data using species-area models. *Journal of Applied Ecology* 34(5): 1222–1228. https://doi.org/10.2307/2405233

Maes, J., Teller, A., Erhard, M., Condé, S., Vallecillo, S., Barredo, J.I., Luisa, M., Malak, D.A., Trombetti, M., Vigiak, O., Zulian, G., Addamo, A.M., Grizzetti, B., Somma, F., Hagyo, A., Vogt, P., Polce, C., Jones, A., Marin, A.I., Santos-martín, F., et al., 2020. *Mapping and Assessment of Ecosystems and Their Services: An EU Wide Ecosystem Assessment in Support of the EU Biodiversity Strategy*. European Commission, Brussels. https://doi.org/10.2760/757183

Malley, J.D., Kruppa, J., Dasgupta, A., Malley, K.G. and Ziegler, A., 2012. Probability machines: consistent probability estimation using nonparametric learning machines. *Methods of Information in Medicine* 51(1): 74–81. https://doi.org/10.3414/ME00-01-0052

Manfreda, S., Dvorak, P., Mullerova, J., Herban, S., Vuono, P., Arranz Justel, J. and Perks, M., 2019. Assessing the accuracy of digital surface models derived from optical imagery acquired with unmanned aerial systems. *Drones* 3(1): 15. https://doi.org/10.3390/drones3010015

Mao, J., Yin, X., Zhang, G., Chen, B., Chang, Y., Chen, W., Yu, J. and Wang, Y., 2022. Pseudo-labeling generative adversarial networks for medical image classification. *Computers in Biology and Medicine* 147: 105729. https://doi.org/10.1016/j.compbiomed.2022.105729

Marcinkowska-Ochtyra, A., Gryguc, K., Ochtyra, A., Kopeć, D., Jarocińska, A. and Sławik, Ł., 2019. Multitemporal hyperspectral data fusion with topographic indices – improving classification of Natura 2000 grassland habitats. *Remote Sensing* 11(19): 2264. https://doi.org/10.3390/rs11192264

Martin, J.R., O'Neill, F.H. and Daly, O.H., 2018. *The Monitoring and Assessment of Three EU Habitats Directive Annex I Grassland Habitats*. Irish Wildlife Manuals, No. 102. National Parks and Wildlife Service, Dublin.

Marzialetti, F., Giulio, S., Malavasi, M., Sperandii, M.G., Acosta, A.T.R. and Carranza, M.L., 2019. Capturing coastal dune natural vegetation types using a phenology-based mapping approach: the potential of Sentinel-2. *Remote Sensing* 11(12): 1506. https://doi.org/10.3390/rs11121506

Matese, A., Toscano, P., Di Gennaro, S.F., Genesio, L., Vaccari, F.P., Primicerio, J., Belli, C., Zaldei, A., Bianconi, R. and Gioli, B., 2015. Intercomparison of UAV, aircraft and satellite remote sensing platforms for precision viticulture. *Remote Sensing* 7(3): 2971–2990. https://doi.org/10.3390/rs70302971

Mathew, S., Pellicer, X.M., Caloca, S., Monteys, X., Zarroca, M. and Jiménez-Martín, D., 2019. Bull Island: characterisation and development of a modern barrier island triggered by human activity in Dublin Bay, Ireland. *Irish Geography* 52(1): 75–100. https://doi.org/10.55650/igj.2019.1378

Mehner, H., Cutler, M., Fairbairn, D. and Thompson, G., 2004. Remote sensing of upland vegetation: the potential of high spatial resolution satellite sensors. *Global Ecology and Biogeography* 13(4): 359–369. https://doi.org/10.1111/j.1466-822X.2004.00096.x

Mesas-Carrascosa, F.J., Torres-Sánchez, J., Clavero-Rumbao, I., García-Ferrer, A., Peña, J.M., Borra-Serrano, I. and López-Granados, F., 2015. Assessing optimal flight parameters for generating accurate multispectral orthomosaicks by UAV to support site-specific crop management. *Remote Sensing* 7(10): 12793–12814. https://doi.org/10.3390/rs71012793

MicaSense, 2019. Altum-PT specifications. Available online: https://ageagle.com/drone- sensors/altum-pt-camera/ (accessed 29 June 2022).

Michez, A., Piégay, H., Lisein, J., Claessens, H. and Lejeune, P., 2016. Classification of riparian forest species and health condition using multi-temporal and hyperspatial imagery from unmanned aerial system. *Environmental Monitoring and Assessment* 188: 146. https://doi.org/10.1007/s10661-015-4996-2

Millennium Ecosystem Assessment, 2003. *Ecosystems and Human Well-being: A Framework for Assessment*. Island Press, Washington, DC.

Mollot, G., Pantel, J.H. and Romanuk, T.N., 2017. The effects of invasive species on the decline in species richness: a global meta-analysis. In Bohan, D.A., Dumbrell, A.J. and Massol, F. (eds), *Networks of Invasion: A Synthesis of Concepts.* Elsevier, Oxford, UK, pp. 61–83. https://doi.org/10.1016/bs.aecr.2016.10.002

Mücher, I.S. and Hazeu, G., 2021. Contribution of remote sensing techniques for monitoring Natura 2000 sites. In Schmidt, A.M. and Van der Sluis, T. (eds), *Improving the Availability of Data and Information on Species, Habitats and Sites*. Wageningen Environmental Research/Ecologic Institute/Milieu. Wageningen, Netherlands, pp. 40–67.

Müller, J. and Brandl, R., 2009. Assessing biodiversity by remote sensing in mountainous terrain: the potential of LiDAR to predict forest beetle assemblages. *Journal of Applied Ecology* 46(4): 897–905. https://doi.org/10.1111/j.1365-2664.2009.01677.x

Muller, A.C. and Guido, S., 2017. *Introduction to Machine Learning with Python: A Guide for Data Scientists*. O'Reilly Media Inc, Sebastopol, CA.

Müllerová, J., Gago, X., Bučas, M., Company, J., Estrany, J., Fortesa, J., Manfreda, S., Michez, A., Mokroš, M., Paulus, G., Tiškus, E., Tsiafouli, M.A. and Kent, R., 2021. Characterizing vegetation complexity with unmanned aerial systems (UAS) – a framework and synthesis. *Ecological Indicators* 131: 108156. https://doi.org/10.1016/j.ecolind.2021.108156

Nagendra, H., Lucas, R., Honrado, J.P., Jongman, R.H.G., Tarantino, C., Adamo, M. and Mairota, P., 2013. Remote sensing for conservation monitoring: assessing protected areas, habitat extent, habitat condition, species diversity, and threats. *Ecological Indicators* 33: 45–59. https://doi.org/10.1016/j.ecolind.2012.09.014

Nehring, S. and Adsersen, H., 2006. *NOBANIS – Invasive Alien Species Fact Sheet:* Spartina anglica. Online Database of the European Network on Invasive Alien Species. Available online: https://www.nobanis.org (accessed 12 November 2024).

NPWS (National Parks and Wildlife Service), 2008. *The Status of EU Protected Habitats and Species in Ireland*. National Parks and Wildlife Service, Dublin.

NPWS (National Parks and Wildlife Service), 2013a. *The Status of EU Protected Habitats and Species in Ireland*. National Parks and Wildlife Service, Dublin.

NPWS (National Parks and Wildlife Service), 2013b. *Site Synopsis: Tralee Bay and Magharees Peninsula, West to Cloghane SAC*. National Parks and Wildlife Service, Dublin.

NPWS (National Parks and Wildlife Service), 2013c. *Site Synopsis: North Dublin Bay SAC*. National Parks and Wildlife Service, Dublin.

NPWS (National Parks and Wildlife Service), 2016. *Site Synopsis: Slieve Mish Mountains SAC*. National Parks and Wildlife Service, Dublin. Available online: https://www.npws.ie/protected-sites/sac/002185 (accessed 8 October 2024).

NPWS (National Parks and Wildlife Service), 2017. *Site synopsis: Wicklow Mountains SAC*. National Parks and Wildlife Service, Dublin. Available online: https://www.npws.ie/protected-sites/sac/002122 (accessed 26 September 2024).

NPWS (National Parks and Wildlife Service), 2018. *Natura 2000 Standard Data Form: Tralee Bay and Magharees Peninsula, West to Cloghane SAC*. National Parks and Wildlife Service, Dublin.

NPWS (National Parks and Wildlife Service), 2019. *The Status of EU Protected Habitats and Species in Ireland. Volume 1: Summary Overview*. National Parks and Wildlife Service, Dublin.

O'Connell, J., Connolly, J. and Holden, N.M., 2014. A monitoring protocol for vegetation change on Irish peatland and heath. *International Journal of Applied Earth Observation and Geoinformation* 31: 130–142. https://doi.org/10.1016/j.jag.2014.03.006

O'Connell, J., Bradter, U. and Benton, T.G., 2015. Wide-area mapping of small-scale features in agricultural landscapes using airborne remote sensing. *ISPRS Journal of Photogrammetry and Remote Sensing* 109: 165–177. https://doi.org/10.1016/j.isprsjprs.2015.09.007

Osco, L.P., Nogueira, K., Marques Ramos, A.P., Faita Pinheiro, M.M., Furuya, D.E.G., Gonçalves, W.N., de Castro Jorge, L.A., Marcato Junior, J. and dos Santos, J.A., 2021. Semantic segmentation of citrus-orchard using deep neural networks and multispectral UAV-based imagery. *Precision Agriculture* 22(4): 1171–1188. https://doi.org/10.1007/s11119-020-09777-5

Pajares, G., 2015. Overview and current status of remote sensing applications based on unmanned aerial vehicles (UAVs). *Photogrammetric Engineering and Remote Sensing* 81(4): 281–330. https://doi.org/10.14358/PERS.81.4.281

Pal, M., 2005. Random forest classifier for remote sensing classification. *International Journal of Remote Sensing* 26(1): 217–222. https://doi.org/10.1080/01431160412331269698

Parker, N., Naumann, E.-K., Medcalf, K., Young, R.H., Potschin, M., Kretsch, C., Parker, J. and Burkhard, B., 2016. *National Ecosystem and Ecosystem Service Mapping Pilot for a Suite of Prioritised Services*. Irish Wildlife Manuals No. 95. National Parks and Wildlife Service, Dublin.

Pedregosa, F., Varoquaux, G., Gramfort, A., Michel, V., Thirion, B., Grisel, O., Blondel, M., Prettenhofer, P., Weiss, R., Dubourg, V., Vanderplas, J., Passos, A., Cournapeau, D., Brucher, M., Perrot, M. and Duchesnay, E., 2011. Scikit-learn: machine learning in Python. *Journal of Machine Learning Research* 12: 2825–2830.

Perez, L. and Wang, J., 2017. The effectiveness of data augmentation in image classification using deep learning. *Convolutional Neural Networks Vis. Recognit*. https://doi.org/10.48550/arXiv.1712.04621

Perrin, P.M., O'Hanrahan, B., Roche, J.R. and Barron, S.J., 2009. *Scoping Study and Pilot Survey for a National Survey and Conservation Assessment of Upland Habitats and Vegetation in Ireland*. National Parks and Wildlife Service, Dublin. Available online: http://www.botanicalenvironmental.com/wp-content/uploads/2010/03/Perrin_et_al_2009_Upland_Pilot.pdf (accessed 26 September 2024).

Perrin, P.M., Roche, J.R., Barron, S.J., Daly, O.H., Hodd, R.L. and Devaney, F.M., 2014a. *National Survey of Upland Habitats: Slieve Mish Mountains cSAC (002185), Co. Kerry*. Site Report No. 15. National Parks and Wildlife Service, Dublin. Available online: https://www.npws.ie/sites/default/files/publications/pdf/NSUH13_Slieve_Mish_Mountains_01b_M.pdf (accessed 26 September 2024).

Perrin, P.M., Barron, S.J., Roche, J.R. and O'Hanrahan, B., 2014b. *Guidelines for a National Survey and Conservation Assessment of Upland Vegetation and Habitats in Ireland (Version 2.0)*. Irish Wildlife Manuals, No. 79. National Parks and Wildlife Service, Dublin. Available online: https://www.npws.ie/sites/default/files/publications/pdf/IWM79.pdf (accessed 26 September 2024).

Perrin, P.M., Roche, J.R., Daly, O.H. and Simon, J.B., 2017. *Blanket Bog Turf-cutting Management System: Wicklow Mountains SAC (002122)*. Site Report No. 1. National Parks and Wildlife Service, Dublin.

Proença, B., Frappart, F., Lubac, B., Marieu, V., Ygorra, B., Bombrun, L., Michalet, R. and Sottolichio, A., 2019. Potential of high-resolution Pléiades imagery to monitor salt marsh evolution after *Spartina* invasion. *Remote Sensing* 11(8): 968. https://doi.org/10.3390/rs11080968

Psuty, N.P., 2007. The coastal foredune: a morphological basis for regional coastal dune development. In Martinez, M.L. and Psuty, N.P. (eds), *Coastal Dunes: Ecology and Conservation.* Springer, New York, pp. 11–27.

Qian, W., Huang, Y., Liu, Q., Fan, W., Sun, Z., Dong, H., Wan, F. and Qiao, X., 2020. UAV and a deep convolutional neural network for monitoring invasive alien plants in the wild. *Computers and Electronics in Agriculture* 174: 105519. https://doi.org/10.1016/j.compag.2020.105519

Raab, C., Stroh, H.G., Tonn, B., Meißner, M., Rohwer, N., Balkenhol, N. and Isselstein, J., 2018. Mapping semi-natural grassland communities using multi-temporal RapidEye remote sensing data. *International Journal of Remote Sensing* 39(17): 5638–5659. https://doi.org/10.1080/01431161.2018.1504344

Ronneberger, O., Fischer, P. and Brox, T., 2015. U-Net: convolutional networks for biomedical image segmentation. In Navab, A., Hornegger, N., Wells, J. and Frangi, W. (eds), *Medical Image Computing and Computer-assisted Intervention – MICCAI 2015*. Springer, New York, pp. 234–241. https://doi.org/10.1007/978-3-319-24574-4_28

Sales, M.H.R., De Bruin, S., Souza, C. and Herold, M., 2022. Land use and land cover area estimates from class membership probability of a random forest classification. *IEEE Transactions on Geoscience and Remote Sensing* 60: 4402711. https://doi.org/10.1109/TGRS.2021.3080083

Schmidt, T., Schuster, C., Kleinschmit, B. and Förster, M., 2014. Evaluating an intra-annual time series for grassland classification – how many acquisitions and what seasonal origin are optimal? *IEEE Journal of Selected Topics in Applied Earth Observations and Remote Sensing* 7(8): 3428–3439. https://doi.org/10.1109/JSTARS.2014.2347203

Scholefield, P., Morton, D., McShane, G., Carrasco, L., Whitfield, M.G., Rowland, C., Rose, R., Wood, C., Tebbs, E., Dodd, B. and Monteith, D., 2019. Estimating habitat extent and carbon loss from an eroded northern blanket bog using UAV derived imagery and topography. *Progress in Physical Geography: Earth and Environment* 43(2): 282–298. https://doi.org/10.1177/0309133319841300

Seebens, H., Blackburn, T.M., Dyer, E.E., Genovesi, P., Hulme, P.E., Jeschke, J.M., Pagad, S., Pyšek, P., Winter, M., Arianoutsou, M., Bacher, S., Blasius, B., Brundu, G., Capinha, C., Celesti-Grapow, L., Dawson, W., Dullinger, S., Fuentes, N., Jäger, H., Essl, F., et al., 2017. No saturation in the accumulation of alien species worldwide. *Nature Communications* 8: 14435. https://doi.org/10.1038/ncomms14435

Shannon, C.E., 1948. A mathematical theory of communication. *Bell System Technical Journal* 27: 623–656. https://doi.org/10.1002/j.1538-7305.1948.tb00917.x

Sharma, S., Ball, J.E., Tang, B., Carruth, D.W., Doude, M. and Islam, M.A., 2019. Semantic segmentation with transfer learning for off-road autonomous driving. *Sensors* 19(11): 2577. https://doi.org/10.3390/s19112577

Shorten, C. and Khoshgoftaar, T.M., 2019. A survey on image data augmentation for deep learning. *Journal of Big Data* 6(60): 60. https://doi.org/10.1186/s40537-019-0197-0

Smith, G.F., O'Donoghue, P., O'Hora, K. and Delaney, E., 2011. *Best Practice Guidance for Habitat Survey and Mapping*. The Heritage Council, Kilkenny, Ireland. Available online: https://www.heritagecouncil.ie/content/files/best_practice_guidance_habitat_survey_mapping_onscreen_version_2011_8mb.pdf (accessed 26 September 2024).

Stokes, K., O'Neill, K. and McDonald, R.A., 2006. *Invasive Species in Ireland.* National Parks and Wildlife Service, Dublin.

Suo, C., McGovern, E. and Gilmer, A., 2019. Coastal dune vegetation mapping using a multispectral sensor mounted on an UAS. *Remote Sensing* 11(15): 1814. https://doi.org/10.3390/rs11151814

Taddia, Y., Corbau, C., Zambello, E. and Pellegrinelli, A., 2019. UAVs for structure-from-motion coastal monitoring: a case study to assess the evolution of embryo dunes over a two-year time frame in the Po River Delta, Italy. *Sensors (Switzerland)* 19(7): 1717. https://doi.org/10.3390/s19071717

Tuanmu, M.N., Viña, A., Roloff, G.J., Liu, W., Ouyang, Z., Zhang, H. and Liu, J., 2011. Temporal transferability of wildlife habitat models: implications for habitat monitoring. *Journal of Biogeography* 38(8): 1510–1523. https://doi.org/10.1111/j.1365-2699.2011.02479.x

Van Beijma, S., Comber, A. and Lamb, A., 2014. Random forest classification of salt marsh vegetation habitats using quad-polarimetric airborne SAR, elevation and optical RS data. *Remote Sensing of Environment* 149: 118–129. https://doi.org/10.1016/j.rse.2014.04.010

van Iersel, W., Straatsma, M., Middelkoop, H. and Addink, E., 2018. Multitemporal classification of river floodplain vegetation using time series of UAV images. *Remote Sensing* 10(7): 1144. https://doi.org/10.3390/rs10071144

Villoslada, M., Bergamo, T.F., Ward, R.D., Burnside, N.G., Joyce, C.B., Bunce, R.G.H. and Sepp, K., 2020. Fine scale plant community assessment in coastal meadows using UAV based multispectral data. *Ecological Indicators* 111: 105979. https://doi.org/10.1016/j.ecolind.2019.105979

Wood, E.M., Pidgeon, A.M., Radeloff, V.C. and Keuler, N.S., 2012. Image texture as a remotely sensed measure of vegetation structure. *Remote Sensing of Environment* 121: 516–526. https://doi.org/10.1016/j.rse.2012.01.003

Yakubovskiy, P., 2019. Segmentation models. GitHub. Available online: https://github.com/qubvel/segmentation_models (accessed 26 September 2024).

Yan, L., Gou, Z. and Duan, Y., 2009. A UAV remote sensing system: design and tests. In Li, D., Shan, J. and Gong, J. (eds), *Geospatial Technology for Earth Observation*. Springer Science & Business Media, New York, pp. 27–44. https://doi.org/10.1007/978-1-4419-0050-0

Young, J., Watt, A., Nowicki, P., Alard, D., Clitherow, J., Henle, K., Johnson, R., Laczko, E., McCracken, D., Matouch, S., Niemela, J. and Richards, C., 2005. Towards sustainable land use: identifying and managing the conflicts between human activities and biodiversity conservation in Europe. *Biodiversity and Conservation* 14(7): 1641–1661. https://doi.org/10.1007/s10531-004-0536-z

Yousefi Lalimi, F., Silvestri, S., Moore, L.J. and Marani, M., 2017. Coupled topographic and vegetation patterns in coastal dunes: remote sensing observations and ecomorphodynamic implications. *Journal of Geophysical Research: Biogeosciences* 122(1): 119–130. https://doi.org/10.1002/2016JG003540

Yu, H., Yang, Z., Tan, L., Wang, Y., Sun, W., Sun, M. and Tang, Y., 2018. Methods and datasets on semantic segmentation: a review. *Neurocomputing* 304: 82–103. https://doi.org/10.1016/j.neucom.2018.03.037

Zheng, Q., Yang, M., Tian, X., Jiang, N. and Wang, D., 2020. A full stage data augmentation method in deep convolutional neural network for natural image classification. *Discrete Dynamics in Nature and Society* 2020: 4706576. https://doi.org/10.1155/2020/4706576

Zlinszky, A. and Kania, A., 2016. Will it blend? Visualization and accuracy evaluation of high-resolution fuzzy vegetation maps. *International Archives of the Photogrammetry, Remote Sensing and Spatial Information Sciences – ISPRS Archives* 41: 335–342. https://doi.org/10.5194/isprsarchives-XLI-B2-335-2016

Zuleta, D., Russo, S.E., Barona, A., Barreto-Silva, J.S., Cardenas, D., Castaño, N., Davies, S.J., Detto, M., Sua, S., Turner, B.L. and Duque, A., 2018. Importance of topography for tree species habitat distributions in a terra firme forest in the Colombian Amazon. *Plant and Soil* 450: 133–149. https://doi.org/10.1007/s11104-018-3878-0

Zuo, P., Zhao, S., Liu, C., Wang, C. and Liang, Y., 2012. Distribution of *Spartina* spp. along China's coast. *Ecological Engineering* 40: 160–166. https://doi.org/10.1016/j.ecoleng.2011.12.014

Abbreviations

DSM	Digital surface model
DTM	Digital terrain model
FPN	Feature Pyramid Network
GCP	Ground control point
GIS	Geographic information system
GNSS	Global Navigation Satellite System
GPS	Global positioning system
GPU	Graphics processing unit
HD	Habitats Directive
IAS	Invasive alien species
IOU	Intersection over Union
mIOU	Mean Intersection over Union
PCA	Principal component analysis
RF	Random forest
RGB	Red, green and blue
SAC	Special Area of Conservation
SSL	Semi-supervised learning
UAV	Unoccupied aerial vehicle

An Ghníomhaireacht Um Chaomhnú Comhshaoil

Tá an GCC freagrach as an gcomhshaol a chosaint agus a fheabhsú, mar shócmhainn luachmhar do mhuintir na hÉireann. Táimid tiomanta do dhaoine agus don chomhshaol a chosaint ar thionchar díobhálach na radaíochta agus an truaillithe.

Is féidir obair na Gníomhaireachta a roinnt ina trí phríomhréimse:

Rialáil: Rialáil agus córais chomhlíonta comhshaoil éifeachtacha a chur i bhfeidhm, chun dea-thorthaí comhshaoil a bhaint amach agus díriú orthu siúd nach mbíonn ag cloí leo.

Eolas: Sonraí, eolas agus measúnú ardchaighdeáin, spriocdhírithe agus tráthúil a chur ar fáil i leith an chomhshaoil chun bonn eolais a chur faoin gcinnteoireacht.

Abhcóideacht: Ag obair le daoine eile ar son timpeallachta glaine, táirgiúla agus dea-chosanta agus ar son cleachtas inbhuanaithe i dtaobh an chomhshaoil.

I measc ár gcuid freagrachtaí tá:

Ceadúnú

- Gníomhaíochtaí tionscail, dramhaíola agus stórála peitril ar scála mór;
- Sceitheadh fuíolluisce uirbigh;
- Úsáid shrianta agus scaoileadh rialaithe Orgánach Géinmhodhnaithe;
- Foinsí radaíochta ianúcháin;
- Astaíochtaí gás ceaptha teasa ó thionscal agus ón eitlíocht trí Scéim an AE um Thrádáil Astaíochtaí.

Forfheidhmiú Náisiúnta i leith Cúrsaí Comhshaoil

- Iniúchadh agus cigireacht ar shaoráidí a bhfuil ceadúnas acu ón GCC;
- Cur i bhfeidhm an dea-chleachtais a stiúradh i ngníomhaíochtaí agus i saoráidí rialáilte;
- Maoirseacht a dhéanamh ar fhreagrachtaí an údaráis áitiúil as cosaint an chomhshaoil;
- Caighdeán an uisce óil phoiblí a rialáil agus údaruithe um sceitheadh fuíolluisce uirbigh a fhorfheidhmiú
- Caighdeán an uisce óil phoiblí agus phríobháidigh a mheasúnú agus tuairisciú air;
- Comhordú a dhéanamh ar líonra d'eagraíochtaí seirbhíse poiblí chun tacú le gníomhú i gcoinne coireachta comhshaoil;
- An dlí a chur orthu siúd a bhriseann dlí an chomhshaoil agus a dhéanann dochar don chomhshaol.

Bainistíocht Dramhaíola agus Ceimiceáin sa Chomhshaol

- Rialacháin dramhaíola a chur i bhfeidhm agus a fhorfheidhmiú lena n-áirítear saincheisteanna forfheidhmithe náisiúnta;
- Staitisticí dramhaíola náisiúnta a ullmhú agus a fhoilsiú chomh maith leis an bPlean Náisiúnta um Bainistíocht Dramhaíola Guaisí;
- An Clár Náisiúnta um Chosc Dramhaíola a fhorbairt agus a chur i bhfeidhm;
- Reachtaíocht ar rialú ceimiceán sa timpeallacht a chur i bhfeidhm agus tuairisciú ar an reachtaíocht sin.

Bainistíocht Uisce

- Plé le struchtúir náisiúnta agus réigiúnacha rialachais agus oibriúcháin chun an Chreat-treoir Uisce a chur i bhfeidhm;
- Monatóireacht, measúnú agus tuairisciú a dhéanamh ar chaighdeán aibhneacha, lochanna, uiscí idirchreasa agus cósta, uiscí snámha agus screamhuisce chomh maith le tomhas ar leibhéil uisce agus sreabhadh abhann.

Eolaíocht Aeráide & Athrú Aeráide

- Fardail agus réamh-mheastacháin a fhoilsiú um astaíochtaí gás ceaptha teasa na hÉireann;
- Rúnaíocht a chur ar fáil don Chomhairle Chomhairleach ar Athrú Aeráide agus tacaíocht a thabhairt don Idirphlé Náisiúnta ar Ghníomhú ar son na hAeráide;
- Tacú le gníomhaíochtaí forbartha Náisiúnta, AE agus NA um Eolaíocht agus Beartas Aeráide.

Monatóireacht & Measúnú ar an gComhshaol

- Córais náisiúnta um monatóireacht an chomhshaoil a cheapadh agus a chur i bhfeidhm: teicneolaíocht, bainistíocht sonraí, anailís agus réamhaisnéisiú;
- Tuairiscí ar Staid Thimpeallacht na hÉireann agus ar Tháscairí a chur ar fáil;
- Monatóireacht a dhéanamh ar chaighdeán an aeir agus Treoir an AE i leith Aeir Ghlain don Eoraip a chur i bhfeidhm chomh maith leis an gCoinbhinsiún ar Aerthruailliú Fadraoin Trasteorann, agus an Treoir i leith na Teorann Náisiúnta Astaíochtaí;
- Maoirseacht a dhéanamh ar chur i bhfeidhm na Treorach i leith Torainn Timpeallachta;
- Measúnú a dhéanamh ar thionchar pleananna agus clár beartaithe ar chomhshaol na hÉireann.

Taighde agus Forbairt Comhshaoil

- Comhordú a dhéanamh ar ghníomhaíochtaí taighde comhshaoil agus iad a mhaoiniú chun brú a aithint, bonn eolais a chur faoin mbeartas agus réitigh a chur ar fáil;
- Comhoibriú le gníomhaíocht náisiúnta agus AE um thaighde comhshaoil.

Cosaint Raideolaíoch

- Monatóireacht a dhéanamh ar leibhéil radaíochta agus nochtadh an phobail do radaíocht ianúcháin agus do réimsí leictreamaighnéadacha a mheas;
- Cabhrú le pleananna náisiúnta a fhorbairt le haghaidh éigeandálaí ag eascairt as taismí núicléacha;
- Monatóireacht a dhéanamh ar fhorbairtí thar lear a bhaineann le saoráidí núicléacha agus leis an tsábháilteacht raideolaíochta;
- Sainseirbhísí um chosaint ar an radaíocht a sholáthar, nó maoirsiú a dhéanamh ar sholáthar na seirbhísí sin.

Treoir, Ardú Feasachta agus Faisnéis Inrochtana

- Tuairisciú, comhairle agus treoir neamhspleách, fianaise-bhunaithe a chur ar fáil don Rialtas, don tionscal agus don phobal ar ábhair maidir le cosaint comhshaoil agus raideolaíoch;
- An nasc idir sláinte agus folláine, an geilleagar agus timpeallacht ghlan a chur chun cinn;
- Feasacht comhshaoil a chur chun cinn lena n-áirítear tacú le hiompraíocht um éifeachtúlacht acmhainní agus aistriú aeráide;
- Tástáil radóin a chur chun cinn i dtithe agus in ionaid oibre agus feabhsúchán a mholadh áit is gá.

Comhpháirtíocht agus Líonrú

- Oibriú le gníomhaireachtaí idirnáisiúnta agus náisiúnta, údaráis réigiúnacha agus áitiúla, eagraíochtaí neamhrialtais, comhlachtaí ionadaíocha agus ranna rialtais chun cosaint chomhshaoil agus raideolaíoch a chur ar fáil, chomh maith le taighde, comhordú agus cinnteoireacht bunaithe ar an eolaíocht.

Bainistíocht agus struchtúr na Gníomhaireachta um Chaomhnú Comhshaoil

Tá an GCC á bainistiú ag Bord lánaimseartha, ar a bhfuil Ard-Stiúrthóir agus cúigear Stiúrthóir. Déantar an obair ar fud cúig cinn d'Oifigí:

1. An Oifig um Inbhunaitheacht i leith Cúrsaí Comhshaoil
2. An Oifig Forfheidhmithe i leith Cúrsaí Comhshaoil
3. An Oifig um Fhianaise agus Measúnú
4. An Oifig um Chosaint ar Radaíocht agus Monatóireacht Comhshaoil
5. An Oifig Cumarsáide agus Seirbhísí Corparáideacha

Tugann coistí comhairleacha cabhair don Ghníomhaireacht agus tagann siad le chéile go rialta le plé a dhéanamh ar ábhair imní agus le comhairle a chur ar an mBord.

EPA Research

Webpages: www.epa.ie/our-services/research/
LinkedIn: www.linkedin.com/showcase/eparesearch/
Twitter: @EPAResearchNews
Email: research@epa.ie